

CHAPTER 2

Stratospheric Ozone and Surface Ultraviolet Radiation

Coordinating Lead Authors:

A. Douglass
V. Fioletov

Lead Authors:

S. Godin-Beekmann
R. Müller
R.S. Stolarski
A. Webb

Coauthors:

A. Arola
J.B. Burkholder
J.P. Burrows
M.P. Chipperfield
R. Cordero
C. David
P.N. den Outer
S.B. Diaz
L.E. Flynn
M. Hegglin
J.R. Herman
P. Huck
S. Janjai
I.M. Jánosi
J.W. Krzyściński
Y. Liu
J. Logan
K. Matthes
R.L. McKenzie
N.J. Muthama
I. Petropavlovskikh
M. Pitts
S. Ramachandran
M. Rex
R.J. Salawitch
B.-M. Sinnhuber
J. Staehelin
S. Strahan
K. Tourpali
J. Valverde-Canossa
C. Vigouroux

Contributors:

G.E. Bodeker
T. Canty
H. De Backer
P. Demoulin
U. Feister
S.M. Frith
J.-U. Groöß
F. Hase
J. Klyft
T. Koide
M.J. Kurylo
D. Loyola
C.A. McLinden
I.A. Megretskaja
P.J. Nair
M. Palm
D. Papanastasiou
L.R. Poole
M. Schneider
R. Schofield
H. Slaper
W. Steinbrecht
S. Tegtmeier
Y. Terao
S. Tilmes
D.I. Vyushin
M. Weber
E.-S. Yang

CHAPTER 2

STRATOSPHERIC OZONE AND SURFACE ULTRAVIOLET RADIATION

Contents

SCIENTIFIC SUMMARY	1
INTRODUCTION	5
2.1 OZONE OBSERVATIONS	5
2.1.1 State of Science in 2006	5
2.1.2 Update on Methods Used to Evaluate the Effect of ODSs on Ozone	5
2.1.3 Update on Total Ozone Changes	6
2.1.3.1 Measurements	6
2.1.3.2 Total Ozone Changes and Trends	8
2.1.4 Update on Ozone Profile Changes	10
2.1.4.1 Measurements	10
2.1.4.2 Ozone Profile Changes	12
2.2 POLAR OZONE	17
2.2.1 State of Science in 2006	17
2.2.2 Polar Ozone Chemistry	18
2.2.2.1 Laboratory Studies of the ClOOCI UV Absorption Spectrum	19
2.2.2.2 Field Observations of Chlorine Partitioning	21
2.2.2.3 Other Issues Related to Polar Ozone Chemistry	25
2.2.3 Polar Stratospheric Cloud Processes	25
2.2.3.1 New Observational Data Sets	26
2.2.3.2 PSC Composition	27
2.2.3.3 PSC Forcing Mechanisms	27
2.2.3.4 Use of Proxies to Represent PSC Processes	28
2.2.4 Arctic Polar Temperatures and Ozone	29
2.2.5 Antarctic Polar Temperatures and Ozone	30
2.2.6 The Onset of Antarctic Ozone Depletion	31
2.3 SURFACE ULTRAVIOLET RADIATION	31
2.3.1 State of Science in 2006	31
Box 2-1 Radiation Amplification Factor for Erythral Irradiance	32
2.3.2 Update on Factors Affecting UV Radiation	33
2.3.2.1 Ozone Effects	33
2.3.2.2 Other Influences on UV	34
2.3.3 Ground-Based and Satellite UV Data	35
2.3.3.1 Ground-Based UV Measurements	35
2.3.3.2 Ground-Based UV Reconstruction	35
2.3.3.3 UV Estimates from Satellite Observations	36
2.3.4 Long-Term Changes in UV	37
2.3.4.1 Ground-Based Observations	37
2.3.4.2 Reconstructed UV Data	38
2.3.4.3 Satellite Estimates of Irradiance Changes	40
2.3.4.4 Consistency of UV Estimates from Observations, Reconstructions, and Satellite Data	41
2.4 INTERPRETATION OF OBSERVED OZONE CHANGES	41
2.4.1 State of Science in 2006	41

2.4.2	Updates to Kinetic and Photochemical Data.....	43
2.4.2.1	Update from JPL 2002 to JPL 2006.....	43
2.4.2.2	Updates since JPL 2006.....	43
2.4.3	The Distribution and Variability of Stratospheric Ozone and Their Representation in Models.....	44
2.4.3.1	Annual Cycle and Natural Variability.....	44
2.4.3.2	Solar Cycle.....	44
2.4.3.3	Volcanic and Aerosol Effects.....	46
2.4.3.4	Evaluation of Simulated Transport.....	47
2.4.3.5	Evaluation of the Chemical Mechanism and Its Implementation.....	49
2.4.3.6	Evaluation of Simulations of the Upper Troposphere/Lower Stratosphere.....	49
2.4.4	Recovery Detection and Attribution.....	50
2.4.4.1	Dynamical Contributions to Apparent Trend.....	50
2.4.4.2	Greenhouse Gas Effects on Ozone Trends.....	50
2.4.4.3	Polar Loss and Dilution to Midlatitudes.....	51
2.4.5	Simulation of Ozone Changes for the Last Three Decades.....	51
2.4.5.1	Total Ozone Trends.....	51
2.4.5.2	Midlatitude Profile Trends.....	53
2.4.5.3	Tropical Profile Trends.....	55
2.4.5.4	Polar Trends.....	55
2.4.5.5	Trends and Recovery in the Upper Troposphere and Lower Stratosphere.....	58
REFERENCES.....		59

SCIENTIFIC SUMMARY

Global Ozone Observations and Interpretation

As a result of the Montreal Protocol, ozone is expected to recover from the effect of ozone-depleting substances (ODSs) as their abundances decline in the coming decades. The 2006 Assessment showed that globally averaged column ozone ceased to decline around 1996, meeting the criterion for the first stage of recovery. Ozone is expected to increase as a result of continued decrease in ODSs (second stage of recovery). This chapter discusses recent observations of ozone and ultraviolet radiation in the context of their historical records. Natural variability, observational uncertainty, and stratospheric cooling necessitate a long record in order to attribute an ozone increase to decreases in ODSs. Table S2-1 summarizes ozone changes since 1980.

The primary tools used in this Assessment for prediction of ozone are chemistry-climate models (CCMs). These CCMs are designed to represent the processes determining the amount of stratospheric ozone and its response to changes in ODSs and greenhouse gases. Eighteen CCMs have been recently evaluated using a variety of process-based comparisons to measurements. The CCMs are further evaluated here by comparison of trends calculated from measurements with trends calculated from simulations designed to reproduce ozone behavior during an observing period.

Total Column Ozone

- **Average total ozone values in 2006–2009 have remained at the same level for the past decade, about 3.5% and 2.5% below the 1964–1980 averages respectively for 90°S–90°N and 60°S–60°N.** Average total ozone from CCM simulations behaves in a manner similar to observations between 1980 and 2009. The average column ozone for 1964–1980 is chosen as a reference for observed changes for two reasons: 1) reliable ground-based observations sufficient to produce a global average are available in this period; 2) a significant trend is not discernible in the observations during this period.
- **Southern Hemisphere midlatitude (35°S–60°S) annual mean total column ozone amounts over the period 2006–2009 have remained at the same level as observed during 1996–2005, approximately 6% below the 1964–1980 average.** Simulations by CCMs also show declines of the same magnitude between 1980 and 1996, and minimal change after 1996, thus both observations and simulations are consistent with the expectations of the impact of ODSs on southern midlatitude ozone.
- **Northern Hemisphere midlatitude (35°N–60°N) annual mean total column ozone amounts over the period 2006–2009 have remained at the same level as observed during 1998–2005, approximately 3.5% below the 1964–1980 average.** A minimum about 5.5% below the 1964–1980 average was reached in the mid-1990s. Simulations by CCMs agree with these measurements, again showing the consistency of data with the expected impact of ODSs. The simulations also indicate that the minimum in the mid-1990s was primarily caused by the ozone response to effects of volcanic aerosols from the 1991 eruption of Mt. Pinatubo.
- **The latitude dependence of simulated total column ozone trends generally agrees with that derived from measurements, showing large negative trends at Southern Hemisphere mid and high latitudes and Northern Hemisphere midlatitudes for the period of ODS increase.** However, in the tropics the statistically significant range of trends produced by CCMs (–1.5 to –4 Dobson units per decade (DU/decade)) does not agree with the trend obtained from measurements (+0.3 ± 1 DU/decade).

Ozone Profiles

- **Northern Hemisphere midlatitude (35°N–60°N) ozone between 12 and 15 km decreased between 1979 and 1995, and increased between 1996 and 2009.** The increase since the mid-1990s is larger than the changes expected from the decline in ODS abundances.

- **Northern Hemisphere midlatitude (35°N–60°N) ozone between 20 and 25 km declined during 1979–1995 and has since ceased to decline.** Observed increases between 1996 and 2008 are statistically significant at some locations but not globally.
- **Northern Hemisphere midlatitude (35°N–60°N) ozone between 35 and 45 km measured using a broad range of ground-based and satellite instruments ceased to decline after the mid-1990s, consistent with the leveling off of ODS abundances.** All data sets show a small ozone increase since that time, with varying degrees of statistical significance but this increase cannot presently be attributed to ODS decrease because of observational uncertainty, natural ozone variability, and stratospheric cooling. CCMs simulate the ozone response to changes in ODSs and increases in greenhouse gases; analysis of CCM results suggests that longer observational records are required to separate these effects from each other and from natural variability.
- **In the midlatitude upper stratosphere (35–45 km) of both hemispheres, the profile ozone trends derived from most CCMs from 1980 to 1996 agree well with trends deduced from measurements.** The agreement in both magnitude and shape of the ozone trends provides evidence that increases in ODSs between 1980 and 1996 are primarily responsible for the observed behavior.
- **In the tropical lower stratosphere, all simulations show a negative ozone trend just above the tropopause, centered at about 18–19 km (70–80 hPa), due to an increase in upwelling.** The simulated trends in the lower tropical stratosphere are consistent with trends deduced for 1985–2005 from Stratospheric Aerosol and Gas Experiment (SAGE II) satellite data, although uncertainties in the SAGE II trends are large. The near-zero trend in tropical total ozone measurements is inconsistent with the negative trend found in the integrated SAGE I + SAGE II stratospheric profiles. The tropospheric ozone column does not increase enough to resolve this discrepancy.

Table S2-1. Summary of ozone changes estimated from observations.

	Column Ozone	12–15 km	20–25 km	35–45 km	Comment
Data Sources	Ground-based, satellite	Ozonesondes	Ozonesondes, satellites, FTIR	Satellites, Umkehrs, FTIR	
Northern midlatitudes 1980–1996	Declined by about 6%	Declined by about 9%	Declined by about 7%	Declined by about 10%	1992–1996 column and lower stratosphere data affected by Mt. Pinatubo
Northern midlatitudes 1996–2009	Increased from the minimum values by about 2% by 1998 and remained at the same level thereafter	Increased by about 6%	Increased by about 2.5%	Increased by 1 to 2%, but uncertainties are large	
Southern midlatitudes 1980–1996	Declined by 6%	No information	Declined by about 7%	Declined by about 10%	
Southern midlatitudes 1996–2009	Remained at approximately the same level	No statistically significant changes	No statistically significant changes	Increased by 1 to 3%, but uncertainties are large	

Polar Ozone Observations and Interpretation

- **The Antarctic ozone hole continued to appear each spring from 2006 to 2009.** This is expected because decreases in stratospheric chlorine and bromine have been moderate over the last few years. Analysis shows that since 1979 the abundance of total column ozone in the Antarctic ozone hole has evolved in a manner consistent with the time evolution of ODSs. Since about 1997 the ODS amounts have been nearly constant and the depth and magnitude of the ozone hole have been controlled by variations in temperature and dynamics. The October mean column ozone within the vortex has been about 40% below 1980 values for the past fifteen years.
- **Arctic winter and spring ozone loss has varied between 2007 and 2010, but remained in a range comparable to the values that have prevailed since the early 1990s.** Chemical loss of about 80% of the losses observed in the record cold winters of 1999/2000 and 2004/2005 has occurred in recent cold winters.
- **Recent laboratory measurements of the chlorine monoxide dimer (ClOCl) dissociation cross section and analyses of observations from aircraft and satellites have reaffirmed the fundamental understanding that polar springtime ozone depletion is caused primarily by the ClO + ClO catalytic ozone destruction cycle, with significant contributions from the BrO + ClO cycle.**
- **Polar stratospheric clouds (PSCs) over Antarctica occur more frequently in early June and less frequently in September than expected based on the previous satellite PSC climatology.** This result is obtained from measurements by a new class of satellite instruments that provide daily vortex-wide information concerning PSC composition and occurrence in both hemispheres. The previous satellite PSC climatology was developed from solar occultation instruments that have limited daily coverage.
- **Calculations constrained to match observed temperatures and halogen levels produce Antarctic ozone losses that are close to those derived from data.** Without constraints, CCMs simulate many aspects of the Antarctic ozone hole, however they do not simultaneously produce the cold temperatures, isolation from middle latitudes, deep descent, and high amounts of halogens in the polar vortex. Furthermore, most CCMs underestimate the Arctic ozone loss that is derived from observations, primarily because the simulated northern winter vortices are too warm.

Ultraviolet Radiation

Ground-based measurements of solar ultraviolet (UV) radiation (wavelength 280–400 nanometers) remain limited both spatially and in duration. However, there have been advances both in reconstructing longer-term UV records from other types of ground-based measurements and in satellite UV retrievals. Where these UV data sets coincide, long-term changes agree, even though there may be differences in instantaneous, absolute levels of UV.

- **Ground-based UV reconstructions and satellite UV retrievals, supported in the later years by direct ground-based UV measurements, show that erythemal (“sunburning”) irradiance over midlatitudes has increased since the late 1970s, in qualitative agreement with the observed decrease in column ozone.** The increase in satellite-derived erythemal irradiance over midlatitudes during 1979–2008 is statistically significant, while there are no significant changes in the tropics. Satellite estimates of UV are difficult to interpret over the polar regions.
- **In the Antarctic, large ozone losses produce a clear increase in surface UV radiation.** Ground-based measurements show that the average spring erythemal irradiance for 1990–2006 is up to 85% greater than the modeled irradiance for 1963–1980, depending on site. The Antarctic spring erythemal irradiance is approximately twice that measured in the Arctic for the same season.
- **Clear-sky UV observations from unpolluted sites in midlatitudes show that since the late 1990s, UV irradiance levels have been approximately constant, consistent with ozone column observations over this period.**

- **Surface UV levels and trends have also been significantly influenced by clouds and aerosols, in addition to stratospheric ozone.** Daily measurements under all atmospheric conditions at sites in Europe and Japan show that erythemal irradiance has continued to increase in recent years due to net reductions in the effects of clouds and aerosols. In contrast, in southern midlatitudes, zonal and annual average erythemal irradiance increases due to ozone decreases since 1979 have been offset by almost a half due to net increases in the effects of clouds and aerosols.

INTRODUCTION

This chapter presents information on several topics but is conceptually organized around a single question: is the Montreal Protocol working? This chapter is focused on the observational record and interpretation thereof up to the present, and consolidates information found in three separate chapters in the previous Assessment (WMO, 2007): Chapter 3 (“Global Ozone: Past and Present,” Chipperfield and Fioletov et al., 2007), Chapter 4 (“Polar Ozone: Past and Present,” Newman and Rex et al., 2007), and Chapter 7 (“Surface Ultraviolet Radiation: Past, Present and Future,” Bais and Lubin et al., 2007). There are four sections in this chapter: Ozone Observations, Polar Ozone, Surface Ultraviolet Radiation, and Interpretation of Observed Ozone Changes. Each section begins with a summary of WMO (2007) followed by a combination of updates to the observational records and longer discussion of new discoveries and observations.

2.1 OZONE OBSERVATIONS

2.1.1 State of Science in 2006

The long-term changes in global ozone were reviewed in Chapter 3 of WMO (2007). From the analysis of data from multiple sources, it was shown that the global mean total column ozone values for the period 2002–2005 had stabilized to values similar to those observed in 1998–2001, at approximately 3.5% below the 1964–1980 average values. Differences between the Northern and Southern Hemispheres (NH and SH) were noted, with ozone average values respectively 3% and 5.5% below their pre-1980 average values. The time series behavior of total ozone column was also shown to be different in both hemispheres during the 1990s. Ozone showed a minimum in the NH around 1993 followed by an increase, while it decreased through the late 1990s in the SH and leveled off in about 2000. Seasonal differences between ozone changes over midlatitude regions in both hemispheres were also noticed. The changes with respect to the pre-1980 values were larger in spring in the NH, while no seasonal dependence was found in the SH. Over the tropics, no change in column ozone values was found, which was consistent with the findings of WMO (2003).

Because total ozone column was no longer decreasing in most observations, several methods were discussed in WMO (2003) and WMO (2007) for the evaluation of ozone trends. Previous Assessments had described long-term ozone changes due to chemical destruction by ozone-depleting substances (ODSs) in terms of linear trends estimated using multiple regression analysis. Because the change in ODSs after the mid-1990s was no longer linear

with time, other methods were proposed, e.g., the piecewise linear trend model in which different linear fits are used before and after a turning point, and the fit to the equivalent effective stratospheric chlorine (EESC) function (see Chapter 1 of this Assessment). Such methods have been used in most recent studies on ozone trends and are also discussed in the present Assessment.

Regarding changes in the vertical ozone distribution, satellite and ground-based measurements showed that in the upper stratosphere, the ozone decrease had stopped and ozone values were relatively constant since 1995. Similar stabilization was found in the lower stratosphere between 20 and 25 kilometers (km) altitude. In the lowermost stratosphere below 15 km altitude in the NH, a significant increase was found from 1996, after the strong decrease observed between 1979 and 1995. This change in the lowermost stratosphere had a substantial impact on the total ozone column. Such an ozone increase was not observed in the SH. The lowermost stratosphere is defined and discussed in more detail in Section 2.4 below.

All studies in WMO (2007) pointed out the stabilization of ozone both in total column and in the vertical distribution at various levels, various locations, and at the global scale. They concurred that the first stage of recovery (i.e., slowing of ozone decline attributable to ODS changes) had already occurred and that the second stage (i.e., onset of ozone increase) was expected to become evident within the next two decades.

2.1.2 Update on Methods Used to Evaluate the Effect of ODSs on Ozone

As discussed in previous Assessments, the long-term and short-term variability of ozone in the stratosphere is generally estimated using multi-regression statistical models that quantify the relationship between ozone and different explanatory variables describing natural or anthropogenic forcings (e.g., SPARC, 1998). The long-term trend components representing the effect of ODSs are extracted simultaneously with other regression terms and autocorrelated noise.

To describe the long-term trend in ozone that is related to ODSs, the equivalent effective stratospheric chlorine (EESC) (see Section 1.4.4 of Chapter 1) is commonly used as a proxy in statistical models (Stolarski et al., 2006; Dhomse et al., 2006; Brunner et al., 2006; Randel and Wu, 2007; Wohltmann et al., 2007; Mäder et al., 2007; Vyushin et al., 2007; Harris et al., 2008). Statistical methods are used to quantify the relationship between ozone changes and EESC, and verify whether the EESC-related term is statistically significant. Analysis of the residuals, for example, by the Cumulative Sum of Residuals (CUSUM) technique (Reinsel et al., 2002;

Newchurch et al., 2003) then can be used to check that a statistical model with the EESC term adequately describes the observed ozone changes.

The EESC depends on latitude and altitude. Moreover, the present estimates of EESC are different from those used, for example, in WMO (2003), as discussed in Section 1.4.4 of Chapter 1. As a result, all of the ozone trend studies mentioned above did not use the same EESC function. While a particular shape of the EESC curve has little effect on the EESC-based trend estimates in the past (they all represent a linear decline during the 1980s and early 1990s with leveling off thereafter), the shape of an EESC function will have more impact on the estimated trend value as time moves from the EESC turning point. The shape of the EESC curve is particularly important for the detectability of future trends (Vyushin et al., 2010). On the other hand, once the EESC shape is specified, the sensitivity of ozone to EESC obtained from this type of statistical analysis varies little as a result of small differences in the length of record.

A statistically significant EESC-related term can be used as evidence of the ODS-related destruction of ozone. The EESC was a linear function of time in the 1980s and thus the EESC fit to ozone can be expressed in terms of linear changes at that time, with results reported in ozone changes (% or Dobson units (DU)) per decade. WMO (2007, Section 3.2.1) discussed ozone trends in terms of EESC. Adding four more years to 25-year-long observation records discussed in WMO (2007) does not change the trend estimates for that period significantly. Similarly, the EESC is nearly a linear function in the 2000s and therefore the expected rate of ozone increase during the declining phase of the EESC can be expressed in % or DU per decade.

WMO (2007) concluded that the first stage of the ozone recovery, i.e., the slowing of ozone decline, identified as the occurrence of a statistically significant reduction in the rate of decline in ozone due to changing EESC, had already occurred. The second stage of the ozone recovery or the onset of ozone increases (turnaround) is identified as the occurrence of statistically significant increases in ozone above previous minimum values due to declining EESC.

The ozone increase after the minimum can be estimated by fitting the data with a linear function or by calculating a piecewise linear trend (PWLT) with a turning point near the EESC maximum (Reinsel et al., 2005; Miller et al., 2006; Vyushin et al., 2007; S.-K. Yang et al., 2009). The slope estimated from ozone data during the declining phase of EESC should agree with the slope expected from the EESC fit if the ozone increase is indeed related to the EESC decline.

As discussed by WMO (2007, Section 3.4.2) a sizable fraction of the long-term ozone changes, particularly

over northern mid and high latitudes, can be related to dynamical processes. Estimation of ozone trends requires a proper accounting for the effect of these processes on ozone. One approach is to add more terms to the statistical model used for trend calculations using a purely statistical approach and letting the regression model find the best proxies (e.g., Mäder et al., 2007) or by adding proxies based on possible physical processes that cause the ozone changes (e.g., Wohltmann et al., 2007). However the physical mechanisms underlying these additional terms are often not well understood, and therefore it is difficult to account for them properly in a statistical model. This issue is addressed in detail in Section 2.4. Another approach is to consider the contribution from dynamical processes as noise. This results in a larger uncertainty in the trend estimates and also requires an additional analysis of the autocorrelation function of the residuals (Vyushin et al., 2007). In both approaches, the eleven-year solar activity cycle and the quasi-biennial oscillation (QBO) are typically included in the statistical model because these oscillations are located in a narrow frequency range.

2.1.3 Update on Total Ozone Changes

2.1.3.1 MEASUREMENTS

Ground-Based Measurements

Dobson, Brewer, and filter instruments provide long-term ground-based total ozone time series. The instrumental precision of well maintained Dobson and Brewer instruments was recently estimated by Scarnato et al. (2010) to be respectively 0.5% and 0.15% (1-sigma). When comparing ground-based total ozone measurements with satellite overpass data, the standard deviation of monthly differences was on average about 1.5% and within 0.6–2.6% for 90% of Dobson and Brewer network stations and on average about 2% and within 1.5–3.5% for 90% of stations equipped with filter instruments M-124 (Fioletov et al., 2008). The agreement between various instruments can be further improved as new ozone absorption cross sections are adopted (Scarnato et al., 2009). A recently established committee is presently addressing the issue of ozone cross sections used in ground-based and satellite measurements (see <http://igaco-o3.fmi.fi/ACSO/>). Since the end of the 1980s, other instruments have been implemented for the monitoring of total ozone. Long-term and regular ground-based Fourier transform infrared (FTIR) measurements are performed at many stations around the world and these data were used to assess ozone trends over Western Europe from 79°N to 28°N (Vigouroux et al., 2008). The precision of FTIR ozone total columns

is about 4%, but it has been demonstrated that it can reach 1 DU in some conditions (Schneider et al., 2008). No calibration is needed, but the instrumental line shape must be known in order to avoid introducing a bias in the ozone retrievals. UV-Visible spectrophotometers such as the System d'Analyse par Observation Zenitale (SAOZ) instruments (Pommereau and Goutail, 1988) retrieve total ozone as well as nitrogen dioxide (NO₂) column amounts from zenith sky measurements using Differential Optical Absorption Spectroscopy (DOAS). A new version of the zenith-sky retrieval algorithm using improved air mass factors was recently introduced. SAOZ observations were used here in addition to Dobson, Brewer, and filter instrument data to form the ground-based zonal mean data set as described by Fioletov et al. (2002). This data set with the list of contributed stations is available from http://woudc.org/data_e.html.

Satellite Measurements

Satellite instruments have observed the total ozone distributions at the global scale since 1970, when the Nimbus 4 satellite was launched with the Backscatter Ultraviolet (BUV) instrument onboard. To date, the longest total ozone records are provided by the series of Total Ozone Mapping Spectrometer (TOMS) and Solar Backscatter Ultraviolet 2 (SBUV/2) instruments. Since 2004, the TOMS total ozone record has been taken over by the Ozone Monitoring Instrument (OMI), an instrument on the Aura satellite. TOMS, BUV, and SBUV/2 data presented here are retrieved with the version 8 algorithm (Bhartia et al., 2004; Flynn, 2007). There are two operationally available OMI satellite total ozone column data products, based on the OMI-TOMS and the OMI-DOAS retrieval algorithms, but outputs of the OMI-TOMS algorithm agree better with the most accurate ground-based measurements than those for the OMI-DOAS algorithm (Balis et al., 2007). The TOMS algorithm uses only two wavelengths (317.5 and 331.2 nanometers (nm)) to derive total ozone (four other wavelengths are used for diagnostics and error correction). The version 8.5 OMI algorithm is similar to the TOMS version 8 algorithm and is used to process OMI data presented here.

In order to obtain long-term total ozone records, several data sets merging various satellite ozone records have been constructed. The TOMS+OMI+SBUV(2) merged ozone data set (MOD) (Stolarski and Frith, 2006), used in WMO (2007), has been updated through December of 2009. The input now includes version 8.5 data from OMI and version 8.0 data from NOAA-17 SBUV/2. Data from 1970 through 1972 have also been added from the Nimbus 4 BUV experiment in 1970–1977. The merged

ozone data set (MOD) can be obtained at http://acdb-ext.gsfc.nasa.gov/Data_services/merged/.

Version 8 ozone retrievals from Nimbus 7 SBUV, and NOAA-9, -11, -14, -16, -17, and -18 SBUV/2 instruments were used in a NOAA cohesive SBUV(2) total ozone data set (S.K. Yang et al., 2009) available at ftp://ftp.cpc.ncep.noaa.gov/long/SBUV_v8_Cohesive.

The European instruments Global Ozone Monitoring Experiment (GOME) on the European Remote Sensing Satellite (ERS-2) (1995–2003, global coverage), Scanning Imaging Absorption Spectrometer for Atmospheric Cartography (SCIAMACHY) on the Environmental Satellite (Envisat; 2002–present), and GOME-2 on Meteorological Operational satellite (MetOp)-A (2006–present) apply the DOAS algorithm technique in the continuous 325–335 nm wavelength range (Burrows et al., 1999) to retrieve total ozone estimates. Different types of DOAS algorithms have been developed: WFDOAS (Coldewey-Egbers et al., 2005), TOGOMI/TOSOMI (Eskes et al., 2005), and SDOAS/GDOAS/GDP (Van Roozendaal et al., 2006). By comparing to Brewer/Dobsons and other satellite data, all algorithms applied to GOME were shown to be in good agreement (Weber et al., 2005; Balis et al., 2007; Fioletov et al., 2008). Overall good agreement was also found in the comparison of SCIAMACHY total ozone to ground data and other satellite data over more than six years (Lerot et al., 2009). However, a downward drift of total ozone from SCIAMACHY with respect to GOME and other correlative data has been identified that is independent of the algorithm used (Lerot et al., 2009; Loyola et al., 2009a). GOME-2 has almost three years of total ozone data. First validation results have been reported (Antón et al., 2009). A merged data set from GOME, SCIAMACHY, and GOME-2 by successive scaling of SCIAMACHY and GOME-2 monthly-mean zonal mean data to GOME is described in Loyola et al. (2009a). They report that a scaling of +2 to +3% was required to match GOME-2 to the GOME data record.

The GOME-SCIAMACHY data is based on combined GOME, SCIAMACHY, and GOME-2 records, with SCIAMACHY and GOME-2 records adjusted using a stable record of the GOME instrument (although with a limited coverage after 2003). While multiple versions of the data processing algorithm and merged data sets exist (Weber et al., 2007; Loyola et al., 2009a), they produce nearly identical records of zonal monthly-mean ozone values.

Measurements from four TOMS instruments, GOME, four SBUV(2) instruments, and OMI are used to produce the New Zealand National Institute of Water and Atmospheric Research (NIWA) combined total ozone data set (Bodeker et al., 2005; Müller et al., 2008). Offsets and drifts between all of the satellite-based data sets are removed through intercomparisons with the

Dobson and Brewer ground-based network. The NIWA data set is available from <http://www.bodekerscientific.com/data/ozone>.

2.1.3.2 TOTAL OZONE CHANGES AND TRENDS

The quasi-global (60°S–60°N) ozone record from the MOD is shown in Figure 2-1. The annual variation and an 11-year periodical component are evident from the plot and are discussed in detail in WMO, 2007 (Chipperfield and Fioletov et al., 2007). The total ozone deviations for the 60°S–60°N, 90°S–90°N, 25°S–25°N, 35°N–60°N, and 35°S–60°S latitude belts are shown in Figure 2-2. The approach used in Fioletov et al. (2002) and WMO (2007) is again used here. Five data sets of 5°-wide zonal averages of total ozone values are analyzed in this Assessment. Area-weighted annual averages are calculated for different latitude belts and for the globe. All panels of Figure 2-2 indicate that average total ozone deviations in 2006–2009 display very little change as compared to the 2002–2005 values reported in WMO (2007). The global and 60°S–60°N averages were about 3.5% and 2.5% below the 1964–1980 average values, respectively. The total column ozone for 1964–1980 is chosen as a reference for observed changes for two reasons: (1) reliable ground-based observations sufficient to produce a global average are available in this period; and (2) a significant trend is not discernible in the observations during this period. In midlatitude regions of both hemispheres, ozone values in the NH and SH stabilized at respectively about 3.5% and 6% lower than the 1964–1980 average, with little sign of increase in recent years.

Several authors have examined the zonally averaged total ozone data and find statistically significant positive trends since the second half of the 1990s. S.-K. Yang et al. (2009) find a positive trend of about $1.2 \pm 0.8\%$ /decade for the period 1996–2007 in the averaged 50°S–50°N SBUV(2) satellite data using the PWLT model. Using Dobson total ozone measurements, Angell and Free (2009) find positive trends in the same regions after application of 5-year running linear trends to the smoothed individual station ground-based data. They used 11-year running means to minimize the 11-year solar and QBO effects in the ozone time series. It should be mentioned however, that the positive trend in 50°S–50°N region is largely associated with an ozone increase in the tropical belt related to relatively low ozone values there in the mid-1990s and relatively high values during the recent solar activity minimum. Loyola et al. (2009b) analyzed the merged GOME(2)+SCIAMACHY data set as well the MOD set for the period from June 1995 to April 2009. They report a statistically significant positive linear trend between 5°S and 30°N for both satellite data sets. All these findings seem to contradict previous estimates of the number of

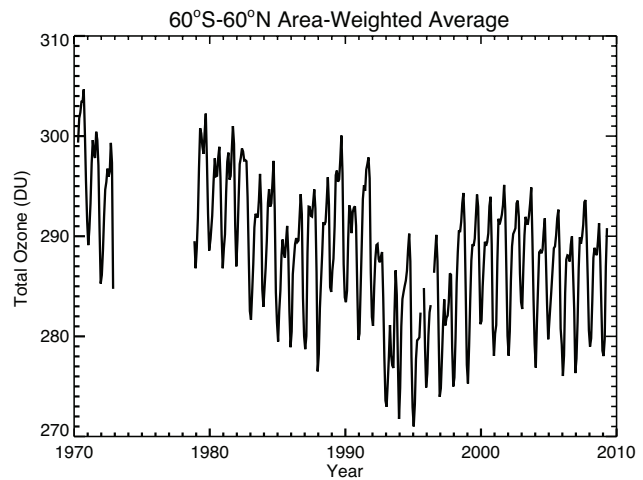


Figure 2-1. Quasi-global (60°N–60°S) average of total ozone distribution (Dobson units) for the period 1970–2009 from the BUV/TOMS/SBUV(2) merged ozone data set.

years required to detect statistically significant ozone trend expected from the decline of ODSs (Weatherhead et al., 2000; Vyushin et al., 2007). These studies predicted that statistically significant ozone trends will be detectable first at southern midlatitudes but that this will not be possible earlier than 2015–2020.

Comparison of the PWLT (or linear trend) estimates with results based on the EESC fit, shows that these recent positive ozone trends are larger than those expected from the decline in ODSs. As mentioned above, knowing the EESC decreasing rate after the turning point in the late 1990s, the corresponding linear term in total ozone regression can be compared to positive trends in PWLT models. Figure 2-3 (updated Figures 8 and 9 of Vyushin et al., 2007) illustrates the ozone zonal trends by PWLT and EESC models with the solar and QBO terms applied to the MOD set for the periods 1979–2008, with the turning point for the PWLT in 1996. Figure 2-3 shows the rate of ozone increase based on the EESC fit for the period corresponding to the declining phase of EESC and the estimates for the linear trend after the turning point of the PWLT. The gray areas indicate 95% confidence intervals for the PWLT estimate. The two trends are fairly similar in southern middle and high latitudes, although the uncertainties on the observed trends encompass zero. In northern middle and high latitudes, however, the observed linear trend is roughly four times the EESC-predicted trend and is actually statistically significant over northern middle and low latitudes according to the PWLT estimate of the noise. In these regions, the ODS decrease induces a positive trend but it is overwhelmed by large dynamically driven variations. This result is confirmed by several

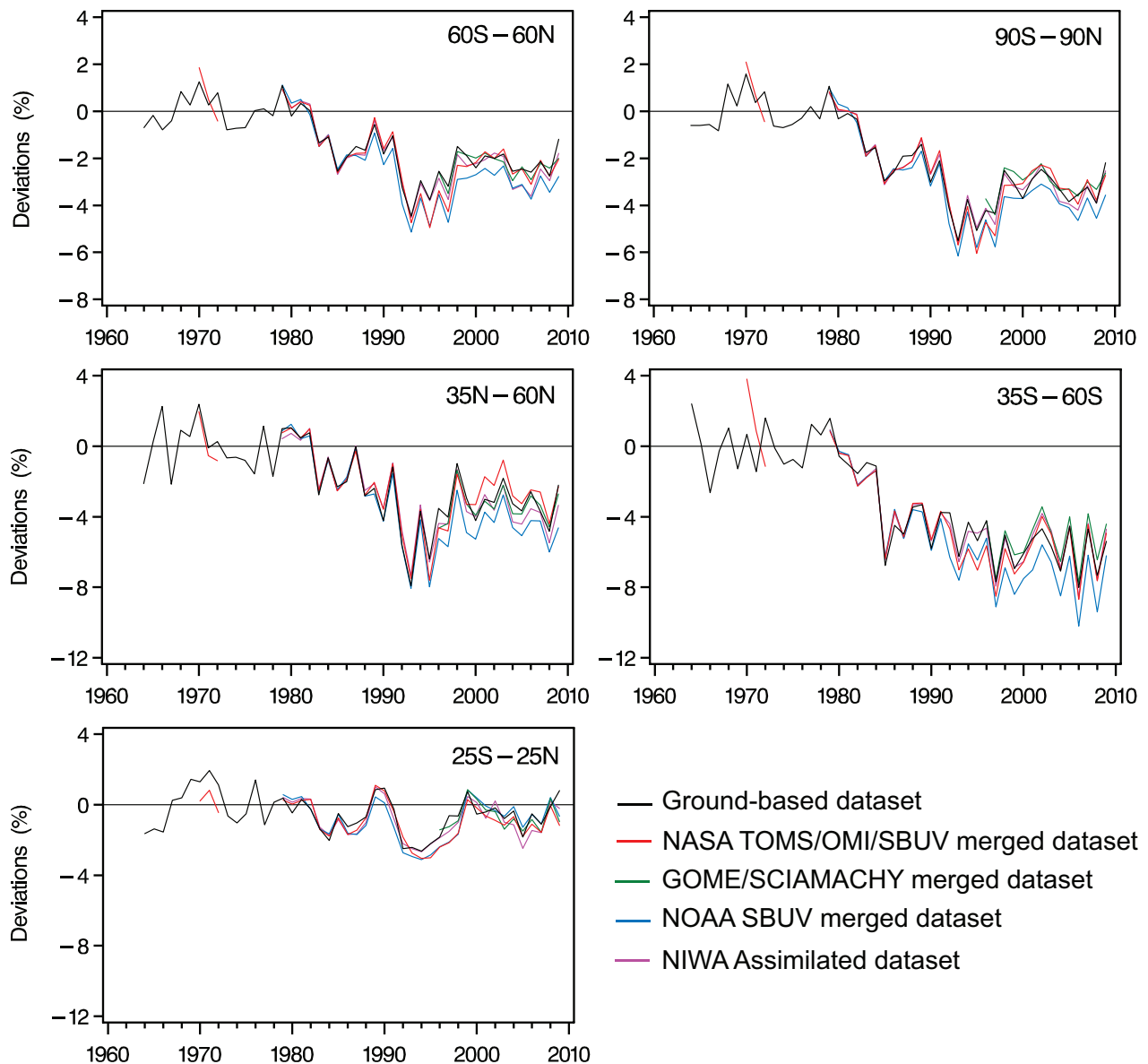


Figure 2-2. Annual mean area-weighted total ozone deviations from the 1964–1980 means for the latitude bands 90°S–90°N, 60°S–60°N, 25°S–25°N, 35°N–60°N, and 35°S–60°S, estimated from different global data sets: ground-based (black), NASA TOMS/OMI/SBUV(/2) merged satellite data set (red), National Institute of Water and Atmospheric Research (NIWA) assimilated data set (magenta), NOAA SBUV(/2) (blue), and GOME/SCIAMACHY merged total ozone data (green). Each data set was deseasonalized with respect to the period 1979–1987. The average of the monthly-mean anomalies for 1964–1980 estimated from ground-based data was then subtracted from each anomaly time series. Deviations are expressed as percentages of the ground-based time average for the period 1964–1980. Figure updated from Chapter 3 of WMO, 2007.

authors, who indicate that the EESC decrease since the mid-1990s is not a major contributor to the recent increase in ozone (Reinsel et al., 2005; Dhomse et al., 2006; Wohltmann et al., 2007; Harris et al., 2008).

On a regional scale, Krzyścin and Borkowski (2008) evaluate the ozone trend variability over Europe using 10-year blocks of reconstructed total ozone time

series since 1950. Statistically significant negative trends of 1 to 5%/decade are found almost over the whole of Europe only in the period 1985–1994. Trends up to –3%/decade appeared over small areas in earlier periods when the anthropogenic forcing on the ozone layer was weak. Vigouroux et al. (2008) provide total ozone trends from homogenized FTIR measurements in European stations,

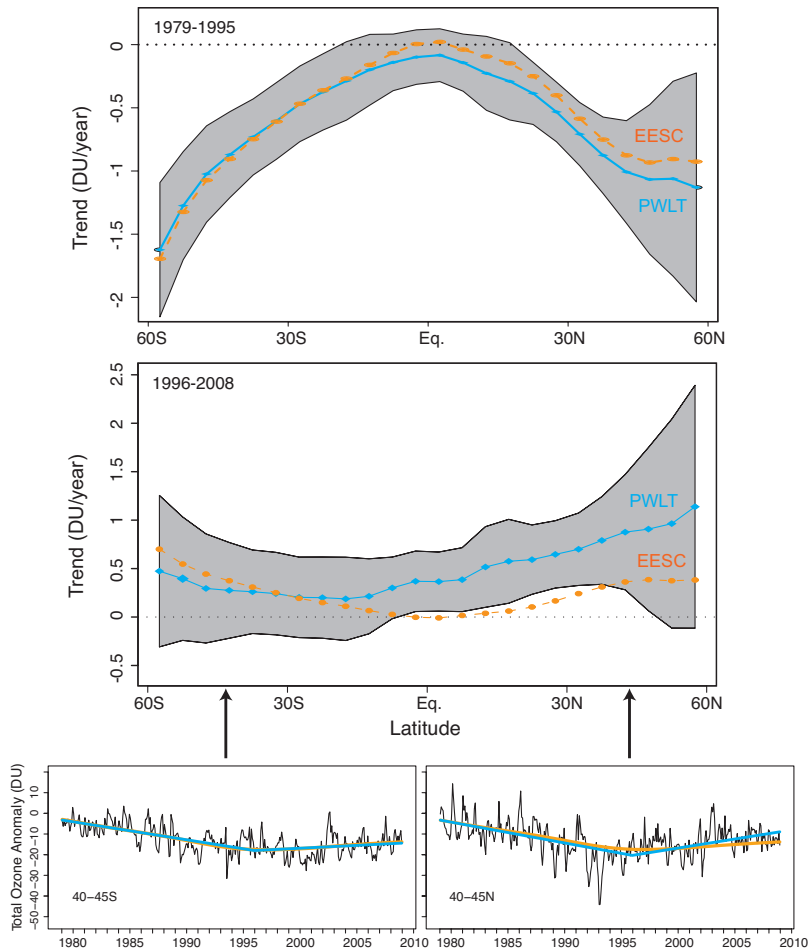


Figure 2-3. (top) The EESC-based linear trend in ozone (Dobson units/year) calculated for the increasing part of EESC (yellow solid circles connected by the yellow line) is compared to the first (declining) slope of the PWLT fit for the period 1979–1995 (blue diamonds connected by the solid blue line) with 95% confidence intervals (gray shading) for the PWLT fit. (middle) The EESC-based linear trend in ozone (DU/year) calculated for the declining part of EESC (yellow solid circles connected by the yellow line) is compared to the second (increasing) slope of the PWLT fit for the period 1996–2008 (blue diamonds connected by the solid blue line) with 95% confidence intervals (gray shading) for the PWLT fit. (bottom) Monthly and zonal mean total ozone anomalies for the 40°S–45°S and 40°N–45°N latitude bands obtained by filtering out the seasonal cycle, QBO, and solar flux, together with the EESC (yellow) and PWLT (blue) fits. Updated from Vyushin et al. (2007). The MOD set was used.

over the 1995–2004 period. These trends have been updated for the 1995–2009 period for the present Assessment and are summarized in Table 2-1. Because the time series are too short to employ the multi-regression models described in Section 2.1.2, a bootstrap resampling method was used, which allows for non-normally distributed data and gives an independent evaluation of the uncertainty in the trend value (Gardiner et al., 2008). The total column trends are close to zero and not significant at all stations except at Kiruna, where the trend is significantly positive.

2.1.4 Update on Ozone Profile Changes

2.1.4.1 MEASUREMENTS

Ground-Based Measurements

Ozonesondes, Dobson and Brewer spectrometers using the Umkehr method, lidars, and microwave instruments provide long-term measurements of ozone vertical distribution. Various recent studies have focused on

assessing the quality and stability of ozonesonde data. Differences ranging from 5 to 10% were found between data obtained with sondes produced from different manufacturers or with different sensing solutions (Thompson et al., 2007; Smit et al., 2007; Kivi et al., 2007; Deshler et al., 2008; Stübi et al., 2008). The Umkehr method retrieves ozone profiles from Dobson and Brewer measurements with a vertical resolution of about 5 km in the stratosphere. Current Umkehr data are retrieved using the UMK04 algorithm already released for the previous Assessment (Petropavlovskikh et al., 2005a, 2005b). Lidars and microwave spectrometers provide range-resolved measurements from the lower stratosphere to about 50 km for the lidar and higher for the microwave. Lidar measurements are characterized by a higher vertical resolution than microwave measurements, but they require clear skies so fewer measurements are obtained. A detailed description of the characteristics of ozonesondes, Umkehr, lidar, and microwave measurements in terms of accuracy and vertical resolution can be found in WMO (2007) and SPARC (1998).

A new ozone profile data source has been introduced for this Assessment, based on the inversion of FTIR measurements (Hase, 2000; Pougatchev et al., 1995). The

Table 2-1. Annual ozone trends and uncertainties (95% confidence limits), in %/decade, for partial and total columns. The measurements at Ny-Ålesund and Kiruna are restricted to the March–September and January–November period, respectively. Updated from Vigouroux et al. (2008).

FTIR Station	Latitude	Period	Ozone Trend (%/decade)			Total Column
			10–18 km	18–27 km	27–42 km	
Ny-Ålesund	79°N	1995–2009	0.0 ± 5.4	−0.8 ± 2.8	5.7 ± 2.7	0.0 ± 2.6
Kiruna	68°N	1996–2009	−1.0 ± 3.9	4.2 ± 2.3	11.4 ± 2.5	2.8 ± 2.2
Harestua	60°N	1995–2009	−11.4 ± 6.2	4.9 ± 2.3	7.2 ± 2.6	0.3 ± 2.7
Jungfraujoch	47°N	1995–2009	−1.9 ± 3.6	0.4 ± 0.9	0.8 ± 0.9	−0.1 ± 1.1
Izaña	28°N	1999–2009	−3.6 ± 4.2	1.8 ± 1.1	1.0 ± 1.2	0.5 ± 1.1

inversion is based on the optimal estimation method (Rodgers, 2000) and leads to 4–5 degrees of freedom in the whole column (Barret et al., 2002). Therefore, in addition to total column ozone, FTIR measurements can provide ozone profile data in 4 vertical layers (approximately ground–10 km; 10–18 km; 18–27 km; and 27–42 km). The precision of these four ozone partial columns is about 9.5%, 6.5%, 8.5%, and 6.0%, respectively (Vigouroux et al., 2008).

Satellite Measurements and Merged Data Sets

The second Stratospheric Aerosol and Gas Experiment (SAGE II) and Halogen Occultation Experiment (HALOE) satellite instruments that provided long and stable global observations of the ozone vertical distribution using the solar occultation technique ceased operation in 2005. Their long observational records, which were used in the previous Assessments, cover the periods 1984–2005 and 1991–2005 respectively. The longest ozone profile record based on a single instrument type still in operation is now provided by the series of SBUV and SBUV/2 instruments in operation since 1978. Retrieved profiles however have much lower vertical resolution than SAGE II or HALOE. The data are retrieved with the version 8 algorithm also used for total ozone retrieval (Bhartia et al., 2004; Flynn, 2007).

Data availability and quality remain the key issues in assessing changes in ozone profiles from satellite data. Jones et al. (2009) estimated that the smallest detectable linear trend in the midlatitude upper stratosphere from accurate but sparse SAGE occultation data was ~2.9%/decade (for the 1979–1997 period), while a trend of 1.5%/decade could be detected if the SAGE time series are combined with HALOE and much more frequent SBUV(/2) nadir observations. The SBUV(/2) record is comprised of data from multiple instruments. Biases between some of these instruments are comparable with

long-term ozone changes (e.g., Terao and Logan, 2007; Fioletov, 2009) that make the combined record difficult to use for the trend estimates.

In the last decade, several satellite instruments providing ozone profile measurements according to various measuring techniques have been launched onboard various satellite platforms, e.g., Odin (launched in 2001), Envisat (2002), SCISAT (2003), Aura (2004), and MetOp-A (2006), but their records are too short to contribute to this analysis on their own. Evaluation of the impact of the stabilization and subsequent decrease of ODS abundances in the stratosphere thus requires the merging of multiple data sets.

Merging the various satellite ozone profile data sets into a single, homogeneous data record suitable for trend studies is a challenge since each record is subject to its own instrument effects (noise, systematic errors, degradation, aging) and sampling issues (vertical and horizontal sampling, resolution, repeat time). Several such data sets have been introduced, based on single instrument type, such as SBUV and SBUV(/2) (Frith et al., 2004) or multiple instruments, e.g., sondes and solar occultation instruments (Randel and Wu, 2007; Hassler et al., 2008), or satellite instruments using different measurement techniques (Jones et al., 2009). McLinden et al. (2009) provide another data set based on SAGE and SBUV(/2) data spanning 1979–2005 where drifts in individual SBUV instruments and inter-SBUV biases are corrected using SAGE I and II by calculating differences between coincident SAGE-SBUV(/2) measurements. In this way the daily, near-global coverage of SBUV(/2) is combined with the stability and precision of SAGE to provide a homogeneous ozone record. Another approach is used by Jones et al. (2009): in order to remove biases between individual instrument records, ozone anomalies (deviations from the annual cycle) in overlapping periods are compared and then corrected for the difference. The data quality issue for trend estimates has become particularly important after

August 2005, when the SAGE II instrument stopped its operation, ending its long and stable data record. Because both SAGE II and HALOE ceased operations in 2005, few trend analyses using satellite ozone profile data were performed since the WMO (2007) report.

2.1.4.2 OZONE PROFILE CHANGES

Profile Trends in Altitude and Pressure Coordinates

As discussed in the previous Ozone Assessments, care must be taken when comparing trends in ozone derived from data in different geophysical units and/or different vertical coordinate systems (WMO, 2007). This is due to simultaneous trends in temperature that impact the air density directly and the altitude of a pressure surface indirectly. Rosenfield et al. (2005) demonstrated using a two-dimensional model that trends in upper stratospheric ozone may differ by 1 to 2%/decade depending on the units and vertical coordinate of the time series. Terao and Logan (2007) show differences up to 4%/decade between SAGE trends in altitude and pressure coordinates if National Centers for Environmental Prediction (NCEP) temperature reanalysis data are used for the conversion. An analysis of SBUV(2) and SAGE ozone time series suggests that this difference can be as much as 4% in the upper stratosphere if SAGE trends calculated in number density versus altitude are compared to SBUV(2) partial pressure versus pressure trends (Figure 2-4). However, if SAGE data are converted to the same units as SBUV(2) using temperature data with proper temperature trends (Randel et al., 2009) and are adjusted to match SBUV(2) vertical resolution as was done in the SAGE-corrected SBUV data set (McLinden et al., 2009), the ozone trends derived from SAGE and SBUV(2) are consistent at the 1–2%/decade level, roughly that of the trend uncertainties.

Ozone Changes in the Upper Stratosphere

The upper stratosphere (35–45 km) is the region where the effects of ODSs are expected to be the easiest to quantify, since the destruction of ozone there is mainly due to processes linked to homogeneous chemistry (WMO, 1999). Most studies performed in that region show a strong and statistically significant decline (6–8% per decade) for the period up to the mid-1990s and a near-zero or slightly positive trend thereafter (e.g., Randel and Wu, 2007; Steinbrecht et al., 2009; Jones et al., 2009; McLinden et al., 2009).

The ozone variability in the upper stratosphere (35–45 km) was examined by Steinbrecht et al. (2009) from various satellites and five ground-based lidar stations located in northern midlatitudes, tropical latitudes, and

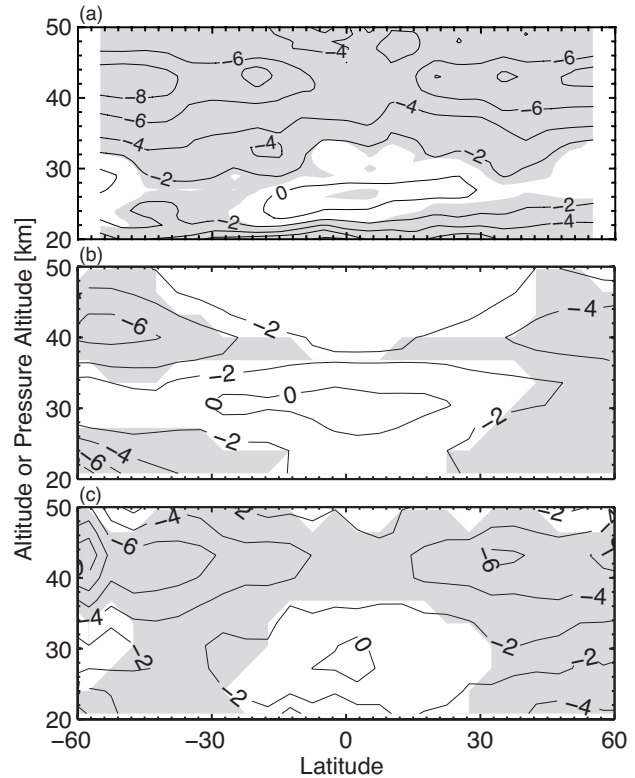
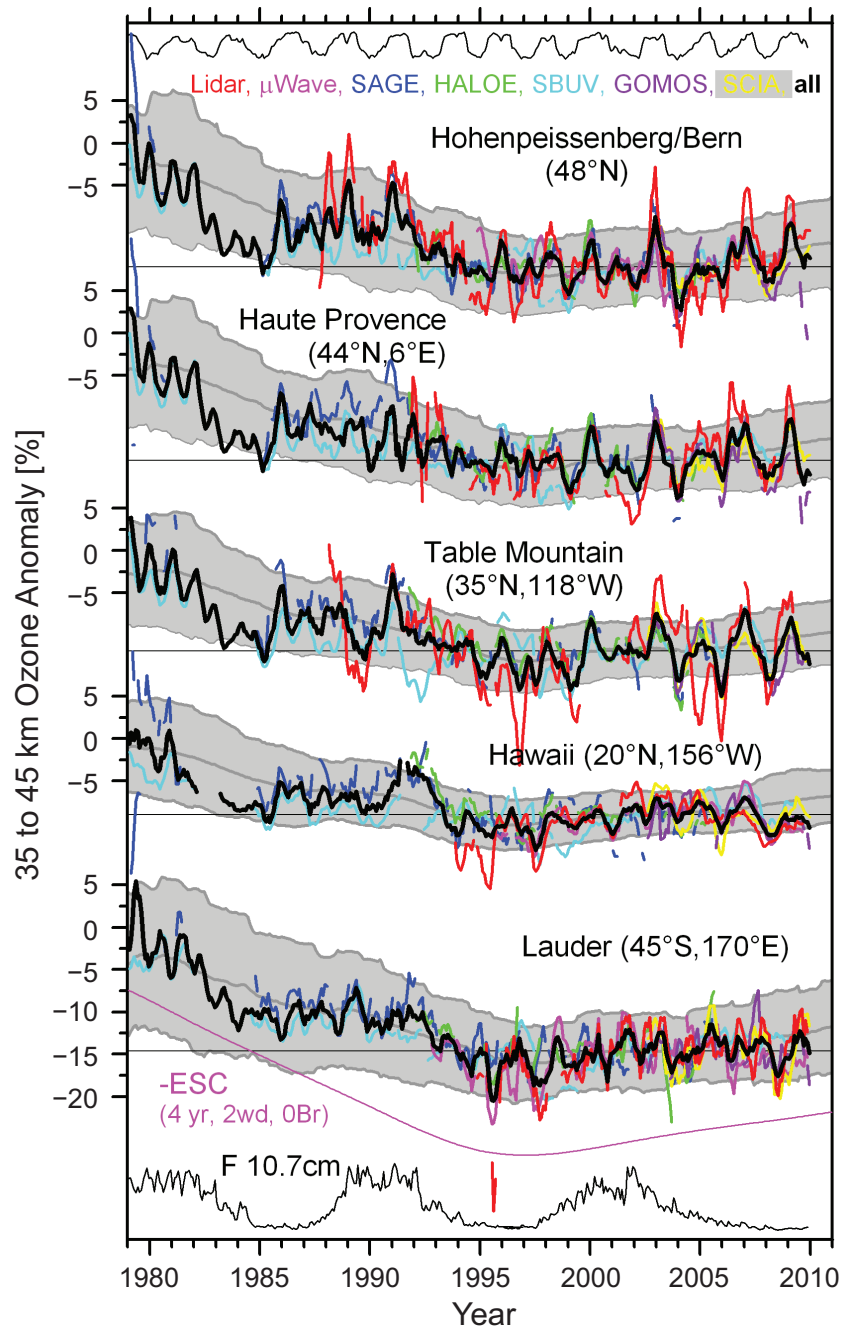


Figure 2-4. Stratospheric ozone trends as functions of latitude and altitude or pressure altitude from various data sources. The trends were estimated using regression to an EESC curve and converted to % per decade using the variation of EESC with time in the 1980s. The plots display trend estimates from various published data sets: (a) SAGE I+II (adapted from Randel and Wu, 2007), (b) the NASA merged SBUV(2) data set, (c) SAGE-corrected SBUV(2) (McLinden et al., 2009). For panel (c) SAGE I+II data are converted onto a pressure using a temperature trend from Randel et al. (2009) and then vertically smoothed to match the SBUV vertical resolution. Shading indicates the trends are significant at the 2σ level. Panel (a) is plotted in altitude, the remaining panels in pressure-altitude. Pressure-altitude is defined as $z^* = -16 \log_{10}(p/1000)$, where p is in hPa and z^* is km. Trend contours are every 2% per decade.

southern midlatitudes (Figure 2-5). This study extends results mentioned in WMO (2007) and includes an evaluation of temperature variability over the same locations. The new analysis confirms that the upper stratospheric ozone decline apparent from 1979 until the mid-1990s has stopped and ozone has stabilized since 1995–1996, depending on the latitude. Tatarov et al. (2009) analyzed 20 years (1988–2008) of stratospheric ozone and temperature

Figure 2-5. Ozone anomalies over the 1979 to early 2010 period from different data sets at five NDACC stations. Anomalies are averaged over the 35–45 km range. Light blue: SBUV(/2)-MOD version 8. Dark blue: SAGE I and II version 6.20. Green: HALOE version 19.0. Red: Lidar. Magenta: Microwave. Yellow: SCIAMACHY IUP–Bremen version 2.0. Violet: GOMOS ESA IPF 5.00. Black: Average of all available instruments. Gray underlay: CCMVal model simulations, 24-month running average ± 2 standard deviations. Observed data are smoothed by a five-month running mean. Lidar and microwave data are station means; all other data are zonal means. The thin black lines at the top and bottom show negative 10 hPa zonal wind at the equator as a proxy for the QBO, and 10.7 cm solar flux as a proxy for the 11-year solar cycle, respectively. The thin magenta line near the bottom shows inverted effective stratospheric chlorine as a proxy for ozone destruction by chlorine (ESC, 4 years mean age, 2 years spectral width, no bromine; see Newman et al., 2006). Updated from Steinbrecht et al. (2009).



profiles measured by differential absorption lidar (DIAL) data at the National Institute for Environmental Studies in Tsukuba (36°N , 140°E), Japan. Ozone data in the upper stratosphere exhibit a strong negative trend from 1988 to 1997 and a statistically insignificant trend after 1998.

Similar results were obtained for SAGE II coincident data over the station.

The lack of a significant ozone trend during the recent period (since 1996) in the upper stratosphere has also been found in the Arosa Umkehr data (Zanis et al., 2006).

In contrast, analyses of the homogenized Umkehr record for Belsk yielded a statistically significant upward trend in the upper stratosphere in the period 1996–2007 but not a decisive trend at other altitudes (Krzyścin and Rajewska-Wiech, 2009). From FTIR measurements, trends in the upper stratospheric layer of the ozone profile retrieval (27–42 km) range from an insignificant 0.8% per decade trend at Jungfraujoch (47°N) to a significant positive trend of up to 11% per decade at high latitude stations (see Table 2-1). Trend results from relatively short time series in the Arctic should be considered with caution due to the high variability of ozone in this region, especially during wintertime.

Jones et al. (2009) provide a global estimate of ozone trends from the average of various satellite ozone anomaly records. Using the PWLT statistical model with a turning point in 1997, they find that the largest statistically significant ozone declines in 1979–1997 are found in the midlatitude regions between 35 and 45 km altitude in both hemispheres, with trend values of approximately -7% /decade. For the period 1997 to 2008, they derive trends of 1.4 and 0.8%/decade in the NH and SH respectively, but these are not statistically significant (see Table 2-2).

Ozone Changes in the Lower Stratosphere

The lower stratosphere between 20 and 25 km over middle latitudes is another region where a statistically significant decline of about 4 to 5%/decade (or 7–8% total decline) occurred between 1979 and the mid-1990s, followed by stabilization or a slight (2–3%) ozone increase thereafter.

Angell and Free (2009) analyzed long-term ozone profile time series from four Northern Hemisphere Dobson Umkehr and 9 ozonesonde stations for trend analysis between 1970 and 2007. The 5-year trends were derived

from the 11-year running mean of the time series to minimize the impact of the 11-year solar cycle and QBO signals in the data. Both Umkehr and sonde data showed that nearly half of the increase in north temperate total-ozone trend between 1989 and 2000 was due to an increase in the 10–19 km layer in the lower stratosphere, with the troposphere contributing only about 5% of the change. Nonsignificant positive ozone trends at the end of the record in 2000 were found at four Umkehr layers in the middle and high stratosphere, as well as between 10 and 32 km altitude in sonde data.

Murata et al. (2009) could not detect any trend from a 14-year data set of ozone profiles measured with a balloonborne optical ozone sensor beginning in 1994 at Sanriku, Japan. This lack of trend was attributed to the leveling off of ODSs in the stratosphere. The extension of the FTIR trend analysis up to 2009 shows no significant trend at the midlatitudes station for the 18–27 km layer (Table 2-1). Similarly, the global trend analysis of Jones et al. (2009) shows no significant trend for the 20–25 km altitude range in the NH and SH midlatitudes for the period 1997–2008.

Figures 2-6a and 2-6b show the temporal evolution of deseasonalized ozone monthly means in three pressure ranges (upper, lower, and lowermost stratosphere) based on ozonesondes, Umkehr, and SBUV(2) observations over Europe and Lauder in the SH, respectively (adapted from Terao and Logan, 2007). The various time series show very similar interannual variation, although some biases are apparent between the measurements. In the upper and lower stratosphere, ozone levels have stabilized after a decrease from the early 1980s to the mid-1990s. In the lower stratosphere, the decrease was more pronounced over Europe than in the SH. In the lowermost stratosphere, no significant long-term variation is observed at

Table 2-2. Average ozone trends and uncertainties (95% confidence limits) in %/decade in the lower and upper stratosphere in the NH and SH midlatitudes, from various data sources for the period 1996–2008. The ozonesondes and Umkehr results correspond to the PWLT trends in Figure 2-7. The FTIR results are for the Jungfraujoch station only, for the 1995–2009 period, and correspond to respectively the 18–27 km and the 27–42 km altitude ranges for the lower and upper stratosphere.

Data Source	Ozone Trend 30°S–60°S (%/decade)		Ozone Trend 30°N–60°N (%/decade)	
	20–25 km	35–45 km	20–25 km	35–45 km
Satellite (from Jones et al., 2009)	-1.0 ± 2.0	0.8 ± 2.1	0.2 ± 1.9	1.4 ± 2.3
Umkehr	0.2 ± 2.6	2.0 ± 1.5	3.2 ± 2.1	1.5 ± 1.3
Ozonesondes			1.5 ± 0.6	
FTIR (updated from Vigouroux et al., 2008)			0.4 ± 0.9	0.8 ± 0.9

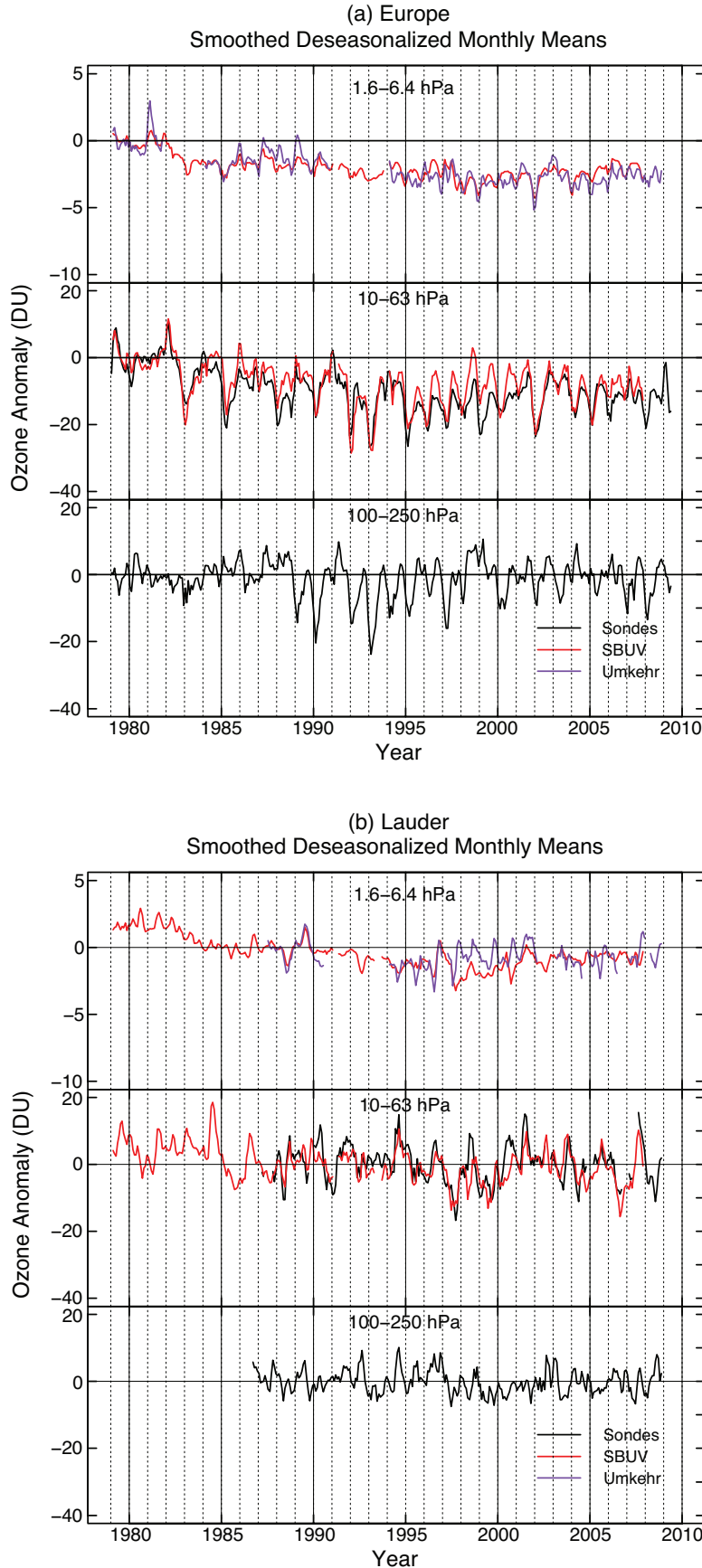


Figure 2-6. (a) Monthly ozone anomalies in Dobson units for Europe as measured by ozonesondes (black line), SBUV(/2) (red line), and Umkehr (blue line) at three pressure layers. The monthly anomalies were computed as the difference between a given monthly mean and the average of monthly means for 1979–1987 for each data set. The average of the monthly-mean anomalies for 1979–1981 was then subtracted from each anomaly time series to set the zero level in each panel. A three-month running mean was applied to the anomalies. The SBUV(/2) data were selected within a grid box of 45°N–55°N and 10°W–30°E. The ozonesonde data are the average of measurements at three European stations: Hohenpeissenberg, Payerne, and Uccle. The Umkehr data are from Arosa, Belsk, and Haute-Provence Observatory. The sonde and SBUV(/2) analysis is updated from Terao and Logan (2007). (b) Same as for (a) but for the Southern Hemisphere. The sonde data are from Lauder, New Zealand. The SBUV(/2) data were selected within a grid box of 40°S–50°S and 150°E–170°W. The monthly anomalies were computed using the monthly means for 1987–1991.

either location over the whole period, but higher short-term variability was seen during the nineties in Europe.

The vertical profile of ozone trends computed from SBUV(/2), Umkehr, and ozonesonde data over Northern midlatitudes stations is displayed in Figure 2-7 for both the increasing and decreasing periods of EESC (e.g., 1979–1995 and 1996–2008). The trends were derived using EESC as a regression term accounting for the variation of mean age of air as a function of altitude (see Waugh and Hall (2000) for a discussion of age of air and its spatial dependence). In the case of ozonesondes, trends were computed as the average of trends derived for nine northern midlatitude stations, as in the previous Ozone Assessment (Chapter 3). For Umkehr, the trend was derived from the average of ozone anomalies at four northern midlatitude stations and for SBUV(/2), the 40°N–50°N zonal mean data were used. Piecewise linear trends with inflection

point in January 1996 derived from ozonesonde and Umkehr data are also represented in the figure. As shown in WMO (2007), ozone trends during the first increasing period of EESC display two maxima in the upper and lower stratosphere, reaching -5 to -7% /decade and -4 to -5% /decade respectively (total decline of about 10% and 7% respectively), with generally good agreement between the various observations, except for Umkehr in the lower stratosphere. In both cases, the EESC and PWLT trend models give similar results for this period. For the decreasing EESC period, positive ozone trends are derived. In the upper and lower stratosphere, EESC and PWLT models provide similar trends of about 2%/decade. The PWLT trends are significant in the lower stratosphere and barely significant in the upper stratosphere. These results indicate that while the decrease of ODSs is indeed causing an increase of ozone over these midlatitude stations, this in-

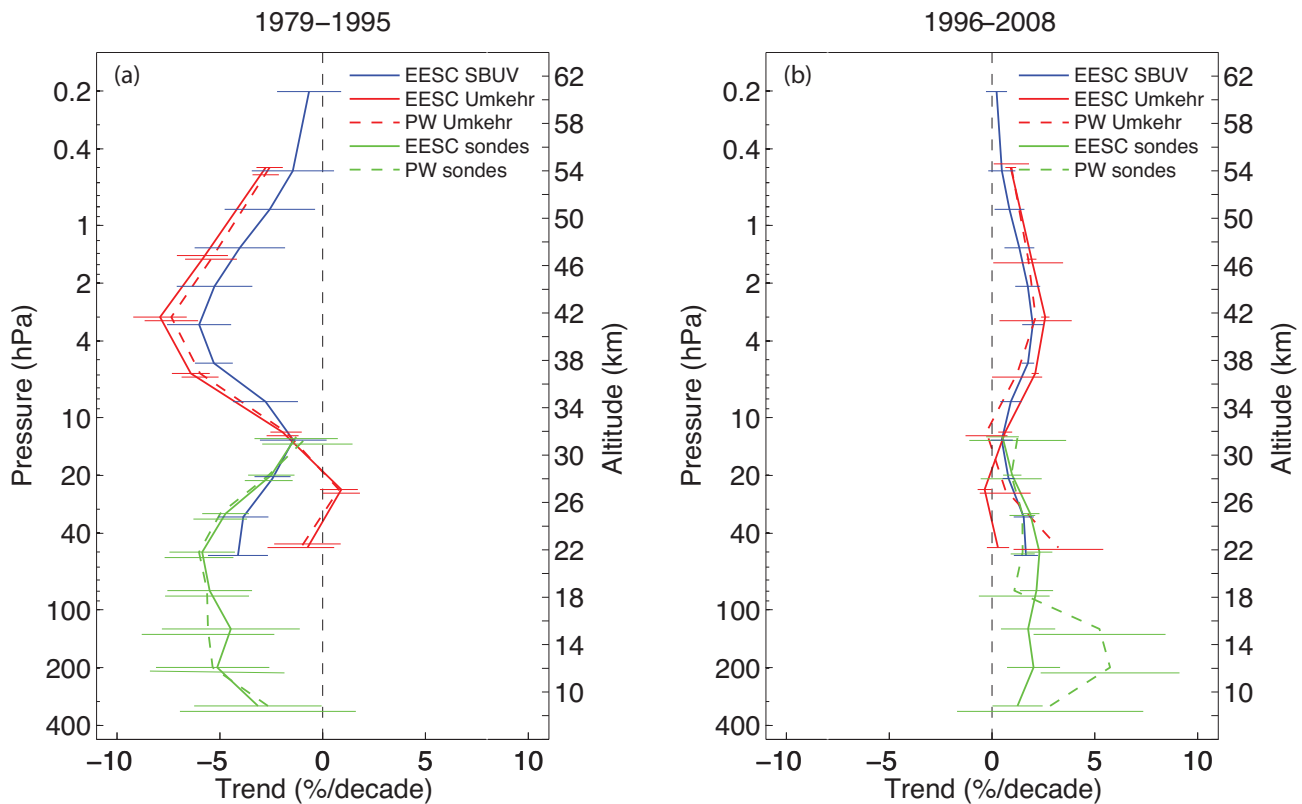


Figure 2-7. Vertical profile of ozone trends over Northern midlatitudes estimated from ozonesondes, Umkehr, and SBUV(/2) measurements for the period 1979–2008. The trends were estimated using regression to an EESC curve and converted to % per decade using the variation of EESC with time from 1979 to 1995 in panel (a) and from 1996 to 2008 in panel (b). Piecewise linear trends with inflection point in January 1996 derived from ozonesonde and Umkehr data are also shown. The trend models also include QBO and solar cycle terms. The sonde results are an average of trends for Churchill, Goose Bay, Boulder, Wallops Island, Hohenpeissenberg, Payerne, Uccle, Sapporo, and Tateno, along with two standard errors of the nine trends. The Umkehr trends were derived from averaged ozone anomalies at Belsk, Arosa, OHP, and Boulder. For SBUV(/2), the 40°N–50°N zonal mean data were used. The altitude scale is from the standard atmosphere. The error bars correspond to 95% confidence interval.

crease is still barely significant, especially in the upper stratosphere where trends derived from PWLT and EESC models are expected to show the best agreement. In contrast, in the lowermost stratosphere, EESC and PWLT trends derived from sondes data differ significantly, with large positive trend values in the latter case, suggesting that the ozone increase is due to factors other than chlorine decline, for example dynamical processes (see Section 2.4).

Table 2-2 summarizes the average trends found from various data sources using the PWLT model in the NH and SH midlatitudes in the lower (20–25 km) and upper (35–45 km) stratosphere. Most results show positive ozone trends (1–3% increase) since 1996 in the various regions. These trends are significant at some locations (e.g., over Northern midlatitudes) but the results from global satellite data are still not significant at the 95% confidence level (Jones et al., 2009).

Northern Hemisphere midlatitude (35°N–60°N) ozone between 12 and 15 km decreased by about 9% between 1979 and 1995, and increased by about 6% between 1996 and 2009 (Figure 2-7). The increase since the mid-1990s is larger than the changes expected from the decline in ODS abundances.

2.2 POLAR OZONE

Chapter 4 of WMO (2007) (“Polar Ozone: Past and Present”, Newman and Rex et al., 2007) builds upon the sequence of polar ozone chapters in the WMO Assessment series. The present discussion updates WMO (2007), highlighting changes over the past four years. Discussion of polar ozone recovery is found in Chapter 3 of this Assessment, and interactions of polar chemistry and climate are found in Chapter 4.

2.2.1 State of Science in 2006

The discovery of the Antarctic ozone hole by Farman et al. (1985) prompted considerable effort to develop the scientific basis necessary to model and predict polar ozone loss. As noted in the previous chapter, the stratospheric chlorine burden reached its peak in the late 1990s and has since begun to decrease. During the period of increasing chlorine concentrations, the springtime polar ozone values decreased in both hemispheres. Consistently low values in springtime ozone have been observed since the mid-1980s in the Southern Hemisphere. A unique dynamical situation, the first major sudden stratospheric warming in the Southern Hemisphere, led to the anomalously high ozone levels in 2002; this situation is discussed in detail in Chapter 4 of WMO (2007). The Arctic polar ozone loss is much more variable, depending not just on the stratospheric chlorine level but also on whether or not the winter is cold enough and of sufficient

length for chlorine-catalyzed ozone loss to occur. Because chlorofluorocarbons are long-lived, atmospheric chlorine loading is declining slowly.

The springtime averages of total ozone poleward of 63° latitude in the Arctic and Antarctic are shown in Figure 2-8 (an update of Figure 4-7 from WMO, 2007). Interannual variability in polar stratospheric ozone abundance and chemistry is driven by variability in temperature and transport due to year-to-year differences in dynamics. The horizontal gray lines in Figure 2-8 are the averages of ozone values obtained between 1970 and 1982, and the shading emphasizes the differences between these averages and subsequent years.

WMO (2007) outlined the processes important to polar ozone loss. The rate-limiting step of the dominant cycle for polar ozone destruction is the photolysis of chlorine peroxide (ClOOCl, also known as the chlorine monoxide dimer). Since the previous Assessment, a laboratory study suggesting a much lower photolysis rate of ClOOCl than previously recommended (Pope et al., 2007) prompted a number of subsequent laboratory studies on the subject. The implications of the laboratory studies since WMO (2007) for the interpretation of the observations of chlorine monoxide (ClO) and ClOOCl and for the assessment of the uncertainty in computation of ozone loss rates are discussed below along with other updates to the photochemical data in Section 2.2.2.

WMO (2007) concluded that Antarctic ozone loss had stabilized over the time period 1995–2005, with higher ozone levels in 2002 and 2004 that were dynamically

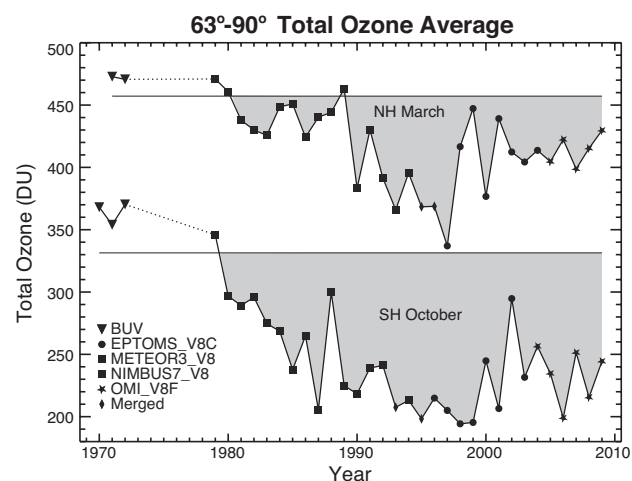


Figure 2-8. Total ozone average (Dobson units) of 63°–90° latitude in March (NH) and October (SH). Symbols indicate the satellite data that have been used in different years. The horizontal gray lines represent the average total ozone for the years prior to 1983 in March for the NH and in October in the SH. Updated from Figure 4-7, WMO (2007).

driven and not related to reductions in the stratospheric halogen load. For the Arctic it was concluded that for the coldest Arctic winters, the volume of air cold enough to support polar stratospheric clouds (PSCs) had increased significantly since the late 1960s. Arctic spring total ozone was reported to be lower than in the 1980s and was also noted to be highly variable from year to year depending on dynamical conditions. This is discussed further in Sections 2.2.4 and 2.2.5.

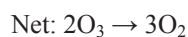
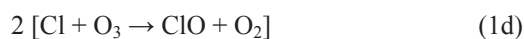
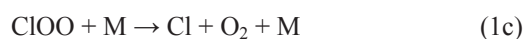
Transport and mixing both affect high-latitude winter ozone, making it challenging to diagnose the chemical loss rate from observations. WMO (2003) presented an overview of various methods that have been used to separate these effects, mainly for the Arctic winter. WMO (2007) included a comparison of the methods, focusing on the 2002/2003 winter. This colder-than-average winter was chosen because aircraft and ground field campaigns provided the data needed to assess our understanding of polar ozone loss, particularly for the large solar zenith angle-conditions of early winter. WMO (2007) noted that the various methods had been refined since WMO (2003) and produced consistent results.

WMO (2007) included evidence that nitric acid trihydrate (NAT) polar stratospheric cloud particles nucleate above the ice frost point and are widespread. Improved NAT mechanisms in chemistry-transport models (CTMs) produce more realistic denitrification, but fail to capture observed interannual variability for the northern winters. Issues concerning polar stratospheric clouds and their representation in models are discussed in Section 2.2.3. This section emphasizes new measurements from the Cloud-Aerosol Lidar and Infrared Pathfinder Satellite Observation (CALIPSO) satellite launched in 2006.

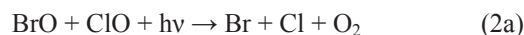
2.2.2 Polar Ozone Chemistry

Chemical loss of polar ozone during winter and spring occurs primarily by two gas-phase catalytic cycles that involve chlorine oxide radicals (Molina and Molina, 1987) and bromine and chlorine oxides (McElroy et al., 1986).

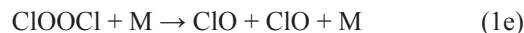
Cycle 1



Cycle 2



Loss of ClOOC by thermal decomposition



or chemical processes that recycle ClO without the formation of O₂ do not cause ozone depletion. Production of Br + OCIO by BrO + ClO also leads to a null cycle. Small contributions to polar ozone loss occur due to cycles involving the reactions ClO + O and ClO + HO₂.

Since WMO (2007), attention has focused on resolving uncertainties in the photolysis cross sections and quantum yields for the ClO dimer, ClOOC. Pope et al. (2007) reported a ClOOC absorption spectrum with cross sections at wavelengths between 300 and 350 nm much lower than recommended and than reported in prior studies (e.g., Sander et al., 2006 (referred to in this chapter as JPL 06-2) and references therein), challenging the fundamental understanding of polar ozone depletion (i.e., Schiermeier, 2007; von Hobe, 2007). Photochemical models using the cross sections reported in Pope et al. (2007), with all other kinetic parameters from JPL 06-2, underestimate the ozone loss rate (von Hobe et al., 2007) as well as observed abundances of ClO (von Hobe et al., 2007; Santee et al., 2008; Schofield et al., 2008). A workshop entitled “The Role of Halogen Chemistry in Polar Stratospheric Ozone Depletion” was convened in summer 2008 to assess the fundamental understanding of polar ozone depletion in light of the Pope et al. (2007) measurements. The following material incorporates findings from this workshop (SPARC, 2009).

The small ClOOC cross sections reported by Pope et al. (2007) have been contradicted by all subsequent laboratory studies, as detailed below. There is now consensus in the community that photolysis of ClOOC occurs much faster than implied by Pope et al. (2007). Further, no credible “missing chemical process” has been proposed that can be included in models that use the Pope et al. (2007) cross section values to adequately account for observed levels of [ClO] (or in some cases [ClO] and [ClOOC]; brackets denote concentration of the species) as well as ozone loss derived from observations. The fundamental understanding that polar ozone depletion is caused primarily by reactions involving ClO + ClO, with significant contribution from reactions involving BrO + ClO, has been strengthened since WMO (2007), based on new laboratory

studies and analyses of field observations. The renewed focus on ClOOCl photolysis has improved knowledge of the UV absorption spectrum and cross sections such that a better quantitative understanding of polar ozone depletion and the relation to halogens has been achieved in the past few years. Present uncertainties in the ClOOCl absorption cross section, as recommended in Sander et al., 2009 (referred to in this chapter as JPL 09-31), are consistent with our fundamental understanding that halogens cause depletion of polar ozone. The following discussion supports the statements given above.

2.2.2.1 LABORATORY STUDIES OF THE ClOOCl UV ABSORPTION SPECTRUM

Figure 2-9 shows the ClOOCl ultraviolet-visible (UV/vis) absorption spectrum, $\sigma_{\text{ClOOCl}}(\lambda)$, reported in the laboratory studies of Burkholder et al. (1990) and Pope et al. (2007) combined with the spectra recommended by Atkinson et al., 2007 (hereafter referenced as IUPAC, 2007) (based on Huder and DeMore, 1995) and JPL 06-2 (Sander et al., 2006) (based on Cox and Hayman, 1988; DeMore and Tschuikow-Roux, 1990; Permien et al., 1988; and Burkholder et al., 1990), which represents the state of knowledge in 2007. The laboratory measurements published after 2007 and the recent NASA JPL Panel for Data Evaluation recommendation (JPL 09-31, Sander et al., 2009) are also shown in Figure 2-9. The JPL Panel revised the recommendations for a number of kinetic parameters for processes important in modeling stratospheric ozone depletion. The recommended ClOOCl cross sections in JPL 09-31 were unchanged from JPL 06-2, since the recommendation was formulated prior to the appearance of several more recent studies, but the recommended uncertainty limits were decreased. The estimated uncertainty limits from JPL 06-2 and JPL 09-31 are included in Figure 2-9, which also illustrates the most critical wavelength region for the calculated photolysis rate constant of ClOOCl (J_{1b}) in polar regions. The uncertainty in the calculated photolysis rate constant stems primarily from the uncertainty in the absorption cross sections and increases considerably for wavelengths (λ) greater than 350 nm, where there is more limited experimental data. At the time of WMO (2007), only Burkholder et al. (1990) and DeMore and Tschuikow-Roux (1990) had reported measured cross section data for $\lambda > 360$ nm, while several other studies provided extrapolated values. The recent studies of von Hobe et al. (2009) and Papanastasiou et al. (2009) confirm substantial contributions to J_{1b} from this spectral region. The uncertainty in the calculated photolysis rate constant is much less using the JPL 09-31 recommendation than using the JPL 06-2 recommendation.

Pope et al. (2007) reported a ClOOCl absorption spectrum at 195 K that was normalized at 245 nm to the

absolute cross section value recommended in JPL 06-2. The ClOOCl spectrum was obtained using a fitting procedure of measured spectra, which contained significant contributions from molecular chlorine (Cl_2). For the photolytically active region $\lambda > 300$ nm, their inferred cross sections are significantly lower than reported in all earlier studies, prompting investigations of the impact of the cross sections reported by Pope et al. (2007) on observations of stratospheric ClO and polar ozone loss (von Hobe et al., 2007; Santee et al., 2008; Schofield et al., 2008; see also Section 2.2.2.2).

Laboratory studies of $\sigma_{\text{ClOOCl}}(\lambda)$ (Papanastasiou et al., 2009), the relative absorption spectrum (von Hobe et al., 2009), and the product of the cross section and quantum yield, $\sigma_{\text{ClOOCl}}(\lambda)\Phi(\lambda)$ (Chen et al., 2009; Lien et al., 2009; Jin et al., 2010; Wilmouth et al., 2009) have been published subsequent to Pope et al. (2007). These studies used complementary experimental techniques designed to reduce the uncertainty in the photochemistry of ClOOCl and to address the discrepancy between Pope et al. (2007) and earlier studies. The more recent laboratory studies either included a method for quantification of Cl_2 (von Hobe et al., 2009; Papanastasiou et al., 2009; Wilmouth et al., 2009) or used a mass-selected detection method independent of interference from Cl_2 and other impurities (Chen et al., 2009; Lien et al., 2009; Jin et al., 2010). Indeed, one of the salient points from the Stratospheric Processes and their Role in Climate (SPARC) initiative was the need for laboratory studies to address the sensitivity of $\sigma_{\text{ClOOCl}}(\lambda)$ to the presence of Cl_2 (e.g., Figure 2.2 of SPARC, 2009). All of these studies indicate that ClOOCl photolyzes much more rapidly than suggested by Pope et al. (2007). These studies have led to a reduction in the overall uncertainty in $\sigma_{\text{ClOOCl}}(\lambda)$ relative to the state of knowledge at the time of WMO (2007). However, only one of the new gas-phase studies (Papanastasiou et al., 2009) extended cross section measurements to $\lambda > 352$ nm and, thus, a higher level of uncertainty remains for the longer wavelengths.

von Hobe et al. (2009) measured a ClOOCl UV absorption spectrum, for λ between 220 and 400 nm, in a neon (Ne) matrix at ~ 10 K. Absolute cross sections were not measured, but cross sections were determined by scaling the measured spectrum to the peak value of the gas-phase cross section reported by JPL 06-2. When interpreting the von Hobe et al. (2009) spectrum it needs to be considered that a spectrum measured in a Ne matrix at 10 K is not directly comparable to a gas-phase spectrum at atmospheric temperatures (> 190 K). For the photolytically active region ($\lambda > 300$ nm), the matrix cross sections are significantly greater than the Pope et al. (2007) cross sections when both spectra are normalized to the same peak cross section. The cross sections reported by von Hobe et al. (2009) are somewhat less than the JPL 06-2

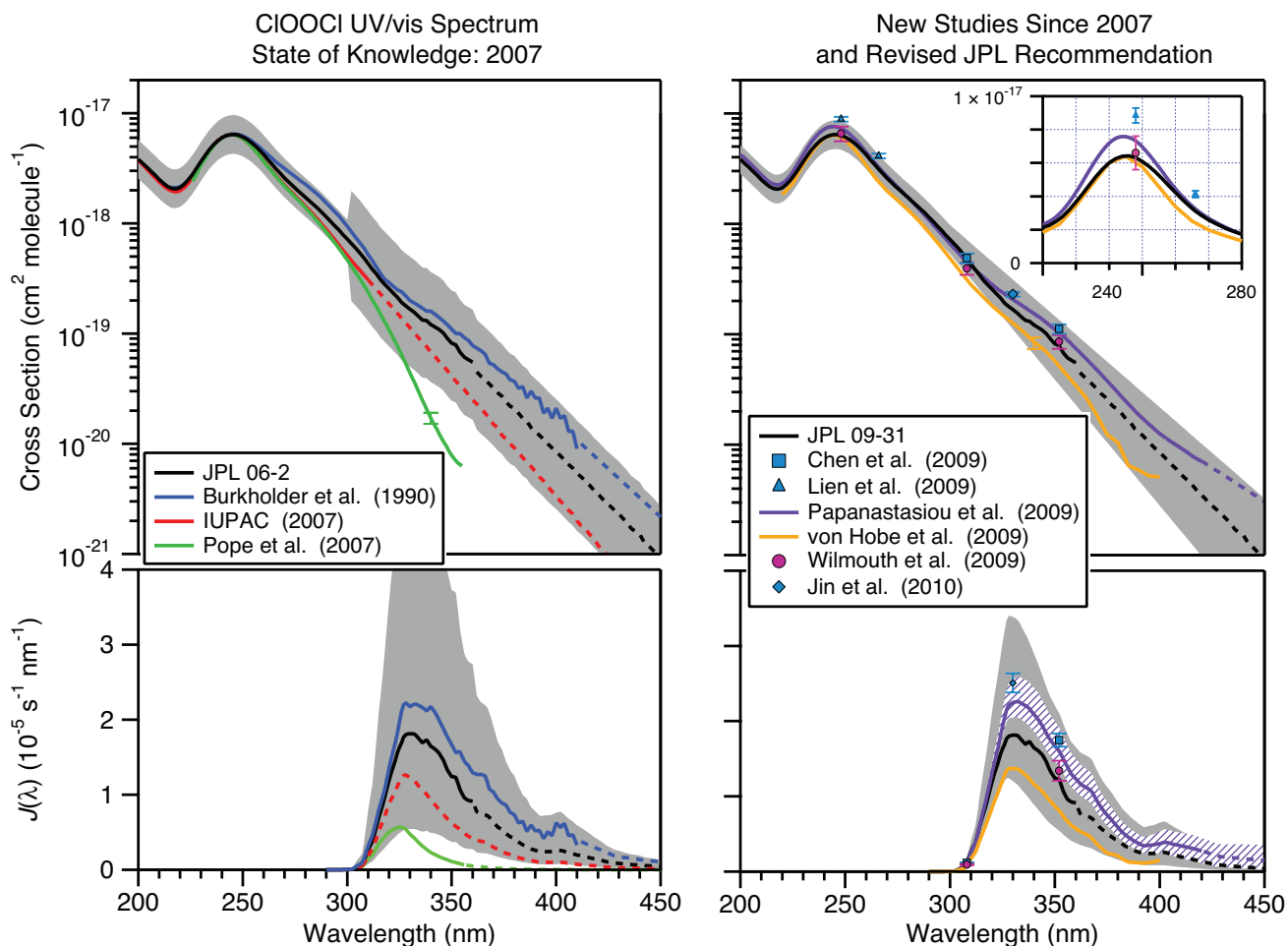


Figure 2-9. The left column summarizes the CIOOCI photochemical state of knowledge (UV/vis absorption spectra, $\sigma(\lambda)$, and representative photolysis rates, $J(\lambda)$, for the polar region) in 2007 and the right column gives the advancements since 2007 (as indicated in the legends). The cross sections for Chen et al. (2009), Lien et al. (2009), and Jin et al. (2010) at 200 K and Wilmouth et al. (2009) at 240 K were calculated from their reported values of $\sigma(\lambda)\Phi(\lambda)$ assuming $\Phi(\lambda) = 1$. The Pope et al. (2007) and Papanastasiou et al. (2009) spectra were recorded at ~ 200 K. Included for comparison is the von Hobe et al. (2009) spectrum recorded in a Ne matrix at ~ 10 K. The dashed lines represent wavelength regions where extrapolated cross section data rather than measured values were reported. The error bars shown were taken from the individual studies. The gray shaded regions in the upper panels are the error limits in $\sigma(\lambda)$ reported in JPL 06-2 and JPL 09-31. $J(\lambda)$ values were obtained for a solar zenith angle of 86 degrees at 20 km and the gray shaded regions are derived from the estimated uncertainties in $\sigma(\lambda)$ from JPL 06-2 and JPL 09-31. The hashed region was derived from the reported 2σ uncertainty in the Papanastasiou et al. (2009) absorption cross section data. Inset in the top right panel shows the absorption spectrum of CIOOCI in the wavelength region 220–280 nm. The choice of a linear y-axis allows a better visual assessment of the uncertainties in the peak absorption.

recommendation in the range 300–350 nm (Figure 2-9). However, significantly greater cross sections would result by scaling the von Hobe et al. (2009) absorption spectrum to a larger value of the peak cross section, as suggested by new observations (see below).

Chen et al. (2009) (308 and 351 nm), Lien et al. (2009) (248 and 266 nm), Jin et al. (2010) (330 nm), and Wilmouth et al. (2009) (248, 308, and 352 nm) have re-

ported values of $\sigma_{\text{CIOOCI}}(\lambda)\Phi(\lambda)$ at the wavelengths given in parentheses (Figure 2-9). The first three of these studies measured the loss of CIOOCI following photolysis in an effusive molecular beam. Assuming $\Phi(\lambda) = 1$, the derived cross sections are greater than those given in JPL 09-31 and agree most closely with those of Burkholder et al. (1990) and Papanastasiou et al. (2009). These three studies also report a weak temperature dependence to the

cross sections at 308, 330, and 352 nm. Wilmouth et al. (2009) used a discharge flow apparatus combined with Cl atom resonance fluorescence detection of photolysis products. Their reported values of $\sigma_{\text{ClOOCl}}(352 \text{ nm})$ at 240 K, assuming $\Phi(352 \text{ nm}) = 1$, are in good agreement with JPL 09-31. These values are a factor of 12 greater than Pope et al. (2007), a factor of 2.3 greater than the IUPAC (2007) recommendation, and $\sim 30\%$ lower than the value reported by Chen et al. (2009). The cross section measurements at several wavelengths from the effusive beam studies (e.g., Figure 5 of Lien et al., 2009) are in agreement with the spectrum reported by von Hobe et al. (2009).

Papanastasiou et al. (2009) reported $\sigma_{\text{ClOOCl}}(\lambda)$ from 200 to 420 nm at $\sim 200 \text{ K}$. The ClOOCl cross sections obtained at $\lambda > 300 \text{ nm}$ are in agreement with values reported by Burkholder et al. (1990). Their measurements agree with the results of Lin and co-workers and Wilmouth et al. (2009), assuming $\Phi(\lambda) = 1$, within the combined estimated measurement uncertainties (Figure 2-9). Their $\sigma_{\text{ClOOCl}}(\lambda > 300 \text{ nm})$ values are significantly greater than those of Pope et al. (2007) and are also somewhat greater than the values recommended in JPL 09-31.

The studies of Papanastasiou et al. (2009) and Lien et al. (2009) report ClOOCl absorption cross sections near the peak of the spectrum of $7.6^{+0.8}_{-0.5} \times 10^{-18} \text{ cm}^2 \text{ molecule}^{-1}$ at 244.25 nm and $(8.85 \pm 0.42) \times 10^{-18} \text{ cm}^2 \text{ molecule}^{-1}$ at 248.4 nm, respectively. These are greater than the JPL 09-31 recommended cross section of $6.4 \times 10^{-18} \text{ cm}^2 \text{ molecule}^{-1}$ at 244 nm. Wilmouth et al. (2009) report a value of $(6.6 \pm 1.0) \times 10^{-18} \text{ cm}^2 \text{ molecule}^{-1}$ at 248 nm, in close agreement with JPL 09-31. The spread in recent measurements of the peak absorption cross section is greater than the estimated uncertainty given by JPL 06-2 and many prior evaluations. Furthermore, the uncertainty limit of the Lien et al. (2009) peak cross section does not overlap with the uncertainty limits reported by Wilmouth et al. (2009) and Papanastasiou et al. (2009) (Figure 2-9). Scaling the absorption spectrum for ClOOCl to the peak cross section reported by Lien et al. (2009) would result in larger values for the ClOOCl cross section, leading to greater photolysis rates for ClOOCl as reported by various prior studies. However, even if the Pope et al. (2007) spectrum was scaled to the maximum cross section compatible with current measurements and the reported error bars, the resulting cross sections for $\lambda > 300 \text{ nm}$ would still be significantly less than reported in all other studies.

Papanastasiou et al. (2009) also reported estimated 2σ uncertainties in the photolysis rate constant of ClOOCl, J_{1b} , based on their cross section data (Figure 2-9). The uncertainty is a function of solar zenith angle (SZA) (i.e., the wavelength dependence of the ClOOCl spectrum) and was estimated to be $+40\%/-15\%$, $+50\%/-20\%$, and $+80\%/-25\%$ at SZAs of 80° , 86° , and 90° , respectively.

Better quantification of σ_{ClOOCl} for $\lambda > 350 \text{ nm}$ would reduce this level of uncertainty.

There is a consensus in the community that photolysis of ClOOCl occurs much faster than implied by the measured spectrum and the determined cross sections reported by Pope et al. (2007). The weight of new laboratory evidence suggests that values of the ClOOCl absorption cross section (σ_{ClOOCl}) in the atmospherically important region of wavelengths greater than 300 nm reported by Pope et al. (2007) are erroneous due to overcorrection of their measured spectra for the contribution of a Cl_2 impurity. The study by von Hobe et al. (2009) showed that ClOOCl exhibits an absorption feature similar to the spectral shape of the Cl_2 . Papanastasiou et al. (2009) demonstrated that the spectral interference by Cl_2 in the Pope et al. (2007) experiment led to an underestimate of σ_{ClOOCl} at $\lambda > 300 \text{ nm}$. The JPL 09-31 recommended value of Φ ($\lambda > 308 \text{ nm}$) is 0.9, although only limited experimental studies are available (Moore et al., 1999; Plenge et al., 2004). The understanding that polar ozone depletion is caused by reactions involving halogens has been reaffirmed by the numerous laboratory studies conducted since the publication of the paper by Pope et al. (2007).

2.2.2.2 FIELD OBSERVATIONS OF CHLORINE PARTITIONING

A large number of field studies over the past several decades have focused on the quantitative understanding of the partitioning of ClO and ClOOCl. The chemistry linking ClO and ClOOCl is thought to be especially simple. During daytime when temperatures are low enough that loss of ClOOCl occurs mainly by photolysis, the ratio $[\text{ClO}]^2/[\text{ClOOCl}]$ essentially equals J_{1b}/k_{1a} (e.g., Stimpfle et al., 2004) (brackets denote concentration of the species). During night after hours of darkness, when loss of ClOOCl occurs exclusively by thermal decomposition, this ratio equals k_{1c}/k_{1a} , which is the equilibrium constant (K_{EQ}) between ClO and ClOOCl. Since the rate of ozone loss by Cycle 1 is controlled by the parameters J_{1b} and k_{1a} , comparisons of measured and modeled daytime values of $[\text{ClO}]$ and $[\text{ClOOCl}]$ provide a quantitative measure of the speed of this cycle in the atmosphere. Thermal decomposition of ClOOCl completes a null cycle. Precise knowledge of K_{EQ} and an accurate measurement of nighttime $[\text{ClO}]$ enable $[\text{ClO}_x]$ ($[\text{ClO}_x] = [\text{ClO}] + 2 \times [\text{ClOOCl}]$) to be estimated in a manner that is independent of σ_{ClOOCl} .

Stimpfle et al. (2004) introduced a quantitative basis for comparison of modeled $[\text{ClO}]^2/[\text{ClOOCl}]$ to the measured value of this quantity at various SZAs during daytime, termed β , to quantify how well models represent the true value of J_{1b}/k_{1a} . The notion that β represents the value of J_{1b}/k_{1a} assumes that the partitioning of ClO and ClOOCl is dominated by the self-reaction of ClO and the

photolysis of ClOOCl (i.e., the temperature is low enough that thermal dissociation of ClOOCl is much slower than photolysis of ClOOCl). The Stimpfle et al. (2004) data were obtained at sufficiently low temperature that this assumption is valid given known chemistry. This data set is also notable for having achieved quantitative closure of the chlorine budget (Wilmouth et al., 2006).

Figure 2-10 (left) shows β , as a function of SZA, for the laboratory studies and recommendations of $\sigma_{\text{ClOOCl}}(\lambda)$

that existed in 2007 and provided enough spectral information for calculation of J_{1b} . The black dotted lines indicate the 1σ uncertainty in β based on measured [ClO] and [ClOOCl], whereas the error bars indicate the uncertainty in the modeled value of β (see caption). The β ratio indicates that the partitioning of ClO and ClOOCl is not consistent with J_{1b}/k_{1a} based on the Pope et al. (2007) measurement of $\sigma_{\text{ClOOCl}}(\lambda)$. The slight change in k_{1a} in JPL 09-31 does not affect this or any other conclusion of this

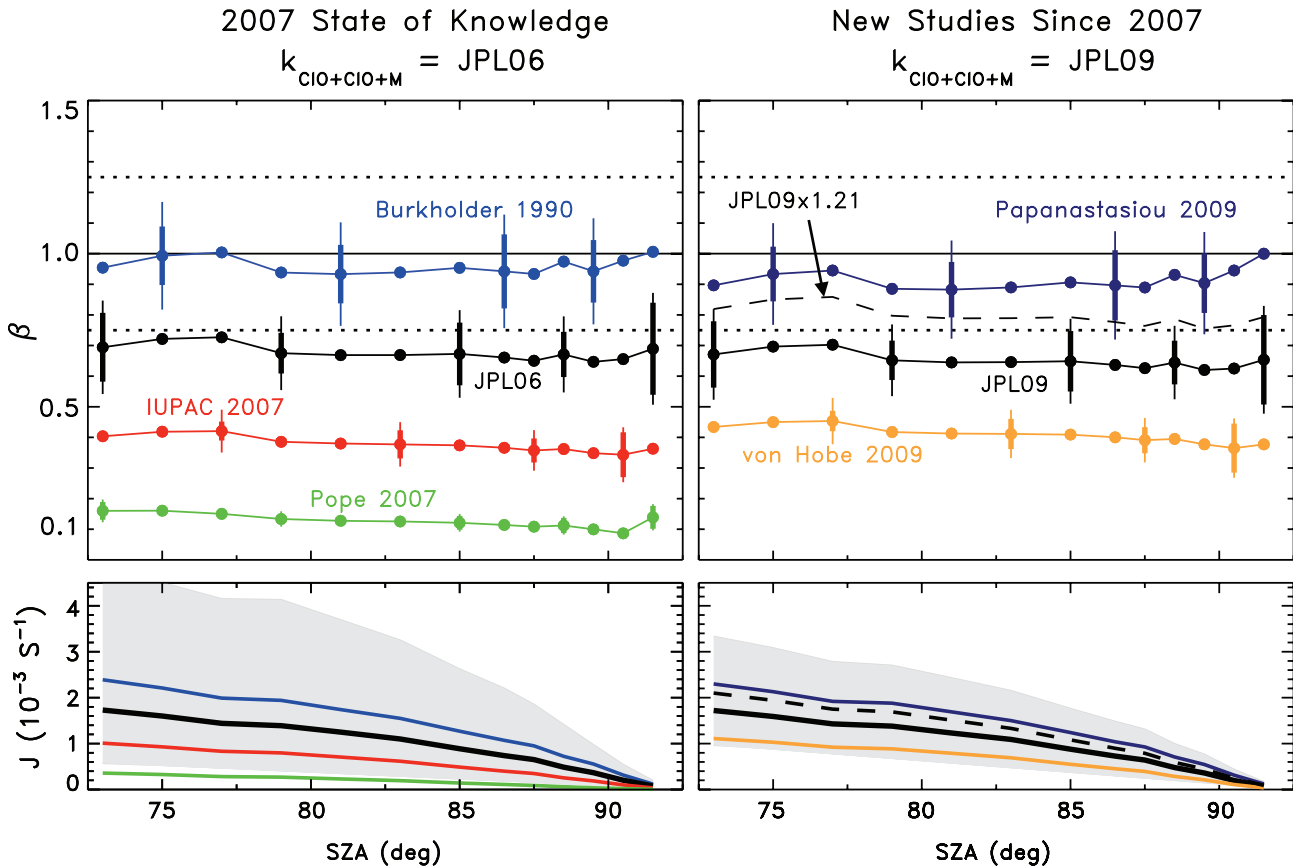


Figure 2-10. Analysis of β versus SZA, for all daytime measurements obtained during the SAGE III Ozone Loss and Validation Experiment (SOLVE), where $\beta = \{([\text{ClO}]^2 / [\text{ClOOCl}])_{\text{MODEL}}\} / \{([\text{ClO}]^2 / [\text{ClOOCl}])_{\text{OBSERVATION}}\}$. The left panel shows results for J_{1b} using values of $\sigma_{\text{ClOOCl}}(\lambda)$ available as of 2007 (same colors and studies as used in Figure 2-9). The right-hand side shows results for J_{1b} using values of $\sigma_{\text{ClOOCl}}(\lambda)$ available after 2007. The black dotted lines depict the $\pm 25\%$ uncertainty (1σ) in β attributable to uncertainties in observations of [ClO] and [ClOOCl]. The thick colored error bars denote the standard deviation about the mean for all of the individual determinations of β within a particular SZA bin. The thin error bar represents total uncertainty in the modeled component of β , found by combining the JPL 06-2 (left panel) or JPL 09-31 (right panel) uncertainty in k_{1a} in a root-sum-square fashion with the standard deviations. If the thin error bar falls within the range of the dotted lines, this is agreement of model and measurements to within combined 1σ uncertainties. The black dashed line on the right hand side depicts results of an illustrative calculation, the scaling of the JPL 09-31 value of $\sigma_{\text{ClOOCl}}(\lambda)$, which minimizes the distance between the scaled cross section and determinations of the peak cross section near 244 nm reported by Lien et al. (2009), Papanastasiou et al. (2009), and Wilmouth et al. (2009). The bottom panel compares J_{1b} as a function of SZA, for the altitude and surface albedo of the observations, for the various values of $\sigma_{\text{ClOOCl}}(\lambda)$ shown in the upper panels. After Stimpfle et al. (2004) and Figure 4-15 of WMO (2007).

section. As noted by Stimpfle et al. (2004), the cross section recommended by IUPAC (2007), based solely on the laboratory study of Huder and DeMore (1995), also yields a value of β inconsistent with field observations. The JPL 06-2 cross section is consistent with the field observations (overlap of error bars) and the Burkholder et al. (1990) value is most consistent (β near unity).

Figure 2-10 (right) shows a similar comparison for the laboratory measurements of $\sigma_{\text{ClOOCl}}(\lambda)$ published since 2007. Here, the JPL 09-31 value of k_{1a} is used. As noted above, von Hobe et al. (2009) normalized their spectrum to the JPL 06-2 peak cross section. Use of this cross section leads to values of β that are outside of the 1σ uncertainty on the measured value of $[\text{ClO}]^2/[\text{ClOOCl}]$. Clearly, if the von Hobe et al. (2009) spectrum were normalized to a higher peak, as perhaps is warranted by more recent measurements of the peak cross section, then β would lie closer to unity (β scales in an approximately linear fashion with the peak cross section). The JPL 09-31 spectrum and cross sections (unchanged since JPL 06-2, except for the uncertainty limits) is consistent with the field observations (overlap of error bars). The Papanastasiou et al. (2009) spectrum and cross sections results in the best agreement (value of β close to unity).

Many of the ClOOCl laboratory studies to date report the wavelength dependence of the ClOOCl spectrum normalized to an absolute value of the cross section near the peak. Typically, the JPL 09-31 peak value of $6.4 \times 10^{-18} \text{ cm}^2$ at 244 nm has been used (e.g., Huder and DeMore, 1995; Pope et al., 2007; von Hobe et al., 2009). The analysis presented in Figure 2-10 is complicated by the fact that three laboratory studies published in 2009 report peak absolute cross sections greater than the JPL 09-31 value (see Figure 2-9). To illustrate the importance of this scaling, the black dashed line in Figure 2-10 (right) shows the result of a calculation where the JPL 09-31 cross section has been multiplied by a factor of 1.21, which scales the peak cross section of JPL 09-31 to the mean of the cross section values near 244 nm reported by Lien et al. (2009), Papanastasiou et al. (2009), and Wilmouth et al. (2009). The JPL 09-31 cross section, scaled in this manner, provides a better representation of field data than found using the recommended cross section. We highlight this sensitivity to illustrate the importance of this laboratory parameter for quantitative understanding of halogen photochemistry in the polar vortex. The Pope et al. (2007) absorption spectrum for ClOOCl is entirely inconsistent with field data, for any reasonable amount of scaling.

The bottom panels of Figure 2-10 show the photolysis first-order rate constant (J_{1b}) as a function of SZA, for various cross section data sets. The shaded region shows propagation of the JPL 06-2 uncertainty (left) and the JPL 09-31 uncertainty (right). This figure reveals consistency

between laboratory studies of $\sigma_{\text{ClOOCl}}(\lambda)$ published after 2007 and the uncertainty given by JPL 09-31, which was not based on these studies. Absorption cross sections derived from the measurements of Lin and co-workers and Wilmouth et al. (2009) at specific wavelengths in the photolytically active region are, as shown in Figure 2-9, generally consistent with the values reported by Papanastasiou et al. (2009). Therefore, all new laboratory studies of $\sigma_{\text{ClOOCl}}(\lambda)$ conducted since 2007 lead to a consistent picture of good understanding of polar ozone chemistry, in contrast to the state of knowledge that existed upon the 2007 publication of the Pope et al. results.

Figure 2-11 extends Figure 2-10 by summarizing the high level findings for J_{1b}/k_{1a} from Stimpfle et al. (2004) as well as seven other studies, relative to the value of J_{1b}/k_{1a} recommended by JPL 06-2. Similar to the conclusions noted above, the seven other studies also suggest the value of J_{1b}/k_{1a} is as large as, or larger than, the value found using $\sigma_{\text{ClOOCl}}(\lambda)$ from JPL 06-2 and JPL 09-31. The field observations are most consistent with values of J_{1b}/k_{1a} found using the cross sections from Burkholder et al. (1990) and Papanastasiou et al. (2009) (the central portion of most of the blue bars lies closest to the arrow denoting J_{1b}/k_{1a} from these two laboratory studies). Both of these laboratory studies measured absolute values of the ClOOCl cross section.

Figure 2-11 shows that field data are not consistent with J_{1b}/k_{1a} found using the recommendation for $\sigma_{\text{ClOOCl}}(\lambda)$ from IUPAC (2007) (based on Huder and DeMore, 1995) or von Hobe et al. (2009) (both spectra scaled to JPL 06-2). As described above, three 2009 studies report values of the peak absolute cross section greater than given in JPL 06-2. The value of J_{1b}/k_{1a} found using the spectra reported by von Hobe et al. (2009) and Huder and DeMore (1995) will exhibit closer agreement with the field data if these spectra are scaled to peak cross section values reported in the new laboratory measurements, as was illustrated by scaling the JPL 09-31 recommended spectrum in Figure 2-10. At present the peak cross section and thus scaling factor has an uncertainty in the 20 to 30% range. Most of the literature is based on the JPL 06-2 estimate (identical to the JPL 09-31 value), which is at the low end of this range. If the peak cross section is revised by future evaluations, these revisions will likely indicate a greater role for ClO in polar ozone loss, since $d\text{O}_3/dt$ is roughly proportional to J_{1b} .

Finally, Figure 2-11 shows that the field data are not consistent with J_{1b}/k_{1a} found using $\sigma_{\text{ClOOCl}}(\lambda)$ from Pope et al. (2007). The range of uncertainty in k_{1a} (red bar) does not come close to encompassing the value of J_{1b}/k_{1a} found using $\sigma_{\text{ClOOCl}}(\lambda)$ from Pope et al. (2007) and the slight revision in k_{1a} in JPL 09-31 is inconsequential. No reasonable scaling of the Pope et al. (2007) spectrum will resolve the inconsistency with field data. An analysis of satellite observations reported by Santee et al. (2008) supports the

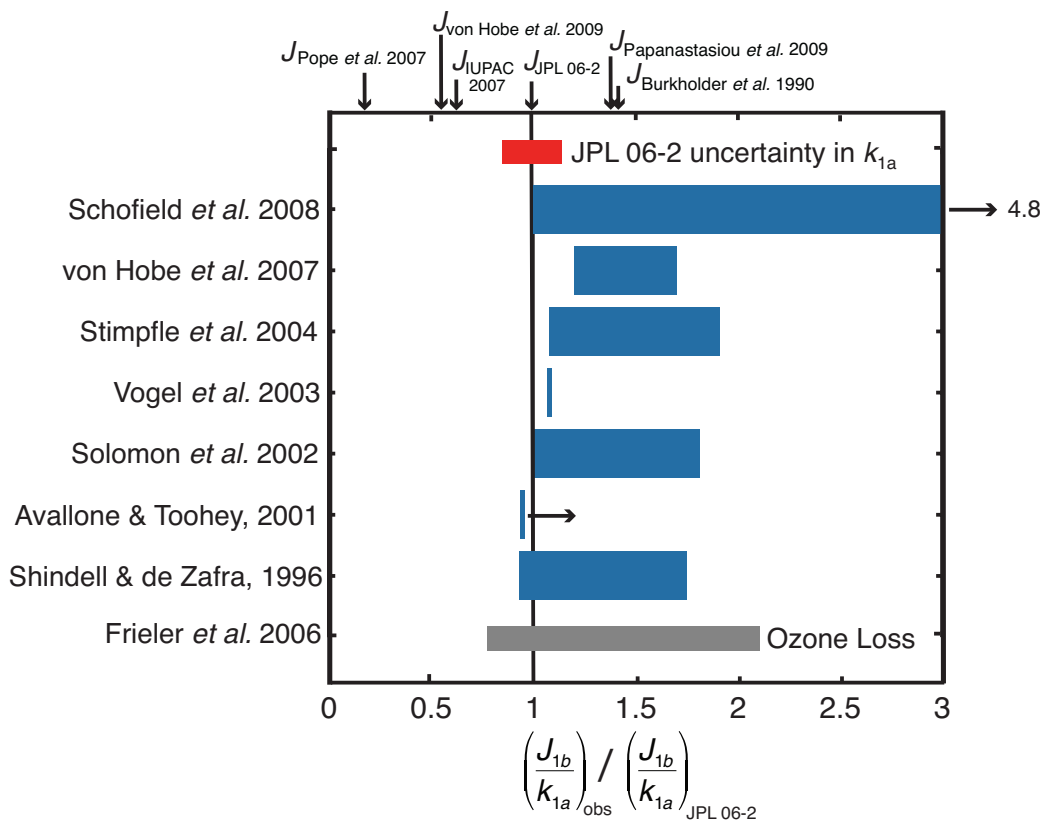


Figure 2-11. The ratio J_{1b}/k_{1a} inferred from analysis of daytime measurements of [ClO] or [ClO] and [ClOOCl] divided by the value of J_{1b}/k_{1a} from JPL 06-2, from various studies (blue bars; length of each bar represents range of uncertainty, generally 1σ). Horizontal black arrows denote lower limits for the ratio determined by two of the studies. The red bar shows the 1σ uncertainty in k_{1a} from JPL 06-2, evaluated at 190 K. The gray bar shows the value of J_{1b}/k_{1a} needed to match observed ozone loss in the Arctic and Antarctic vortices. The value of J_{1b}/k_{1a} using absorption cross sections of ClOOCl from various laboratory studies and data evaluations, relative to the JPL 06-2 value, is indicated by downward pointing arrows. The JPL 06-2 value of k_{1a} was used throughout the analysis because most of the cited papers relied on k_{1a} from JPL 06-2. The slight change in the high-pressure limit of this rate constant recommended by JPL 09-31 has a barely discernable effect on the appearance of this plot. Schofield et al. (2008) analyzed airborne in situ observations of [ClO] during the “self Match flight” of the European Polar Stratospheric Cloud and Lee Wave Experiment (EUPLEX) in the Arctic; von Hobe et al. (2007) examined airborne in situ observations of [ClO] and [ClOOCl] in the Arctic obtained during the SOLVE, EUPLEX, and Envisat Validation campaigns; Stimpfle et al. (2004) analyzed airborne in situ observations of [ClO] and [ClOOCl] in the Arctic obtained during the SOLVE campaign; Vogel et al. (2003) examined balloonborne in situ observations of [ClO] obtained in the Arctic during the Third European Stratospheric Experiment on Ozone (THESEO) 2000; Solomon et al. (2002) and Shindell and de Zafra (1996) analyzed ground-based observations of [ClO] over Antarctica; and Avallone and Toohey (2001) examined airborne in situ observations of [ClO] obtained in the Arctic during Airborne Arctic Stratospheric Expedition (AASE) I and II. Figure first published as Figure 3.1 of SPARC (2009).

conclusion that the Pope et al. (2007) spectrum cannot be reconciled with atmospheric measurements of [ClO].

Section 4.2.1.3 of WMO (2007) examined our understanding of calculated and observed polar ozone loss rates. A major advance is recognition that calculated polar ozone loss rates using values for $\sigma_{\text{ClOOC1}}(\lambda)$ from Pope et al. (2007) are not consistent with ozone loss rates derived from observations (von Hobe et al., 2007; Santee et al., 2008; Schofield et al., 2008; Kawa et al., 2009; SPARC, 2009). A detailed summary is given in SPARC (2009). The gray bar in Figure 2-11 summarizes the understanding articulated in these studies: ozone loss rates derived from observations are consistent with values of J_{1b}/k_{1a} ranging from slightly less than that obtained using the JPL 06-2 recommended cross sections to about a factor of 2 larger than that found using JPL 06-2, with best agreement found for the Burkholder et al. (1990) and Papanastasiou et al. (2009) spectrum and cross sections.

2.2.2.3 OTHER ISSUES RELATED TO POLAR OZONE CHEMISTRY

Kawa et al. (2009) used Monte Carlo model calculations to evaluate the impact and significance of the estimated uncertainties in the kinetic parameters given in JPL 06-2 on polar stratospheric ozone loss. The simulations indicate that the most of the uncertainty in the calculated ozone loss and the rate of ozone loss is due to the uncertainty in the ClOOC1 photolysis reaction. Uncertainties in the BrO + ClO reaction rate coefficient and its product branching ratio were also found to be important. Canty et al. (2005) note an inconsistency between theory and observation of nighttime chlorine dioxide (OCIO) that could be resolved by higher yields of the branches of BrO + ClO that lead to ozone loss. Uncertainties in the rate coefficients for the reactions $\text{ClO} + \text{OH} \rightarrow \text{HCl} + \text{O}_2$ and $\text{Br} + \text{H}_2\text{CO} \rightarrow \text{HBr} + \text{HCO}$ were found to be significant, but to have a smaller overall impact on the calculated polar ozone loss. The uncertainties in these processes were re-evaluated by the NASA JPL Data Panel and reductions in the uncertainties were made in JPL 09-31.

Theoretical calculations by Matus et al. (2008) found the ClClO₂ isomer was more stable than ClOOC1 by 3.1 kcal mol⁻¹ at 298 K. However, as described in SPARC (2009), observational evidence suggests ClClO₂ is not present in appreciable quantities during times of chlorine activation in the Arctic vortex. SPARC (2009) concluded that if unknown chemistry plays a role for the polar ozone loss mechanism, it can only be a minor modification of known mechanisms.

Analyses of field observations by von Hobe et al. (2007), Wetzal et al. (2010), and Santee et al. (2010) are somewhat more consistent with the revised JPL 09-31 recommendation for K_{EQ} at temperatures below ~210 K

than with the JPL 06-2 recommendation. Observations obtained during nighttime conditions when photolysis is negligible all point to higher abundances of ClO and lower abundances of ClOOC1 than found in models using JPL 06-2 kinetics. However, uncertainty in K_{EQ} , which is believed to drive nighttime chemistry, has no bearing on the rate of polar ozone depletion (e.g., Kawa et al. (2009) and references therein). Nevertheless, there is interest in reducing the uncertainty in K_{EQ} because accurate knowledge of this quantity will improve estimates of [ClO_x] from nighttime observations of [ClO]. Such improvement is needed, for example, because representation of polar ozone chemistry in chemistry and transport models (CTMs) and chemistry-climate models (CCMs) is better evaluated by comparing modeled and measured [ClO_x] rather than comparing modeled and measured [ClO]. If [ClO] is used, one must factor in SZA and temperature, which greatly complicates the comparison (Chapter 6 of SPARC CCMVal, 2010).

2.2.3 Polar Stratospheric Cloud Processes

As discussed in previous WMO reports, heterogeneous reactions on the surfaces of stratospheric particles at cold temperatures convert chlorine reservoir species that do not react with ozone, such as hydrogen chloride (HCl) and chlorine nitrate (ClONO₂), to chlorine radical species that lead to catalytic ozone destruction (Solomon et al., 1986). Liquid-phase binary sulfuric acid/water (H₂SO₄/H₂O) droplets, commonly known as background stratospheric aerosols, are ubiquitous throughout the stratosphere. Under cold conditions, these background aerosols take up nitric acid (HNO₃) and H₂O (Carslaw et al., 1994; Tabazadeh et al., 1994) and evolve into ternary HNO₃/H₂SO₄/H₂O droplets, commonly referred to as supercooled ternary solution (STS) polar stratospheric clouds (PSCs). PSC particles may also take the form of H₂O ice and solid hydrates of nitric acid, likely nitric acid trihydrate, or NAT (Voigt et al., 2000). Particle ensembles in the polar winter stratosphere are primarily mixtures of liquid (binary or ternary) droplets and solid particles (NAT and H₂O ice) in varying sizes and number densities (e.g., Toon et al., 2000; Biele et al., 2001; Drdla et al., 2003). Chlorine activation rates on stratospheric particles are dependent on the uptake coefficient of the particle and the particulate surface area density (SAD) (Lowe and MacKenzie, 2008). Both the uptake coefficients and the available surface area of the liquid particles are generally much higher than that of NAT PSC particles, making liquid particles much more efficient in chlorine activation (Portmann et al., 1996; Lowe and MacKenzie, 2008). Liquid particles also increase ozone loss by extending both the height range (Hofmann and Oltmans, 1993) and the season over which heterogeneous chemistry can occur (Portmann et

al., 1996). Solid particles play an important indirect role in ozone depletion by their influence on the abundance of gas-phase nitrogen. Formation and sedimentation of large NAT particles (Waibel et al., 1999; Fahey et al., 2001) can irreversibly redistribute HNO_3 (denitrify) in the polar stratosphere, allowing the ozone depletion process to continue for a longer period by delaying the reformation of the chlorine reservoir ClONO_2 .

2.2.3.1 NEW OBSERVATIONAL DATA SETS

Since the previous Assessment, the PSC observational database has been greatly expanded by measurements from the Cloud-Aerosol Lidar and Infrared Pathfinder Satellite Observation (CALIPSO) satellite that was launched in 2006. Measurements from the polarization-sensitive lidar on CALIPSO (Pitts et al., 2007; Noel et al., 2008) provide comprehensive daily information on the occurrence of PSCs in both the Arctic and Antarctic over the

entire polar region, including the polar night that cannot be sampled by solar occultation instruments. The general climatology of PSCs included in previous Ozone Assessments (e.g., WMO, 1995; WMO, 1999) was established from long-term solar occultation data records (e.g., Poole and Pitts, 1994; Fromm et al., 2003), which were the only available data source at that time. Pitts et al. (2007) compared the PSC frequency observed by CALIPSO in 2006 over the entire Antarctic region (50°S – 82°S) with the PSC frequency derived by subsampling the CALIPSO database only at the time-varying latitudes observed by the SAM II (Stratospheric Aerosol Measurement II) solar occultation sensor, which ranged from 65°S in June to 80°S in September. As shown in Figure 2-12, the temporal distribution of PSCs derived from solar occultation data is not representative of the polar region as a whole. For example, in early June the solar occultation sensor samples only near the edge of the vortex ($\sim 65^\circ\text{S}$) and underestimates the PSC frequency of the vortex as a whole. In September the

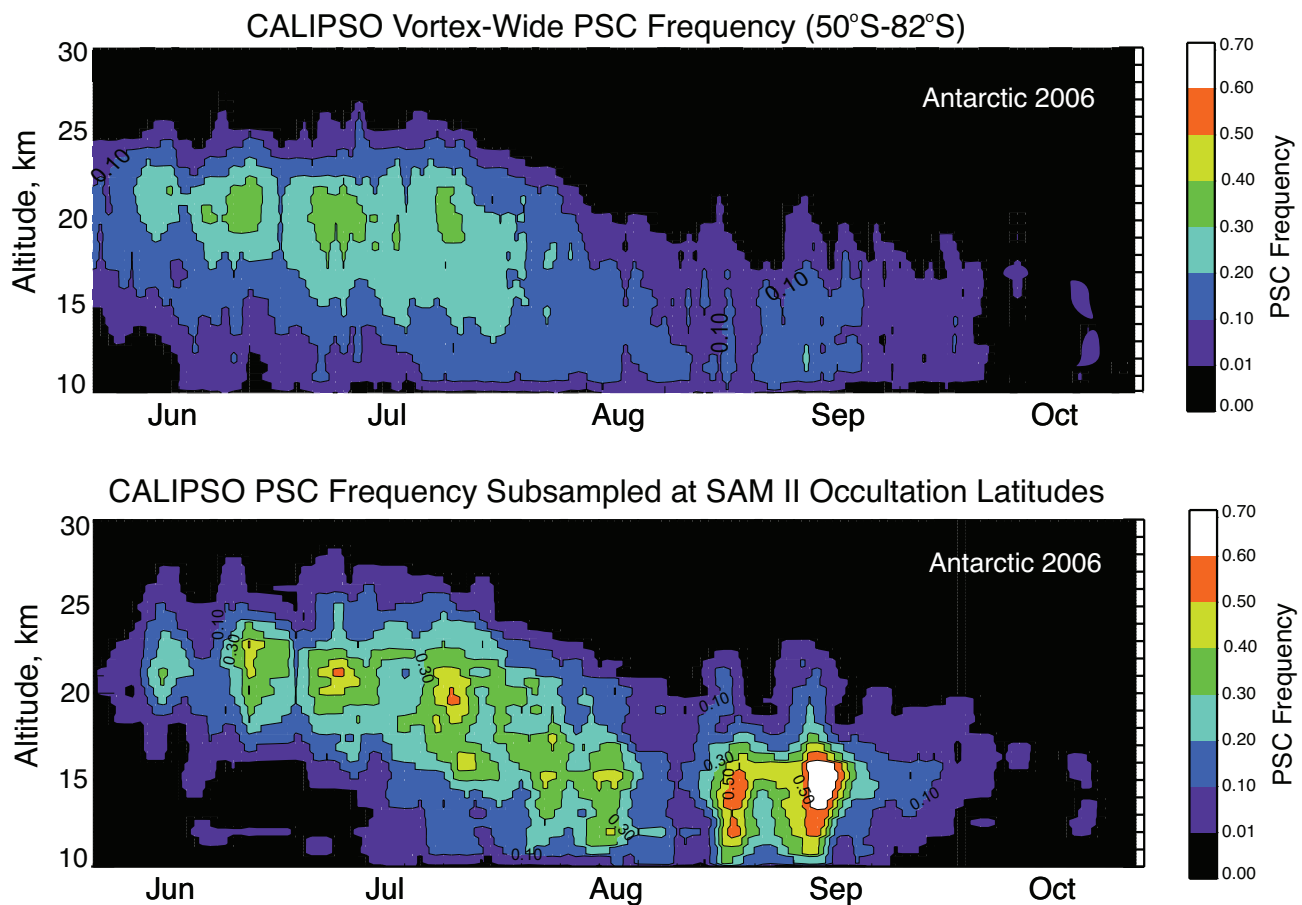


Figure 2-12. PSC frequency for the 2006 Antarctic season (adapted from Pitts et al., 2007). Top panel: PSC frequency as observed by CALIPSO over the entire polar region (50°S – 82°S). Bottom panel: PSC frequency that is deduced by subsampling the CALIPSO data set at measurement latitudes seen by a solar occultation instrument (e.g., SAM II).

occultation sensor samples only near the core of the vortex (80°S) and hence overestimates the PSC frequency of the vortex as a whole. CALIPSO provides a more accurate representation of PSC occurrence on a day-by-day basis over the entire polar region than the historical solar occultation-based observations. But on a season-long basis, both CALIPSO and the historical solar occultation data show that PSCs occur much more frequently and over a longer time period in the Antarctic than in the Arctic.

Optical modeling results (Pitts et al., 2009) suggest that from an ensemble point of view, CALIPSO PSC detection limits are as good as or better than those of historic solar occultation sensors. The ensemble detection limits are also comparable to those of ground-based and airborne lidars, except that CALIPSO cannot resolve very tenuous PSCs with the optical characteristics of a mixture of binary liquid aerosols and very low number densities ($<3-5 \times 10^{-4} \text{ cm}^{-3}$) of NAT particles. For reference, NAT particle surface areas in these PSCs are $<0.1 \mu\text{m}^2 \text{ cm}^{-3}$, which is about 10% of the surface area of the liquid binary aerosols and $<1\%$ of the surface area of a fully developed STS PSC.

2.2.3.2 PSC COMPOSITION

A more complete picture of PSC occurrence and composition has emerged since the previous Assessment. Pitts et al. (2009) examined the seasonal evolution of PSC composition utilizing CALIPSO lidar observations and found that the vast majority of PSC observations over the Antarctic from mid-June until mid-September consisted of liquid/NAT mixtures, while liquid STS clouds were predominant in the Antarctic in late May through early June and again in late September and October. Ice PSCs were much more episodic in nature and accounted for only about 10% of all CALIPSO PSC observations in the Antarctic. Pitts et al. (2009) found that mixtures containing NAT particles in higher number densities/volumes (similar to the so-called type 1a enhanced PSCs) are much more common in the Antarctic than in the Arctic, while the relative frequency of liquid STS clouds is higher in the Arctic than in the Antarctic. These results are generally consistent with the climatologies from ground-based lidars (Adriani et al., 2004; Maturilli et al., 2005; Blum et al., 2005; Massoli et al., 2006).

The spaceborne Michelson Interferometer for Passive Atmospheric Sounding (MIPAS) on Envisat, a limb-sounding infrared spectrometer with full coverage of the Arctic and Antarctic regions, also provides information on PSC composition. Höpfner et al. (2006a) analyzed MIPAS measurements of mid-IR emissions by PSCs during the 2003 Antarctic winter and found evidence of NAT, STS, and water ice clouds. Information on PSC composition is derived from CALIPSO and MIPAS data using

fundamentally different approaches, yet the results are consistent (Höpfner et al., 2009).

2.2.3.3 PSC FORCING MECHANISMS

Several studies have examined formation mechanisms for PSCs. In the NH, Felton et al. (2007) showed that wave-induced temperature perturbations account for about 11% of PSC detections in the Arctic during the SOLVE-THESEO campaign. In the Antarctic, recent studies provide evidence that mountain wave PSCs may be a significant source of NAT particles that can be transported throughout the Antarctic polar vortex. Höpfner et al. (2006b) attribute the large-scale outbreak of NAT particles observed by MIPAS during June 2003 to heterogeneous nucleation on ice in the cooling-phases of large-amplitude mountain waves over the Antarctic Peninsula and Ellsworth Mountains. Eckermann et al. (2009) corroborate this hypothesis, showing that a small region of mountain wave activity over the Antarctic Peninsula on 10–14 June likely served as the source of this circumpolar NAT outbreak. Eckermann et al. (2009) conclude that this is observational evidence of the “mother cloud” theory, which posits that vortex-wide NAT formation and growth are driven by ice formed in mountain wave activity. Noel et al. (2009) used CALIPSO data to examine wave-induced PSCs with near-unity optical depths, concluding that this relatively rare class of PSC can lead to widespread NAT and ice particles downstream from the mountain wave. Based on a combination of Polar Ozone and Aerosol Measurement (POAM) III aerosol extinction measurements and Challenging Minisatellite Payload GPS Radio Occultation (CHAMP GPS/RO) temperature measurements, McDonald et al. (2009) found that gravity wave-induced temperature perturbations may explain enhanced PSC incidence over the Antarctic Peninsula in June, while they contribute to only about 15% of the PSC observations later in the winter at higher latitudes. Innis and Klekociuk (2006), using lidar observations over Davis, Antarctica, also found that gravity wave perturbations influence PSC formation about 15% of the time. Wang et al. (2008) propose a different Antarctic PSC formation mechanism based on their analysis of observations by the NASA A-train satellites that showed two thirds of PSCs over west Antarctica and one half of PSCs over east Antarctica can be related to deep tropospheric cloud systems.

PSCs both influence and are influenced by climate change. Randel et al. (2009) report large trends in temperature in the lower stratosphere in spring. David et al. (2010) show that trends in the mean temperature and also trends in extreme temperatures are important for prediction of PSC occurrence. The long-term trend in global-mean lower stratospheric temperatures reported by Randel et al. (2009) is strongly driven by changes in stratospheric

ozone. Thus, both stratospheric cooling and the increase in PSC occurrence may reverse substantially as ozone will recover in the future. This conclusion is supported by model predictions by Hitchcock et al. (2009).

2.2.3.4 USE OF PROXIES TO REPRESENT PSC PROCESSES

PSC occurrence is often represented in modeling and diagnostic studies of polar ozone loss by simple thermodynamic proxies. A proxy used frequently in the past is that PSCs are present if the ambient temperature is below T_{NAT} , the theoretical threshold temperature for NAT existence. CALIPSO provides the first observational estimates of vortex-wide PSC areal coverage that can be used to directly assess the validity of simple thermo-

dynamic proxies for PSC occurrence. Pitts et al. (2007) showed that the use of T_{NAT} alone is a poor quantitative proxy for PSC occurrence and significantly overestimates the PSC areal extent; Figure 2-13 illustrates this point for the 2007 Antarctic season. The observation that T_{NAT} is not an accurate proxy for PSC occurrence is not surprising since analyses of CALIPSO and MIPAS data, as well as earlier studies, suggest that PSCs are primarily mixtures of liquid droplets and solid particles. However, as discussed below in Section 2.2.4, the empirical relationship between ozone loss and the volume of vortex air below T_{NAT} indicates that T_{NAT} is a useful gauge of low stratospheric temperatures that trigger chlorine activation and ozone loss, even though the activation is primarily occurring on liquid particles.

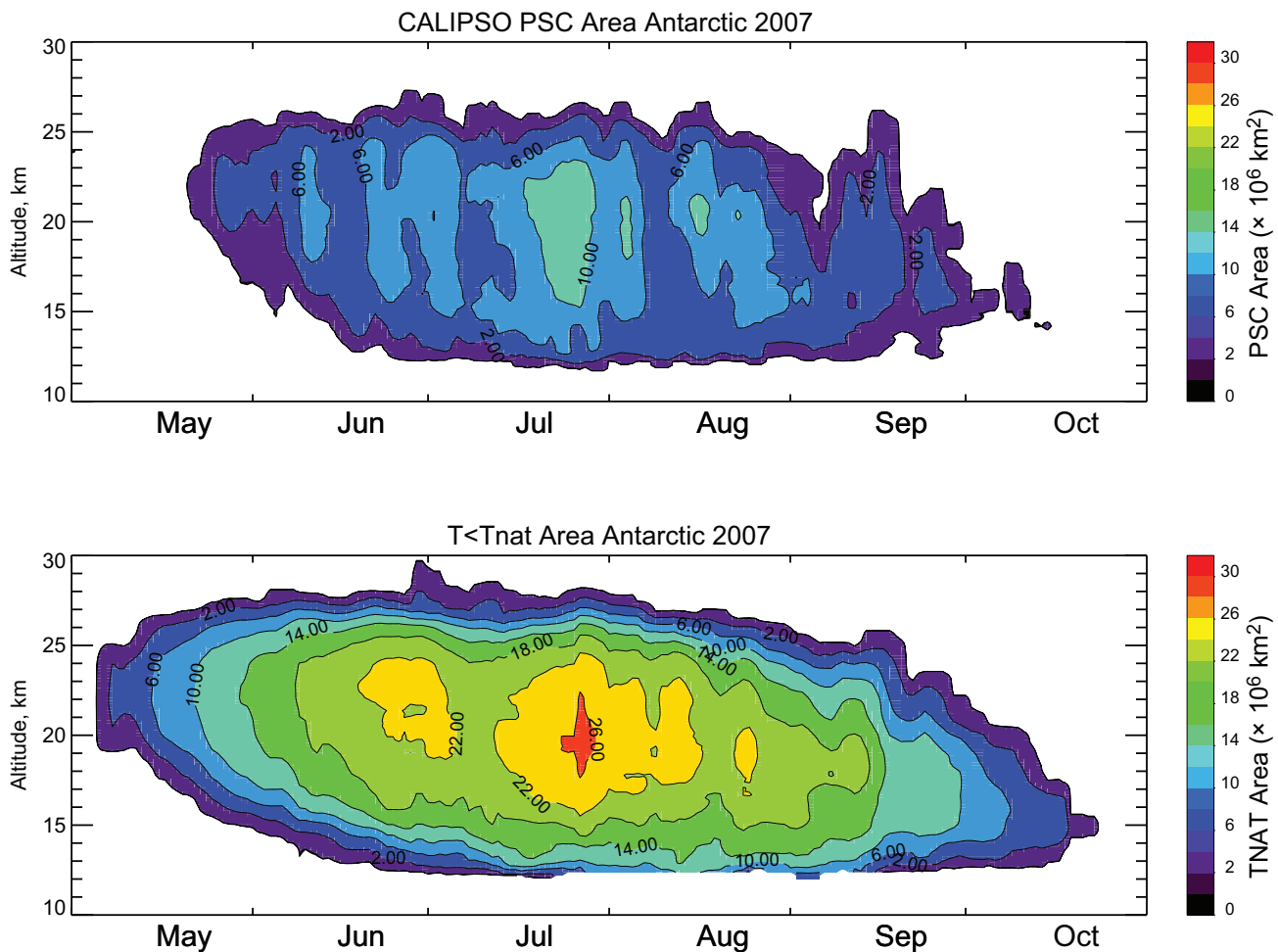


Figure 2-13. Daily time series of CALIPSO PSC area (km^2) versus area with $T < T_{\text{NAT}}$ for the 2007 Antarctic season (adapted from Pitts et al., 2007, and Pitts et al., 2009). Note that very tenuous PSCs containing a mixture of binary liquid aerosols and very low number densities ($<3\text{--}5 \times 10^{-4} \text{ cm}^{-3}$) of NAT particles are below the CALIPSO ensemble detection threshold. NAT particle surface areas in these PSCs are $<0.1 \mu\text{m}^2 \text{ cm}^{-3}$, or about 10% of the surface area of the liquid binary aerosols and $<1\%$ of the surface area of a fully developed STS PSC.

2.2.4 Arctic Polar Temperatures and Ozone

The annual cycle and variability for the minimum temperature poleward of 50° latitude in the Northern Hemisphere for 1979–2004 was shown in WMO (2007) (Newman and Rex et al., 2007, their Figure 4-1, top panel). The temperatures at 50 hPa for recent years fall within this range of variability. Temperatures in the Arctic winter stratosphere exhibit a high degree of natural variability. The winters 2006/2007 and 2007/2008 were among the ten coldest winters from 1965 to present. The 2008/2009 winter was very cold in midwinter but PSC conditions were terminated by a strong warming in late January.

Polar ozone during recent Arctic winters remains low compared with values observed during the 1980s and continues to strongly vary interannually (Figure 2-14, top panel). The figure shows the minimum total ozone over the polar cap for March (calculated as the minimum of the daily average column ozone poleward of 63° equivalent latitude). This is an indicator of polar ozone loss that shows a reasonable correlation with observed chemical ozone depletion (Müller et al., 2008). In the years since WMO (2007), the minimum spring ozone values over the Arctic polar cap remained in a range comparable with values prevailing since the early 1990s (Figure 2-14, top panel). This indicates that substantial chemical loss continues to occur in cold Arctic winters.

Arctic winter and spring ozone loss has varied between 2007 and 2010, but remained in a range comparable to the values that have prevailed since the early

1990s. Chemical ozone destruction on the order of 100 DU (about 80% of the values derived for the record cold winters of 1999/2000 and 2004/2005) is deduced for both Arctic winters 2006/2007 and 2007/2008 (derived from ozonesonde measurements following the approach described by Rex et al., 2006). A strong reduction in column ozone during these winters is in accordance with strong chemical destruction at 475 K in mid-March reported for 2006/2007 based on Odin data (Rösevall et al., 2007) and 2007/2008 based on Microwave Limb Sounder (MLS) data (Kuttippurath et al., 2009). Reliable ozone loss estimates are not possible for the Arctic winter 2008/2009 because a strong midwinter warming in late January led to extensive mixing of air from low latitudes with the polar vortex air.

Tegtmeier et al. (2008) showed that the variability of (1) chemical loss of ozone in the Arctic and (2) the amount of ozone transported into the Arctic during winter each contribute about half of the observed variability of high latitude total ozone during spring (Figure 2-15). The supply of ozone due to transport has so far usually been larger than the chemical loss (with possibly very small net loss only in 1995, 1996, and 2000) such that the total ozone column has not declined in the course of Arctic winters and the extreme ozone anomalies associated with the Antarctic ozone hole are not observed in any long-term Arctic record (Solomon et al., 2007). Tegtmeier et al. (2008) also showed that these terms are correlated and variability in both is driven by variability in wave driving from the troposphere, making both terms sensitive to potential changes in wave driving due to climate change.

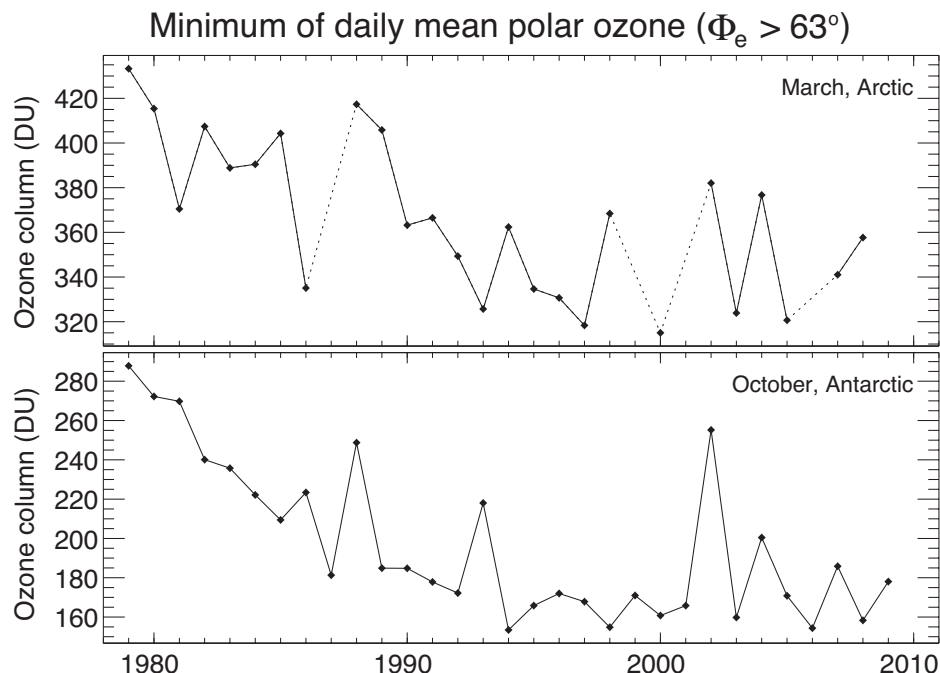


Figure 2-14. Time series of minimum total ozone (Dobson units) over the polar cap, for March in the Arctic (top panel) and October in the Antarctic (bottom panel), calculated as the minimum of daily average column ozone poleward of 63° equivalent latitude. Winters in which the vortex broke up before March (1987, 1999, 2001, and 2006) are not shown for the Arctic time series. Figure adapted from Müller et al. (2008), updated using the NIWA combined total column ozone database (version 2.7).

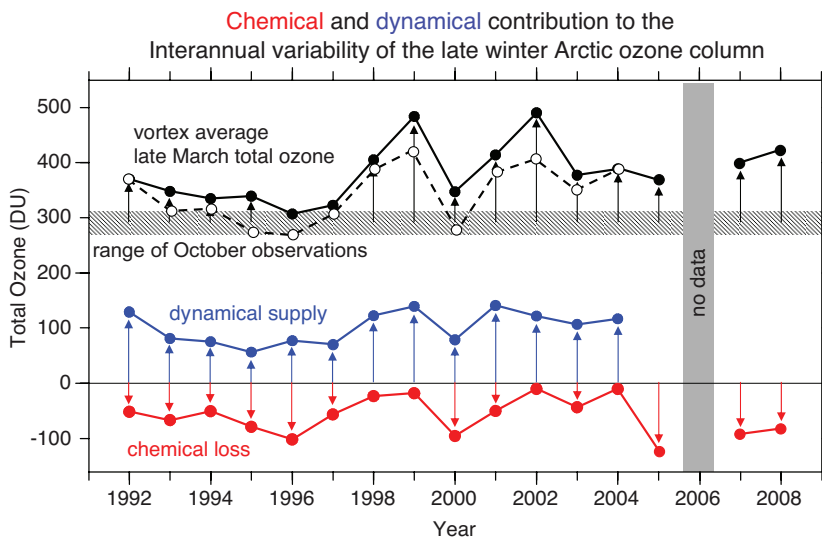


Figure 2-15. Interannual variability of the observed late winter (March) total ozone column (Dobson units) averaged over the polar vortex (black), the dynamical supply of ozone to the polar vortex (blue) and the chemical loss of ozone over the winter inside the vortex (red). The hashed range around 290 DU illustrates the very limited range of early winter (October) variability. The dashed black line close to the late winter observations is the sum of early winter ozone, dynamical supply and chemical loss (updated from Tegtmeier et al., 2008; based on ozonesonde data combined with meteorological data and transport modeling).

Several diagnostics use volume of vortex air below T_{NAT} , the theoretical threshold temperature for NAT existence for typical values of stratospheric water and nitric acid mixing ratios (Rex et al., 2004; Rex et al., 2006; Tilmes et al., 2004). This volume has commonly been referred to as V_{PSC} . Because V_{PSC} calculated in this way is not a good proxy for the existence of NAT particles (see Section 2.2.3.4 above), other proxies for the onset of polar heterogeneous chlorine activation have been considered that involve also the surface area density of binary sulfate aerosol particles, e.g., Tilmes et al. (2008a) consider the potential for activation of chlorine (PACl). However, observations show that T_{NAT} may still be a useful proxy because the onset of chlorine activation does not necessarily occur on NAT particles (Toohey et al., 1993; SPARC, 2009). Therefore, it is meaningful to consider a relation between ozone loss and such calculated values of V_{PSC} . The ozone loss observed in Arctic winters since the previous Assessment falls along the relation between chemical ozone loss and V_{PSC} that was discussed in the previous Assessment (WMO 2007, Figure 4-13).

Rex et al. (2006) noted a tendency toward higher extreme values in the overall volume of air at temperatures below the PSC threshold (V_{PSC}) over the past four decades, i.e., a cooling of the “cold” Arctic winters. An update of this relation is shown in Figure 2-16. Values of V_{PSC} since WMO (2007) were all less than that computed for NH winter 2004/05, but on a statistical basis established over the past four decades, a new maximum occurs about only once in five-year intervals. Therefore, it is not possible to draw a conclusion about the continuation of the changes in the severity of extreme values based on absence of a new record V_{PSC} in the past four years. It is notable that

three of the past four winters had V_{PSC} values in the upper 25% of the long-term distribution even though a midwinter major warming occurred in all of the winters since the previous Assessment.

2.2.5 Antarctic Polar Temperatures and Ozone

Winters remain very cold in the Antarctic, and the seasonal cycles for the minimum temperatures poleward of 50°S for recent years fall within the range of variability for 1979–2005 that is shown in the bottom panel of Figure 4-1 of WMO (2007). Exceptional dynamical activity and associated warming, like that in Antarctic winters 2002 and 2004, has not occurred since the previous Assessment, but in 2006 the springtime increase in the minimum temperature took place slightly later than usual.

The minimum of total ozone over the polar cap for October (calculated as the minimum of the daily average column ozone poleward of 63° equivalent latitude) has remained approximately at the low levels observed in the mid-1990s until 2009 (Figure 2-14 bottom panel). Chemical ozone loss in the Antarctic since the previous Assessment remained stable at the level of the mid-1990s. Ozonesonde observations at South Pole (Hofmann et al., 2009a) consistently indicate that, with the exception of the years 2002 and 2004, more than 90% of the ozone is removed each year since the mid-1990s, at about 18 km (~ 70 hPa). Maximum ozone losses at this altitude reach 99% (Solomon et al., 2005; Solomon et al., 2007). The lowest ozone partial column (2 DU) in the altitude range 14–21 km observed at South Pole (in the time period 1986–2007)

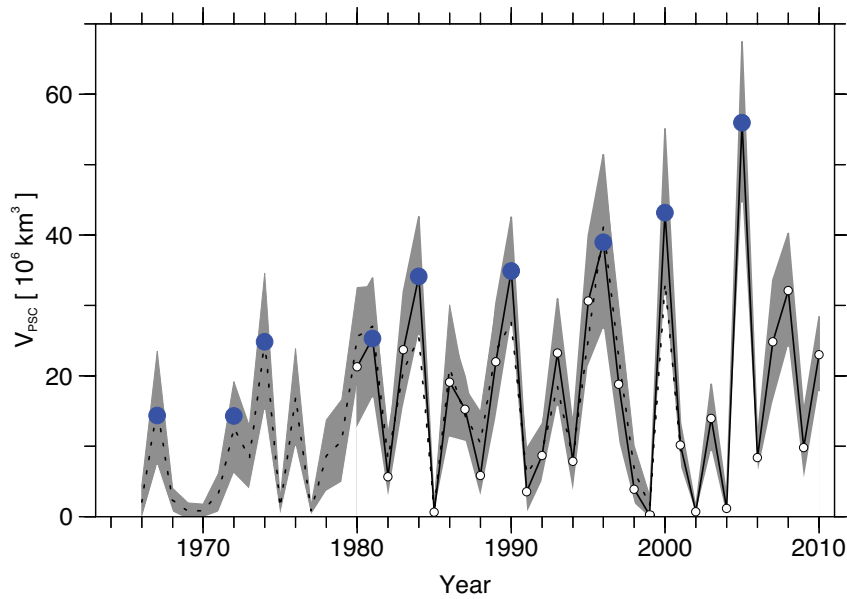


Figure 2-16. Evolution of V_{PSC} (km^3) for the Arctic over the past four decades obtained from European Centre for Medium-Range Weather Forecasts (ECMWF) and Free University of Berlin (FUB) data. The blue dots represent the maximum values of V_{PSC} during five-year intervals. The dotted line is based on radiosonde analyses of the FUB, and the solid line is ECMWF ERA-15 data extended by operational analyses. The gray shading represents the uncertainty of V_{PSC} assuming a 1-K uncertainty of the long-term stability of radiosonde temperatures. Updated from Figure 4-3 of WMO (2007) and Rex et al. (2004).

occurred in 2006 (Hofmann et al., 2009a). The chemical ozone loss in the Antarctic vortex core for the altitude range 350–550 K deduced from satellite data for the period 1992–2005 is ~ 130 DU, more than found for even the coldest Arctic winters (Tilmes et al., 2006).

In summary, ozone loss during Antarctic winters remained stable with little year-to-year variability since the previous Assessment. This is expected since moderate changes in EESC are not expected to have a detectable effect on measures of Antarctic ozone loss (WMO 2007; Newman et al., 2006; see also Section 2.4.5 for further discussion). Since about 1997 the ODS amounts have been nearly constant and the depth and magnitude of the ozone hole have been controlled by variations in temperature and dynamics. The October mean column ozone within the vortex has been about 40% below 1980 values for the past fifteen years.

2.2.6 The Onset of Antarctic Ozone Depletion

The average total ozone poleward of 63° latitude in March (NH) and October (SH) is compared to an average of the observations between 1970 and 1982 to provide an indication of the amount of ozone lost each year due to polar processes (Figure 2-8). This choice of reference level is somewhat arbitrary. The 1970–1982 average includes observations from 1970–1972 and 1979–1982 in the SH and from 1971–1972 and 1979–1982 in the NH. These observations and data from ground-based instruments at several locations suggest that ozone de-

creased between the early 1970s and the early 1980s in both hemispheres, but computing a trend from the satellite observations is not meaningful because of the data gaps. The ground-based data records have smaller gaps but exhibit year-to-year variations and are not representative of the entire polar region. A near-continuous, near-global record of satellite observations of total ozone has been available only since the Nimbus 7 Total Ozone Mapping Spectrometer (TOMS) instrument began taking data late in 1978.

2.3 SURFACE ULTRAVIOLET RADIATION

2.3.1 State of Science in 2006

Chapter 7 of the 2006 Assessment (Bais and Lubin et al., 2007) explored factors that affect surface UV irradiance, examined the methods of assessing this irradiance (ground-based measurements, satellite retrievals, and radiative transfer modeling), and reviewed measurement series, reconstructions, and numerical models of future scenarios to identify past and potential future changes in surface UV irradiance. Much of our understanding of UV radiative transfer remains valid today, while updates since 2006 follow later in the section.

The influence of stratospheric ozone on the transmission of short wavelength UV radiation through the atmosphere is well understood. Since the ozone-related change in UV radiation is wavelength dependent (becoming negligible at wavelengths greater than 340 nm), the way in which UV radiation is defined or measured (e.g.,

spectral, UV-B (280–315 nm) waveband, UV-B + UV-A (315–400 nm), or biologically weighted UV) determines its sensitivity to ozone. Broadband erythemal radiometers are the most widespread instruments for measuring surface UV irradiance, but they cannot identify the contribution of individual wavelengths to the observed change in erythemal irradiance and so cannot separate ozone-induced changes from other influences on UV radiation.

For UV effects for which there is a known action spectrum, e.g., erythemally weighted UV, the sensitivity

to ozone changes is often expressed as a radiation amplification factor (RAF) (see Box 2-1), which differs from the monochromatic RAF.

Clouds, aerosol, surface albedo, and ozone all affect surface UV radiation. For many locations, the observed changes in UV radiation are influenced by changes in all of these. The importance of each varies with latitude, climate, and the amount of atmospheric pollution at each site. Cloud transmission is the greatest and most changeable atmospheric determinant of UV variability at

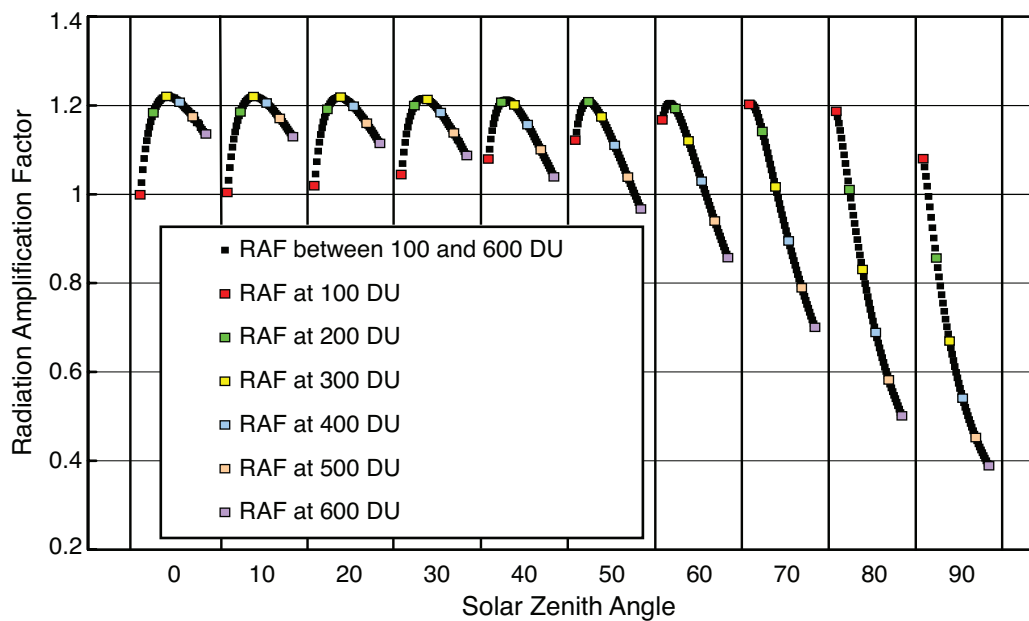
Box 2-1. Radiation Amplification Factor for Erythemal Irradiance

The relationship between change in total column ozone (O_3) and change in biologically effective radiation, e.g., erythemal irradiance (E), can be quantified using the radiation amplification factor (RAF) (Booth and Madronich, 1994). For example, $RAF = 1.5$ means that a 1% decrease in ozone will lead to a 1.5% increase in the biologically effective radiation. For small fractional changes in ozone (of the order of 10%) the RAF for erythema can be defined as

$$RAF = -\left(\frac{\Delta E}{E}\right) / \left(\frac{\Delta O_3}{O_3}\right)$$

where ΔE and ΔO_3 are the respective changes of erythemal irradiance and column ozone.

As the relationship between ozone and erythemal irradiance is nonlinear, the RAF is not a constant in all conditions but depends on factors that change the shape of the solar spectrum, primarily solar zenith angle and ozone column, as illustrated in Figure 1. While for solar zenith angles (SZAs) from 0° to 50° and typical midlatitude ozone the RAF for erythema is 1.1 ± 0.1 , for larger SZAs and large total ozone values the RAF gradually decreases.



Box 2-1, Figure 1. Radiation amplification factor for erythemal irradiance as a function of SZA, for several total column ozone amounts. RAF values were calculated in SZA-steps of 10° and steps of 10 DU in ozone column. The first value in each SZA-bin refers to 100 DU; the last value refers to 600 DU (from WMO, 2008).

the surface. Although UV radiation is reduced slightly less than visible radiation by clouds, heavily overcast conditions can still reduce surface UV irradiance by 90%. Broken-cloud conditions can produce short-term enhancements in UV irradiance up to 25% over clear-sky conditions. Clouds vary on many timescales and thus hinder attempts to identify small ozone-induced changes in UV irradiance from ground-based measurements at locations where ozone depletion has been modest.

Pollutants in the lower troposphere, notably ozone, nitrogen dioxide, and sulfur dioxide, are strong attenuators of UV radiation. Ozone and sulfur dioxide (SO₂) attenuate at UV-B wavelengths, while nitrogen dioxide (NO₂) attenuates most strongly in the range from 330 to 400 nm, with a smaller influence in the UV-B waveband. The UV response to changes in these gaseous pollutants, and UV-absorbing aerosols such as organic carbon from motor vehicles or biomass burning, may be larger than the UV response to changes in stratospheric ozone. In some locations increased pollution and aerosols may have masked an increase in UV irradiance due to ozone decrease in the 1980s and 1990s, and present cleaner air policies may hide the effect of ozone recovery on UV irradiance.

High surface albedo (reflectivity) greatly enhances surface UV irradiance where there is extensive snow and/or ice cover. Enhancements of erythemal irradiance of ~20% have been reported in regions with snow cover; even greater enhancements are seen in Antarctica due to very clean, high-albedo snow over a large area.

In the previous Assessment, ground-based UV measurement records that began in the 1990s covered a period with no significant ozone trends except at high latitudes, and reducing the uncertainties in quantifying surface UV irradiance remained a challenging task. Ozone-related changes in UV irradiance were apparent in unpolluted regions of the SH where previous increases in surface UV irradiance had ceased or reversed along with observed increases in ozone. At polluted midlatitudes in the NH, UV surface irradiance was generally still increasing by small amounts (a few percent per decade) at the time of the previous Assessment, but at unpolluted sites any increase had ceased. Short events with low column ozone and high UV irradiance had also been recorded at a variety of locations.

Satellite-derived erythemal irradiance estimates from 1979, based on ozone, aerosol, and cloud measurements, were being evaluated against ground-based data at the time of WMO (2007). Satellite data have the advantage of providing global coverage, but the retrieved products must be validated. TOMS (Total Ozone Mapping Spectrometer) data, and since July 2004 data from Ozone Monitoring Instrument (OMI) on the Aura spacecraft, had been analyzed. Satellite-estimated UV irradiance compares well with ground-based measurements in clean conditions, but at polluted sites the satellite retrievals failed to

adequately account for tropospheric pollution, leading to overestimates of about 10% and up to 40%.

Both ground-based measured and satellite-estimated UV radiation data have increased in availability since WMO (2007). In addition to improved and reanalyzed ground-based data, there has been substantial progress in development of both satellite-derived UV products and ground-based reconstructed UV time series, and the climatologies and trend estimates derived from them. The following sections detail the advances in our knowledge and understanding since WMO (2007).

2.3.2 Update on Factors Affecting UV Radiation

The main factors affecting UV radiation are well established and recent studies were mostly focused on quantification of the effect of different factors on UV irradiance. In particular, better estimates of the effects of air pollution on UV irradiance, including their magnitude and wavelength dependence, were the subject of many recent studies.

2.3.2.1 OZONE EFFECTS

Where ozone changes are large, e.g., in the Antarctic, they produce a clear signature in the surface UV radiation. Measurements from Summit Station, Greenland (72°N, established in 2004), show that for comparable solar zenith angles, the spring erythemal irradiance at the South Pole is 50–130% larger than at Summit Station, despite the similar location of the two sites on vast high-altitude ice sheets (Bernhard et al., 2008). Bernhard et al. (2008) also show that these differences are almost entirely caused by the difference in spring total ozone at South Pole and Summit.

Due to the ozone decline, the average erythemal irradiance measured at the Pole between 1991 and 2006 was up to 85% larger than the estimate for the years 1963–1980 (Bernhard et al., 2010). At McMurdo, the average erythemal irradiance for October and November is estimated to be about 30–60% higher than historically.

The ozone-related influence on UV radiation can be identified from the spectral dependence of the changes, because ozone absorption increases strongly toward the shorter wavelengths in the UV-B region. Seckmeyer et al. (2008a) demonstrated that the ratio between UV values at Garmisch, Germany, and Lauder, New Zealand, as a function of wavelength clearly shows features related to the ozone absorption spectrum. Monthly erythemal UV radiation is up to 50% lower in the European summer compared to sites with comparable latitudes in New Zealand. These large differences are caused mainly by differences in total ozone (~15%), cloudiness, aerosol loading, and Sun–

Earth separation. At similar SZAs, the ratio between UV irradiance values at Garmisch and Lauder as a function of wavelength clearly shows features related to the ozone absorption spectrum.

2.3.2.2 OTHER INFLUENCES ON UV

Since ozone is not the only influence on surface UV, and may not be the only parameter to change in the future, or to have done so in recent years, we update and further quantify our knowledge of these other influences.

Clouds can cause large and rapid changes (increases as well as decreases) in surface UV radiation and in total radiation (i.e., radiation integrated over the entire spectrum from about 300 nm to 3000 nm). On average, clouds have an attenuating effect of 15–32% in the UV waveband (Seckmeyer et al., 2008a; den Outer et al., 2005), but for any given situation the cloud effect will depend on the cloud type, depth, and distribution across the sky. Thus, cloud transmission of UV irradiance is difficult to quantify in sufficient detail to provide an exact determination of its effect at a given time and place (Thiel et al., 2008). This latter statement becomes important when considering satellite UV retrievals, detailed in Section 2.3.3.3, where cloud effects are averaged over a large field of view.

Another localized influence on surface UV radiation is air pollution, i.e., scattering and absorption by aerosols (black and organic carbon, hydrocarbons, dust, and smoke) as well as absorption by tropospheric O_3 , NO_2 , and other gases. Such pollution can reduce UV radiation by up to 15% at polluted sites, with reductions greater than 25% in highly polluted cities, e.g., occasionally in Los Angeles and frequently in Beijing. McKenzie et al. (2008) show that tropospheric extinctions in Tokyo account for much of the 40% reduction in UV-B radiation when compared to the clean atmosphere of New Zealand, and that UV-A radiation could occasionally be affected by high levels of tropospheric NO_2 .

Black carbon is the main absorbing component present in atmospheric aerosols. In addition, soil dust absorbs radiation in the UV and visible wavebands, and some organic materials absorb at UV wavelengths. Recently there have been several studies including measurements of enhanced UV absorption due to organic carbon. The sources and formation of these compounds and their temporal variability, however, are currently not well understood (Andreae and Gelencsér, 2006; Bergstrom et al., 2007).

The wavelength dependence of aerosol absorption optical depth is often expressed as an Absorption Angstrom Exponent (AAE). The theoretical AAE value for black carbon, assuming spectrally constant refractive index, is one. The higher values (spectrally steeper absorption) are usually attributed to dust and absorbing organic

components. Recent studies that include UV wavelengths show large values of AAE for organic species (Bergstrom et al., 2010; Barnard et al., 2008; Martins et al., 2009; M. Yang et al., 2009).

Corr et al. (2009) analyzed measurements at UV wavelengths from Mexico City and found that there is no significant single scattering albedo (SSA, i.e., the ratio of scattering optical depth to the total optical depth (scattering + extinction) of the atmosphere) variability between 332 and 368 nm. Barnard et al. (2008) analyzed data from the same Megacity Initiative: Local and Global Research Observations (MILAGRO) campaigns and also concluded there was little SSA wavelength dependence between about 300 and 400 nm for aerosols in the Mexico City area. However, Barnard et al. (2008) found a steep increase in SSA between ~400 and 500 nm and attributed the enhanced absorption at UV wavelengths to organic matter. Marley et al. (2009) also concluded that enhanced UV absorption was due to organic aerosols.

Surface reflectivity in the UV is usually less than 0.1, unless the surface is snow covered. The albedo for snow-covered surfaces varies with snow type and age, and can approach unity for fresh, pure snow (Wuttke et al., 2006a; Meinander et al., 2008). The UV irradiance over a high-albedo surface is greater than that above a snow-free surface, and this effect can be further enhanced by cloudiness and the multiple reflections between snow and cloud surfaces (Wuttke et al., 2006a). Changes in the extent and seasonality of snow cover due to climate change could thus change surface UV.

Surface UV radiation is a response to the combination of all influences on UV radiative transfer. Thus, while latitudinal and seasonal variations for UV radiation are firstly determined by the solar zenith angle, instantaneous UV irradiance values at high-latitude sites may sometimes significantly exceed those at lower latitudes due to the effect of clouds, aerosols, or ozone, particularly at sites affected by the ozone hole (Diaz et al., 2006; Vernet et al., 2009). Under similar solar zenith angles, there can still be large differences in UV irradiance between urban and rural locations, or between sites in the NH and generally cleaner sites in the SH. McKenzie et al. (2006), using measurements from the United States Department of Agriculture UV network, show that peak UV Index values at 45°S in New Zealand are approximately 40% greater than those at 45°N in North America. Subsequently, it has been shown that cloud effects are also less severe at SH sites in the South Pacific region compared with similar latitudes in Europe (Seckmeyer et al., 2008a).

Seasonal differences in surface UV irradiance are highly dependent on latitude, moderated by local cloud and aerosol climatologies. They also depend on the UV wavelength/waveband, or biological weighting, of the irradiance being considered or measured. For erythemally

weighted UV, the ratio between summer and winter mean noon erythral irradiance is in the range 17–24 around 55°N (24 in Moscow at 57°N (Chubarova, 2008), and 17 at 53°N, representative of, e.g., Liverpool, U.K., or Berlin, Germany (Seckmeyer et al., 2008b)), while it is 5 at 35°N. These seasonal contrasts tend to be greater, latitude for latitude, in the SH (McKenzie et al., 2009).

2.3.3 Ground-Based and Satellite UV Data

The majority of sites making direct measurements of UV radiation became active in the 1990s. With rare exceptions, ground-based data prior to this are reconstructions. To estimate the long-term evolution of UV radiation at the surface they use proxy data. While the approach is not new, recent studies used it for the first time to reconstruct UV over a large area (Europe) and study regional effects of ozone and clouds on UV irradiance. Satellite retrievals of UV irradiance have the advantage of a nearly global coverage and are available since 1979, the beginning of the almost continuous record of total column ozone and surface reflectivity from satellite instruments. While total ozone data merged from several satellite instruments have long been available (see Section 2.1.3.1), it is only recently that satellite reflectivity measurements have been merged together into a uniform data set (Herman et al., 2009), making it possible to study long-term trends in satellite-derived erythral irradiance over a long period.

2.3.3.1 GROUND-BASED UV MEASUREMENTS

The main classes of instruments presently in use for measuring solar UV irradiance reaching the ground have been described in previous Assessments (WMO 2003; WMO, 2007). Broadband instruments provide a measurement across a specified waveband, most commonly designed to mimic the erythral action spectrum (Hülse et al., 2008; Webb et al., 2006). Multispectral filter instruments measure several narrow wavelength bands (usually less than 10 bands from 1 nm to 10 nm wide) at the same time or sequentially (e.g., Petkov et al., 2006), thus providing some spectral information. Spectroradiometer systems measure the spectrally resolved solar irradiance, ideally at a resolution of 1 nm or better. No instrument is perfect, with uncertainties in the data coming from a variety of instrument-dependent sources (see, e.g., Johnsen et al., 2008; Cordero et al., 2008a; Cordero et al., 2008b). It follows that instruments must be carefully characterized and regularly calibrated (Webb et al., 1998; Wuttke et al., 2006b). Since standards of spectral irradiance have uncertainties in the UV-B of ~3%, Cordero et al. (2008a) estimate uncertainties between 4 and 6% in the absolute calibration of double monochromator-based spectroradi-

ometers. Additional uncertainties (e.g., imperfect cosine response) result in an overall uncertainty for solar measurements of 7–9%. This accords well with the work of Gröbner et al. (2006), who show results of an intercomparison of 25 European spectroradiometers relative to a transportable reference spectroradiometer. Almost half of the instruments had absolute agreement with the reference spectroradiometer to within $\pm 4\%$ for UV-B and UV-A wavelengths. Broadband instruments, usually calibrated by a spectroradiometer, have uncertainties in the range 7–16% (Gröbner et al., 2007), with imperfections in the cosine response being a major source of error.

While absolute calibration is important for comparing measurements at different locations, or between different techniques (e.g., ground versus satellite), the most important requirement for trend detection is good long-term stability in instrument sensitivity. Stability can be determined by repeated checks against standard lamps in the laboratory or by various techniques applied to the data obtained in the field, i.e., the Langley method (Slusser et al., 2000). Some instruments are known to be very stable against standard lamps and can produce radiance stability near 1% (Cede et al., 2006).

Despite the need for geographical comparison between traceable quality-controlled UV measurements, ground-based monitoring stations provide sparse coverage. Most UV measuring stations are located in the NH in Europe and North America, with gradually increasing numbers in Asia. There are a few stations in South America, New Zealand, Australia, and Africa. A well calibrated polar network of seven stations has been maintained by the U.S. National Science Foundation, while the international Network for the Detection of Atmospheric Composition Change (NDACC) also maintains a long-term database of quality-assured UV data from a small number of observation sites. The World Ozone and Ultraviolet Data Center (WOUDC), the repository for Global Atmospheric Watch (GAW) and GAW-related station data, holds both spectral and broadband data.

Given the limited time series of UV measurements at most ground-based sites, there have been recent attempts to extend some of the data sets back in time using other data sets available for the sites, as detailed in the next section.

2.3.3.2 GROUND-BASED UV RECONSTRUCTION

Consistent records of reliable UV data covering more than 15–20 years are generally not available. Recent studies show the possibility of calculating the surface UV irradiance using variables directly affecting UV radiation, e.g., total ozone and cloud characteristics from standard weather station observations. The reconstructed data sets, which can extend backward to the beginning of the UV

proxy observations, are valuable for examining the UV variability in periods without UV measurements.

Radiative transfer calculations and statistical models are additional tools used to reconstruct the UV irradiance reaching the Earth's surface for data-poor periods. These calculations provide hypothetical irradiance that would be measured if input parameters (ozone, aerosols, and ground albedo) were known for selected measuring sites. However, uncertainties in the model input parameters yield uncertainties in the model outputs of about 6% for clean sites, and up to 20% for sites with very large aerosol load (Cordero et al., 2007; Badosa et al., 2007).

The most common hybrid algorithm calculates all-sky UV irradiance by multiplying the radiative transfer model output for clear-sky conditions by an empirical cloud modification factor (CMF) to account for cloud attenuation effects. CMF represents a ratio between measured shortwave radiation and its potential clear-sky value. The UV-relevant CMF is usually derived via model calculations from an empirical formula based on total irradiance, which is measured routinely on many meteorological stations (Staiger et al., 2008; den Outer et al., 2005; den Outer et al., 2010). Comparison of 16 European UV reconstruction models (COST 726, 2010) shows that the models using total irradiance for the CMF calculation prevail over models based on other parameterizations of the cloud effects, since total irradiance represents all the influences on radiation transmission through the atmosphere.

Ultraviolet irradiance data have been reconstructed by merging five different UV reconstruction models and ground-based measurements for eight European sites from Finland to Greece (den Outer et al., 2010) for the period 1963–2004. Reconstruction techniques are based on neural networks (Junk et al., 2007; Janouch and Metelka, 2007), and radiative transfer modeling (Lindfors et al., 2007) or combine radiative transfer modeling with empirical relationships (den Outer et al., 2005; Kazantzidis et al., 2006). Besides total column ozone, all models use pyranometer data (total radiation) to determine the cloud impact on the UV irradiance. The five different models have been validated against ground-based measurements on a range of timescales using daily to yearly sums of erythemally weighted irradiance. Good correspondence between reconstructed and measured data was found for all-sky conditions at sites with concurrent observations of total radiation and total ozone used as input of the reconstruction model. The study by den Outer et al. (2010) compares the output of the models with erythemal doses measured at the eight European stations. Standard deviations in the ratios of modeled to measured daily sums vary between 10 and 30% depending on site and model, and for yearly totals are less than 5%.

While no single model is able to fully represent all sites (each performs best at its site of origin), the combined (best estimate) approach based on all models has resulted in significant reduction in uncertainties in the reconstructed data: the range of deviations compared to measurements is at least halved for the best estimate when compared to the individual models.

Fixed aerosol properties are usually assumed in the UV reconstruction model. Simulations over Europe have used gridded climatological values of aerosol optical depth in the UV range that are calculated on a monthly basis by combining AERONET (AERosol RObotic NETWORK) and MODIS (Moderate Resolution Imaging Spectroradiometer) aerosol data (COST 726, 2010). Variable aerosol properties appear as input to the reconstruction model at a few sites (e.g., Moscow; Chubarova, 2008) and are important where there has been a significant change in aerosols (e.g., in Thessaloniki due to reduction of urban pollution). Kazadzis et al. (2007) found the decrease of aerosol optical depth to be $2.9\% \pm 0.9\%$ per year at 320 nm between 1997 and 2006. den Outer et al. (2010) discuss the dramatic effect of this on the positive trend in the erythemal UV daily sums, up to $1.4\% \pm 0.1\%$ per year, whereas without the aerosol change the trend would be around $0.3\% \pm 0.1\%$ per year. Several authors demonstrate that local pollution (aerosols and trace gases) over urban regions significantly affects surface UV irradiance levels (Chubarova, 2008; McKenzie et al., 2008; Panicker et al., 2009).

A further important input to reconstructions in some climates is elevated ground-albedo during the snow-covered season, which can be incorporated if snow data are available (Rieder et al., 2008; Pribullová and Chmelík, 2008; COST 726, 2010).

While reconstructions provide a historical view of UV irradiance for as long as the required ancillary data are available, recent reconstruction data intended for trend analysis exist only for a small number of sites, concentrated in Europe and Canada (Fioletov et al., 2001).

2.3.3.3 UV ESTIMATES FROM SATELLITE OBSERVATIONS

Global estimates of long-term UV records from satellite ozone and reflectivity data were previously discussed using observations from Nimbus 7 Total Ozone Mapping Spectrometer (N7-TOMS), and have now been updated and extended up to 2008 by Herman (2010). The updated time series, 1979–2008, uses ozone data obtained from the NASA merged satellite data set of monthly and 5° zonal average band values (Stolarski and Frith, 2006). The UV estimates are obtained from measurements of backscattered UV by using radiative transfer calculations

that include ozone, surface reflectivity, and aerosol estimates embedded in a Rayleigh scattering atmosphere adjusted for the local terrain height within a satellite field of view. Another TOMS-based global climatology was published recently (Lee-Taylor et al., 2009). This study also discusses changes in UV irradiance in the 1990s relative to the 1980s and separates contributions from ozone and cloud changes.

Recent validation studies of satellite estimates have focused on OMI data using comparisons to ground-based measurements (Tanskanen et al., 2006; Tanskanen et al., 2007; Ialongo et al., 2008; Buchard et al., 2008; Weihs et al., 2008; Kazadzis et al., 2009a). All find that the OMI UV estimates are biased high, particularly at more polluted sites. In snow-free conditions, they are biased high by 10% compared with ground-based measurements; the high bias is up to 40% in some highly polluted environments. This bias is similar to that for TOMS-based estimates: analysis of Belsk (Poland) data shows that the ratio between satellite-derived and measured erythemally weighted doses calculated for the snowless period (April–October) is stable over the period 1979–2008 (Krzyścin et al., 2011). The ratio for the earliest part of the satellite UV data (from TOMS measurements onboard of the Nimbus 7 satellite in the period 1979–1993) is 1.23 ± 0.06 , only slightly larger than that obtained from the measurements by the TOMS onboard the Earth Probe satellite (1.19 ± 0.07 for the period 1996–2003) and from the measurements by OMI onboard the Aura satellite (1.19 ± 0.05 for the period 2004–2008).

One of the sources of differences is that satellite measurements represent a much larger region (OMI minimum pixel at nadir: $13 \times 24 \text{ km}^2$) than ground-based measurements. Ground-based measurement of erythemal dose at various sites within one OMI satellite pixel showed deviations of $\pm 5\%$ in cloud-free conditions, or 20% if urban areas were included (Weihs et al., 2008; Kazadzis et al., 2009b). For partly cloudy conditions and overcast conditions the discrepancy of instantaneous values between the stations can exceed 200%. If 3-hourly averages are considered, the agreement is better than 20% within a distance of 10 km (Weihs et al., 2008). This spatial discrepancy can explain much of the random variation between ground-based and satellite data but does not generally explain a strong systematic bias. The largest relative differences between the satellite-derived and the measured irradiance are observed in urban areas, where UV-absorbing aerosols play an important role. The OMI overestimate of ground-based UV measurements may be partly explained by the lack of sensitivity of satellite instruments to the boundary layer (Tanskanen et al., 2007; Ialongo et al., 2008; Weihs et al., 2008; Kazadzis et al., 2009a; Buchard et al., 2008). The bias between OMI and ground-based measurements increases with increasing

aerosol absorption optical thickness (Arola et al., 2005; Kazadzis et al., 2009b; Ialongo et al., 2010). The largest positive OMI biases were found at 305 nm (the lowest common wavelength routinely available), reaching 32% and 27% for cloudy and cloudless measurements (Kazadzis et al., 2009b), indicative of ozone variability in addition to aerosol variability.

Additionally, over snow-covered surfaces the OMI-derived daily erythemal dose is generally lower than the ground-based measurement because the OMI surface UV algorithm uses climatological surface albedo that may then be lower than the actual effective surface albedo. Part of the problem is that a portion of the observed reflectivity may be incorrectly interpreted as cloud cover, which reduces the estimated irradiance. All-conditions data and snow-free data have been compared separately to evaluate the effect of albedo. For example, a recent comparison by Buchard et al. (2008) demonstrated that OMI overestimates erythemal daily doses by 14% for days without snow on the surface and only by 8% if days with snow are included in the comparison.

UV irradiance is also derived by using column ozone in conjunction with cloud fraction data from geostationary satellites in combination with polar-orbiting satellites (Verdebout, 2004a and 2004b; Wuttke et al., 2003; Gadhavi et al., 2008; Janjai et al., 2010). The difference of about 10% between satellite and ground-based measurements is due to the limited information from the boundary layer (Arola et al., 2009; Kazadzis et al., 2009a). Schallhart et al. (2008) developed a method to generate near real time UV-index maps from Meteosat Second Generation (MSG) for Austria. The method is similar to that developed by Verdebout (2000) but with an additional input from ground-based UV measurements.

2.3.4 Long-Term Changes in UV

2.3.4.1 GROUND-BASED OBSERVATIONS

Over much of the Earth's surface, long-term increases in UV radiation due to decreases in ozone derived from records of ground-based instruments are small and difficult to separate from the sometimes larger effects of changes in clouds, aerosols, and pollutants. Spectral instruments at clean sites in regions with significant ozone change are in the best position to identify ozone-related changes in UV radiation, either from ozone depletion or recovery. Elsewhere, with small ozone changes, changes in climate (clouds/albedo) and human activities (pollution, gaseous and aerosols) may have greater importance for UV radiation than the ozone.

At clean-air sites such as Lauder, New Zealand, the increase in summertime UV irradiance reported previously

has not continued, and in recent years, the peak summertime UV amounts have been lower than in the late 1990s. Ozone is no longer decreasing at this site, with lowest values occurring in the summer of 1998/1999. However, year-to-year differences are comparable with the measurement uncertainty.

One of the longest series of UV measurements has been taken at Belsk (Poland). The erythemally weighted daily doses have been homogenized for the period 1976–2008 to account for instrument differences and time drift. Figure 2-17 shows that the mean erythemal irradiance level at Belsk in the warm subperiods of the year (April–October) in the 2000s has been ~10% larger than the overall mean level for the whole period of observations 1976–2008 (Krzyściński et al., 2011). The increase for clear-sky days is inferred from a simple model taking into account only ozone anomalies multiplied by the radiation amplification factor (RAF) of 1.1 (see Box 2-1). However, for data measured under all atmospheric conditions, the erythemal irradiance continues to increase when ozone reduction ceases. Borkowski (2008) shows an increase of 2.3% per decade in annual dose during the period 1976–2006 using Belsk’s monthly data.

Similarly, but for a shorter time period, increasing trends in erythemal irradiance have been seen at Sapporo,

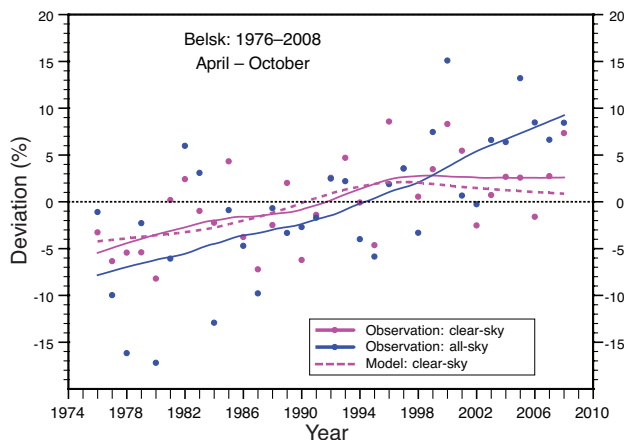


Figure 2-17. Deviations (%) of the monthly mean erythemal dose relative to the long-term (1976–2008) monthly means averaged over the warm subperiod of the year (April–October). The homogenized results of measurements by various broadband instruments at Belsk, Poland, for the period 1976–2008 are shown for all-sky conditions (blue dots) and clear-sky conditions (magenta dots). Curves illustrate the smoothed data. The dashed magenta line shows the modeled ozone signal in the UV series (corresponding total ozone deviations are multiplied by $RAF = 1.1$, see Box 2-1). Adapted from Krzyściński et al. (2011).

Tsukuba, and Naha since the early 1990s. At these sites total ozone was at its lowest around the early 1990s and since then there has been little increase in ozone. The increasing trends in erythemal irradiance since the early 1990s cannot be attributed only to changing ozone (JMA, 2009). Changes in aerosol and weather conditions at the Japanese sites are suggested as reasons for the observed increases in UV radiation.

Analysis of surface 280–320 nm UV irradiance measured by Multi-Filter Rotating Shadowband Radiometer (UV-MFRSR) from the U.S. Department of Agriculture (USDA) network shows annual irradiance changes from -5% per decade to $+2\%$ per decade at eight stations with approximately 10-year records (Hicke et al., 2008). Interannual variability of surface UV-B radiation was 2 to 5% of the mean. Trends at each site were calculated for individual months, but during most months trends were not statistically different from zero.

2.3.4.2 RECONSTRUCTED UV DATA

Using the erythemally weighted yearly doses reconstructed by various models (see Section 2.3.3.2), den Outer et al. (2010) find statistically significant UV trends for eight European sites. The trends vary between 3–6% per decade between 1980 and 2006. Upward trends were observed from 1980 to the mid-1990s for most sites, with levels in the 1980s being lower than the long-term average. Thereafter the rate of change altered at some sites and certainly cannot be extrapolated into the future. Ozone change accounts for $\sim 1\text{--}2\%$ of the increase per decade and clouds account for about 2–3% per decade. Observed increases in surface UV radiation are partly attributed to the decreased pollution since the late 1980s (e.g., Wang et al., 2009). The European continent has “brightened,” possibly due to air pollution abatement policies (e.g., Kazadzis et al., 2007; Ruckstuhl et al., 2008).

Lindfors et al. (2007) reconstructed erythemally weighted irradiance back to the early 1980s at four Northern European stations based on measured total ozone and total irradiance. The reconstructed time series show an increase in erythemal irradiance (3–4% per decade) for the stations having a clear increase in total radiation. Feister et al. (2008) found a similar long-term pattern for Central European stations, with a decrease between the 1950s and 1980 followed by an increase, resulting in UV irradiances $\sim 5\text{--}10\%$ higher than the overall (1950–2004) mean level at the end of the time series. Sites in Finland show similar long-term behavior since the early 1980s, but an increase is found between 1951 and the end of the 1960s, opposite to the Central European sites.

Junk et al. (2007) and Feister et al. (2008) reconstructed series of erythemal irradiance (see Feister et al., 2008, Figure 12) since 1893 based on sunshine duration

measurements at Potsdam. Additional measurements of global and diffuse irradiation were included since 1937, and variability of total ozone was included since 1964. The analysis indicates a few percent decrease in erythemal dose between 1893 and about 1910, a slight increase in the 1950s, followed by a gradual decrease of a few percent until 1980 and a subsequent increase after 1980 of a few percent to the highest levels in the time series. Chubarova (2008) discusses the long-term UV changes over Moscow using reconstructed time series since 1968. The overall trend for 1968–2006 is not statistically significant because of a significant decline (–11% per decade) in cloud transmission at the beginning of time series (1968–1980). Since 1980, the growth of ~6% per decade in the yearly sums of erythemally weighted doses has been caused by a decrease in total ozone (2.5% per decade), cloud (2.1% per decade), and aerosol effects (1.1% per decade). In Austria (Vienna and Sonnblick), changes in erythemally weighted doses relative to a reference decade (1976–1985) showed that changes in total ozone had a larger influence on erythemally weighted doses than changes in cloudiness; here ozone accounted for about 66% of the annually averaged change. However, in recent years the relative influence of changes in cloudiness on UV-doses became larger (reaching 50%) over Vienna (Rieder et al., 2008). Curylo et al. (2007) used reconstructed erythemally weighted data for Poland since 1964 for four stations, finding positive trends in the yearly data (with a maximum trend of about 4% per decade in Warsaw). The trends disappeared over some stations in summer due to increasing cloud attenuation.

Kvalevåg et al. (2009), addressing an extended period, found an extensive reduction of erythemally weighted irradiance of up to 15–20% over most land areas since 1750. An increase is suggested only in polar regions, most strongly in the SH and associated with the appearance of the Antarctic ozone hole. The estimate is based on a UV reconstruction taking into account preindustrial (1750) and present (2000) atmospheric conditions including changes in the stratospheric and tropospheric ozone (within the last 2–3 decades) and centennial changes in SO₂, NO₂, the direct and indirect effects of aerosol changes, and albedo changes. The long-term changes in pollutants could mask an increase of surface UV radiation due to stratospheric ozone decline in recent decades. It seems that the increase of UV extinction by carbonaceous aerosols is mostly responsible for such compensation.

Figure 2-18 presents a summary of estimated changes in UV radiation based on the reconstructions at eight European locations (den Outer et al., 2010). The 10-year running means of the yearly sums of erythemal irradiance are shown separately for all-sky and clear-sky conditions. To make the results of these eight different sites

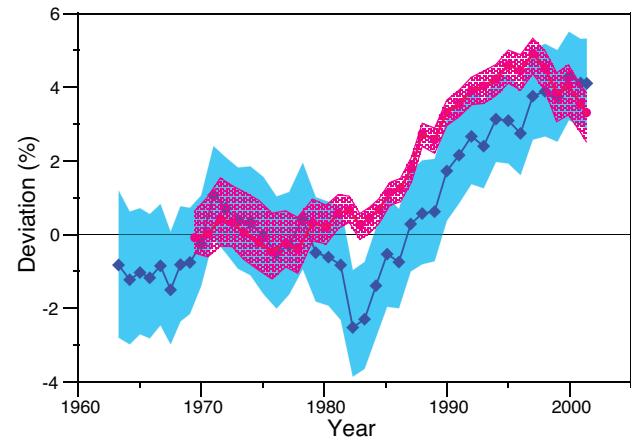


Figure 2-18. The 10-year running means of the yearly sums of erythemal irradiance at eight European sites for all-sky conditions (blue diamonds) and clear sky-only conditions (red dots). Prior to averaging, each reconstructed time series is normalized with respect to the 1970–1980 average. The light blue and red areas depict the uncertainty envelope for all-sky and clear sky-only conditions, respectively. Adapted from den Outer et al. (2010).

comparable, each reconstruction was first normalized with respect to the average level in 1983–2004, which is the overlap period of available data. The uncertainty bands shown in Figure 2-18 stem from the uncertainties in the reconstructed yearly erythemal sums. These uncertainties, assigned to each year separately, were derived from the long-term stability and underlying agreement of the models, and the agreement with actual UV measurements. The uncertainties to higher and lower values than the estimate are independent, and generally differ in magnitude. The high (low) limit of the final uncertainty band is based on the high (low) limits for the individual yearly sums. Summations and averaging in these processes were always carried out with statistical weights assigned to the individual data points. The final running means, as presented in Figure 2-18, are normalized again with respect to the period 1970–1980. Note the divergence between the trends for clear-sky and all-sky data since the mid-1990s, similar to the observations in Figure 2-17.

In conclusion, reconstructed trends, like those observed from direct UV measurement, are a superposition of the ozone, cloud, and aerosol effects on UV radiation. The magnitude of the trend depends very much on the period selected for the trend analyses, and on local characteristics of the cloud and aerosol changes as well as ozone. The statistically significant positive trends in erythemally weighted irradiance identified at many stations in the last half-century are due to reduced attenuation of radiation by

clouds since the beginning of the 1980s, and the general tendency of declining ozone until the mid-1990s.

2.3.4.3 SATELLITE ESTIMATES OF IRRADIANCE CHANGES

Herman (2010) analyzed satellite data (total ozone from multiple satellites) to estimate zonal average percent changes in UV irradiance from 290 to 400 nm and percent changes in biologically weighted irradiance reaching

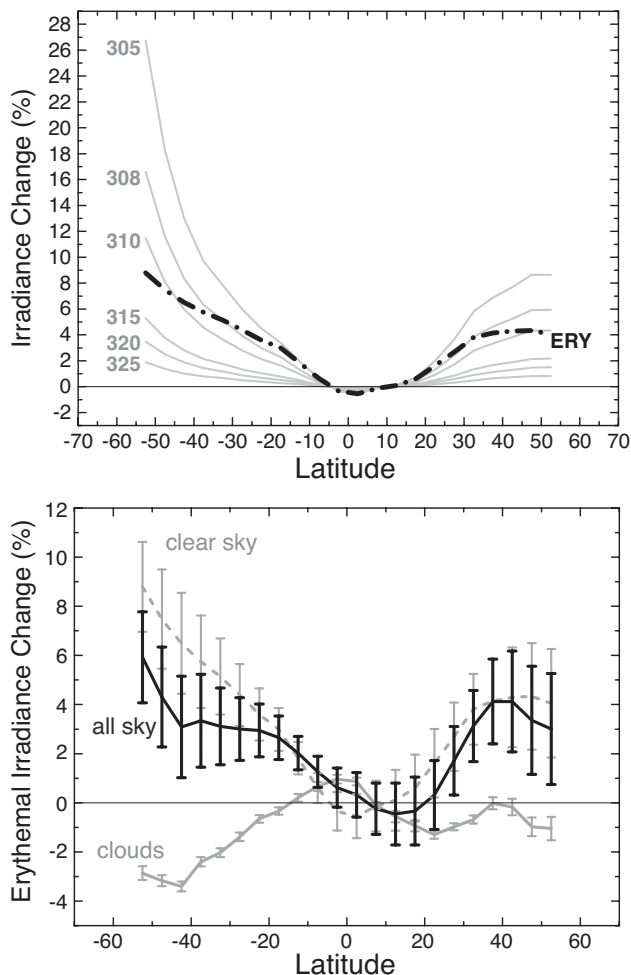


Figure 2-19. (top) Percent changes in erythemal irradiance from total change in ozone amount for 30 years (1979 to 2008). Also shown for comparison are six monochromatic irradiance changes. (bottom) The change in erythemal irradiance (solid black line) caused by changes in reflectivity and cloud transmission (solid gray line) and the changes in ozone amount represented by the clear-sky changes in erythemal irradiance (dashed gray line). Error bars are estimated from the linear least squares fitting procedure. Adapted from Herman (2010).

the Earth's surface (using the concept of RAFs and Beer's Law) for the period 1979 to 2008.

As shown in Figure 2-19 (top), clear-sky biologically weighted UV irradiance increased significantly except in the tropics. The increase was caused by decreases in ozone amount from 1979 to 1998. Since 1998, ozone amounts and UV irradiance levels have been approximately constant. Also shown for comparison are the percent changes in irradiance at six wavelengths (305, 308, 310, 315, 320, and 325 nm), which have different responses to ozone and contribute in different ways to biological effects. The annual estimates of zonal average UV irradiance changes are restricted to latitudes between 53°S and 53°N to avoid SZA > 80° during winter solstice, where spherical geometry effects become significant.

When all atmospheric conditions are considered, changes in cloud and aerosol transmission have a significant effect on UV irradiance in both hemispheres. In the SH the annual average UV increase is partially offset by a decrease in cloud and aerosol transmission (hemispherical dimming), while in the NH the effect was minimal (Figure 2-19, bottom).

For clear skies, the largest increases were at the higher latitudes and in the SH (about 8.5% for erythemally weighted irradiance at 50°S compared to 4% at 50°N). At 30°S the increase was about 5%, which is comparable to the increase at 30–40°N. As mentioned earlier, the weakness in this method is that the satellite sensors do not adequately probe the lowermost regions of the atmosphere, so the method is insensitive to changes in UV-absorbing pollution in the boundary layer of the atmosphere.

The average all-sky changes in erythemally weighted irradiance are more similar at higher latitudes in both hemispheres: 3.1% at 50°N, near the Canadian border, and 5.2% at 50°S latitude near the southern tip of South America. In the SH, changes in cloud transmission partially offset the clear-sky increase. The zonal average irradiance increases vary locally and regionally because of different amounts of local cloud and aerosol cover.

Figure 2-20 shows the monthly percent change in erythemally weighted irradiance, caused by ozone, from 1979 to 2008. Erythemally weighted irradiance has increased dramatically at higher latitudes in the SH and moderately elsewhere. In the SH spring (October and November) the increases are similar to the NH spring (April and May) changes and are about 5% to 7% at 40° to 45° latitude. However the SH summer changes in December to February are much larger than in the NH (June to August) at latitudes >40°. The major population centers in middle and southern South America, Southern Africa, Australia, and New Zealand experience significant increases in erythemally weighted irradiance compared to 30 years ago. The increases have occurred during most of the spring and summer when the solar UV irradiance

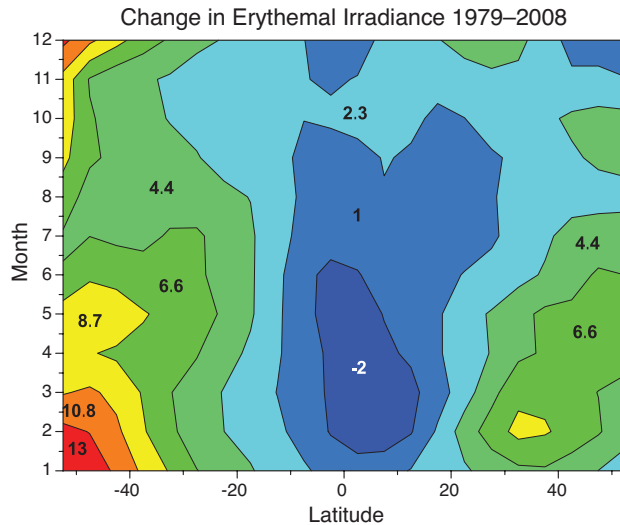


Figure 2-20. Percent change for erythemally weighted irradiance caused by changes in ozone amount for the period 1979 to 2008 as a function of latitude and month. From Herman (2010).

exposure is at a maximum (more clear days as well as seasonally declining ozone going into the summer).

2.3.4.4 CONSISTENCY OF UV ESTIMATES FROM OBSERVATIONS, RECONSTRUCTIONS, AND SATELLITE DATA

Since most of the ground-based UV measurement records are relatively short, they are not suitable for validation of long-term UV trends derived from satellite data. Long-term records of reconstructed data have to be used instead. Figure 2-21 shows summertime daily erythemally weighted doses estimated from ground-based UV measurements, ground-based reconstructions, and satellite estimates for the Northern Hemisphere (May–August) and the Southern Hemisphere (November–February). The comparison was limited to the summertime to avoid conditions with snow on the ground, when satellite estimates are unreliable. In general, satellite estimates are able to reproduce year-to-year variability, although there is a substantial bias between them and ground-based measurements and reconstructions (discussed in Section 2.3.3.3). Linear trend estimates for the period 1980–2003 from ground-based reconstructions and TOMS satellite estimates show a substantial difference between individual sites that reflects the importance of local conditions, and is well captured by both data sets. The average of four linear trend values for seven European sites shown in Figure 2-21 is $4.8\% \pm 1.7\%$ per decade for the reconstructed data and $5.0\% \pm 1.4\%$ per decade for satellite estimates (the uncertainties represent the 95% confidence level of the average of trend values at

individual sites). While satellite estimated irradiance data has a positive bias compared to ground-based data, this does not influence trend detection if the bias is consistent over time. The agreement between independent methods of measurement and trend analysis in Figure 2-21, and discussed in Section 2.3.3.3, implies that at least for the European sites explored, this is the case.

It should be noted that summertime trends over seven European sites with reconstructed data from Figure 2-21 are noticeably larger than those over Toronto, Lauder, and two Japanese stations and substantially larger than trends in zonal mean UV radiation over northern midlatitudes shown in Figure 2-19 (about 4% over the 1979–2008 period). This is likely due to long-term changes in the cloud cover over Europe. The mean trend over the same seven stations (Sodankyla is excluded to avoid snow influence on satellite estimates) is $4.3\% \pm 0.9\%$ per decade for all atmospheric conditions, but the UV trend due to ozone is only $1.5\% \pm 0.4\%$ per decade or about 4% over the entire period (see den Outer et al., 2010, their Table 6, for the trend values at individual sites), which is in line with satellite estimates from Figure 2-20.

2.4 INTERPRETATION OF OBSERVED OZONE CHANGES

The focus of this section is to interpret the observed ozone changes reported earlier in the chapter. This is accomplished primarily through comparisons of observations with simulations produced by chemistry-climate models (CCMs). These models couple the general circulation of the atmosphere with a photochemical mechanism using the latest available evaluation of chemical reaction rates and photolysis cross sections (e.g., JPL 06-2). Eighteen of these models were extensively compared with each other and with data in the second Chemistry-Climate Model Validation (CCMVal) exercise documented in SPARC CCMVal (2010). The models all produced simulations of the past, the future, and a present-day time slice. One of the models included a coupled ocean and some had interactive tropospheric chemistry. Most, but not all, simulated the 11-year solar cycle. Most also simulated the response to large enhancements of aerosol surface area following the eruptions of the El Chichón and Mt. Pinatubo volcanoes.

2.4.1 State of Science in 2006

WMO (2003) concluded that chemistry-transport models (CTMs) including observed changes in halocarbons, other source gases, and aerosols captured the long-term behavior of ozone in the midlatitudes. This conclusion, repeated in WMO (2007) following examination of

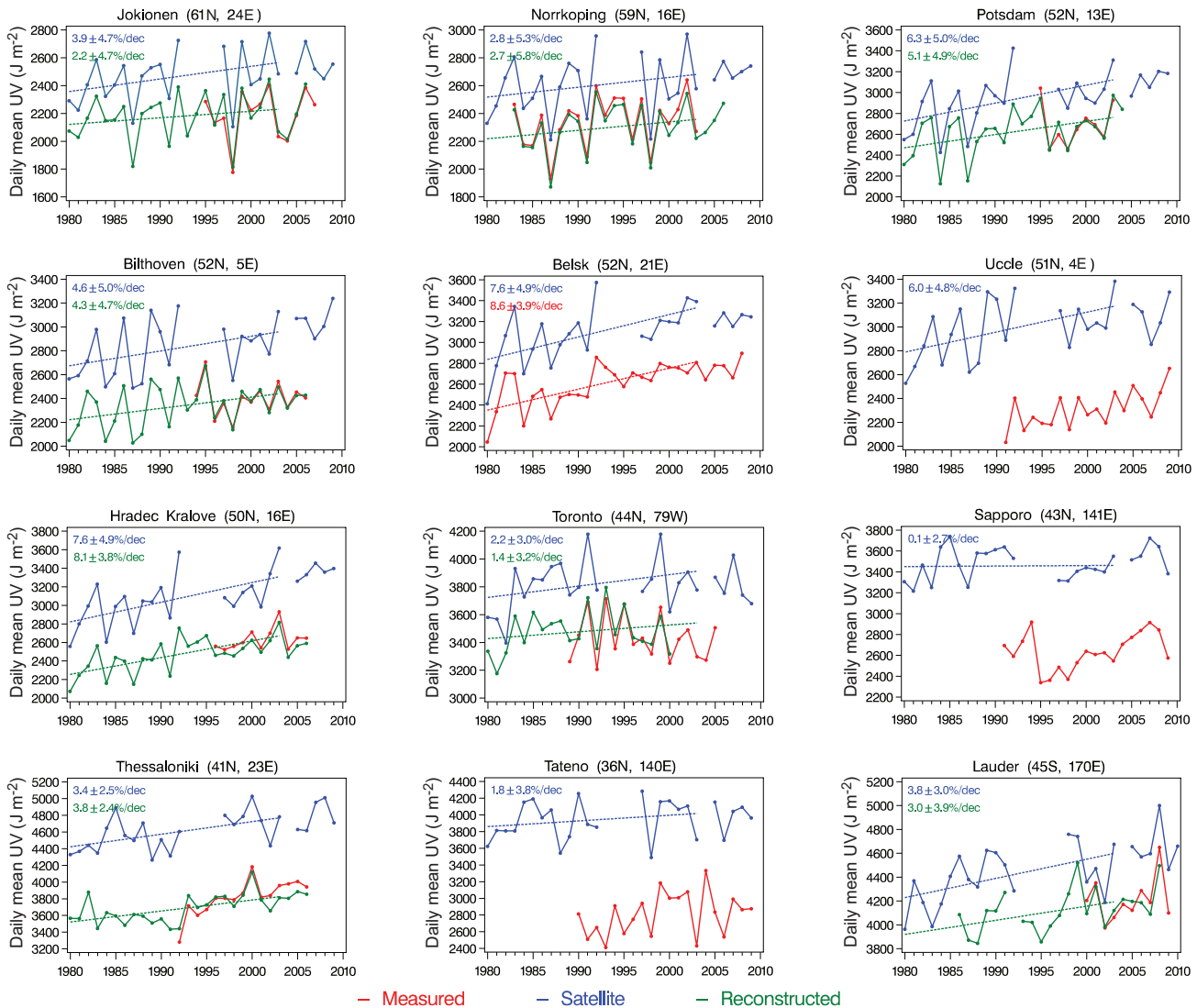


Figure 2-21. Summertime (May–August for NH and November–February for SH) mean daily erythemal UV doses (joules per square meter) from ground-based UV measurements (red), ground-based reconstructions (green), and satellite estimates (blue). The dashed lines show the linear trends for 1980–2004 calculated from reconstructions (green) and satellite estimates (blue). The derived trend values in percent per decade are also shown.

four additional years of measurements and analyses, was based on the faithful representation of general features of the observed ozone changes as functions of latitude, altitude, and season obtained from a suite of models (both CTMs and CCMs).

WMO (2007) pointed out unresolved issues relating to deficiencies of then-current models. These include (1) the failure of models to reproduce the difference between observed southern and northern middle latitude ozone trends; (2) the consistent simulation of a Southern Hemisphere effect of the Mt. Pinatubo aerosols on ozone contrary to observed ozone behavior; and (3) worse comparisons of upper atmospheric ozone trend derived from observations with trends produced by models with tem-

perature feedback than from models without this important process. The models used in WMO (2007) did not include a contribution from short-lived bromine compounds, perhaps leading to an underestimate of the decline in ozone following injection of volcanic aerosols into the stratosphere. Finally, although reproduction of the vertical structure of the solar cycle variation of ozone could be an important critical test of models, observational uncertainties made this test of limited value.

WMO (2007) noted increased evidence that changes in atmospheric dynamics had a significant influence on ozone over the northern midlatitudes on decadal time-scales. WMO (2007) concluded that changes in tropospheric and stratospheric dynamics were partially respon-

sible for both the ozone decline up to the mid-1990s and for the increase after that time.

2.4.2 Updates to Kinetic and Photochemical Data

There have been many revisions to JPL 02-25 (Sander et al., 2003) in chemical rate coefficients, photochemical parameters, and estimated uncertainties reported in JPL 06-2 (Sander et al., 2006) and JPL 09-31 (Sander et al., 2009). These do not result in major changes in our understanding of the response of stratospheric ozone to release of ozone-depleting substances. Recent developments in kinetic parameters of importance to polar ozone chemistry are discussed in Section 2.2.2.

2.4.2.1 UPDATE FROM JPL 2002 TO JPL 2006

An important difference between JPL 02-25 and JPL 06-2 is revision of the recommended rates for reactions of excited-state oxygen atoms $O(^1D)$ with molecular nitrogen (N_2), nitrous oxide (N_2O), H_2O , and methane (CH_4) based on several laboratory studies. Dunlea and Ravishankara (2004) show that the revised rate coefficient for $O(^1D) + H_2O$ reduces the production rate of hydrogen radicals in the stratosphere by 10–15% compared to the 2002 rate coefficient recommendation.

JPL 06-2 introduced the reaction of $O + BrONO_2$ for the first time in the NASA evaluation using data from Soller et al. (2001). Sinnhuber et al. (2002) and Salawitch et al. (2005) showed that including this reaction in chemical models increases the daytime bromine monoxide/total inorganic bromine (BrO/Br_y) ratio by about 20%. The presence of a greater fraction of inorganic bromine in radical form increases the sensitivity of ozone to halogens as well as the contribution of bromine to EESC (Section 1.4.4). The CCMVal-2 comparison (Section 2.4.3.5) shows that many CCM groups did not add this reaction when adopting JPL 06-2 kinetics (Chapter 6 of SPARC CCMVal, 2010). Including this reaction also impacts the amount of Br_y inferred from measured BrO , one method for estimating the impact of very short-lived bromocarbons on the stratospheric bromine budget. The photochemical models used in this Assessment to estimate Br_y from BrO have all included this reaction (Chapter 1, Table 1-14).

The most notable impact of kinetics changes between JPL 02-25 and JPL 06-2 is likely to be the increase in the computed BrO/Br_y ratio. Other reaction rates constants updated in JPL 06-2 include reactions of chlorine atoms (Cl) with hydrochlorofluorocarbons (HCFCs) and hydrofluorocarbons (HFCs); the hydroperoxyl radical (HO_2) self-reaction; OH reactions with oxygenated organics; the yield of pernitrous acid ($HOONO$) from $OH + NO_2$

+ M and $HO_2 + NO_2 + M$; and the photochemistry for a number of organic carbonyl compounds. WMO (2007) used the kinetic evaluations from JPL 02-25 with a few updates. To our knowledge there are no published estimates of the impact on global ozone of the change from JPL 02-25 kinetics to JPL 06-2 kinetics.

2.4.2.2 UPDATES SINCE JPL 2006

$O(^1D)$ Reactions

Additional studies (Carl, 2005; Takahashi et al., 2005; Dillon et al., 2008; Vranckx et al., 2008) have led to a further revision in the recommended $O(^1D) + N_2O$ and CH_4 reaction rate coefficients in JPL 09-31. Recent simulations using the NASA Goddard two-dimensional (2-D) model described by Fleming et al. (2007) show a 1 part per billion by volume (ppbv) increase in NO_y (~8%) due to the increase in the recommended rate coefficient for $O(^1D) + N_2O \rightarrow 2NO$. Atmospheric measurements do not differentiate between these results. The same 2-D model also produces a 10–12% deeper minimum in the Antarctic springtime ozone with the JPL 09-31 rates versus JPL 06-2, with about half of the difference due to the change in the $O(^1D) + N_2O$ reaction rate coefficient.

$HO_2 + NO$

Laboratory studies by Butkovskaya et al. (2007, 2009) examined the reaction product yields of the $HO_2 + NO$ reaction, reporting that the yield of the HNO_3 product increased at lower temperature (223–323 K) and higher pressure, 72–660 Torr (96–880 hPa), and in the presence of water vapor. Cariolle et al. (2008) tested the impact of the updated reaction rate coefficient on the HNO_3 formation from the $HO_2 + NO$ reaction using 2-D and 3-D models and found a significant impact on nitrogen oxides (NO_x) and odd hydrogen (HO_x) in the free troposphere and O_3 abundance in the troposphere at low latitudes. They found only small changes in minor species distributions in the stratosphere.

$ClO + HO_2$

JPL 09-31 revised the recommendation for the rate constant for the reaction $ClO + HO_2$ based on the new laboratory study by Hickson et al. (2007). The revised rate constant has been increased by 25% at room temperature and by 37% at 200 K. Kovalenko et al. (2007) showed that atmospheric measurements of hypochlorous acid ($HOCl$) obtained by several balloonborne instruments are consistent with a value for the $ClO + HO_2$ rate constant considerably larger than values recommended by JPL 06-2 or reported by Hickson et al. (2007). Kovalenko et al. (2007) also showed

good agreement between measured and modeled HOCl using the older rate constant measurement of Stimpfle et al. (1979), which was weighted more heavily in recommendations prior to JPL 02-25. Comparison of measured and modeled HOCl serves as a proxy for the rate of ozone loss by the ClO + HO₂ cycle, which is often the dominant halogen loss process in the midlatitude lower stratosphere. Kovalenko et al. (2007) suggest that models underestimate ozone loss by this process because models using this kinetic input commonly underestimate observed HOCl.

2.4.3 The Distribution and Variability of Stratospheric Ozone and Their Representation in Models

The detection and attribution of trends in ozone depend on both long-term changes in ozone and on the variability of ozone. In Section 2.1, it was noted that ozone concentrations over the last decade or so remained more or less constant. A central problem is attributing these changes to causes such as dynamical variability, long-term climate change, decreasing ODSs, or the changing phase of the solar cycle.

WMO (2007) relied on 2-D models, 3-D CTMs, and CCMs, a mix of models that included and excluded radiative feedback. The current Assessment makes near-exclusive use of 3-D CCMs because they represent the state of the art of our understanding of the physical and chemical processes controlling atmospheric composition. These models have been developed significantly over the last four years. Recently their radiative, dynamical, chemical, and transport processes have been subjected to extensive evaluation using a wide range of diagnostics derived from observations (SPARC CCMVal, 2010). Understanding the mean ozone distribution and ozone variability requires not only analyses of observations but also evaluations of the processes that control the mean distribution and variability found in models.

The following sections summarize some of the key conclusions drawn from extensive evaluations of the 18 CCMs presented in the SPARC CCMVal report (2010). Table 3-1 of Chapter 3 gives a description of the CCMs.

2.4.3.1 ANNUAL CYCLE AND NATURAL VARIABILITY

Stratospheric ozone is known to vary in response to natural factors, such as the QBO, El Niño-Southern Oscillation (ENSO), variations in transport associated with the Brewer-Dobson circulation, and dynamical variability associated with the annular modes. Ozone observations have demonstrated variations on many spatial and temporal scales. Diagnostics for each of the different sources of natural variability in stratospheric ozone have

been applied to the chemistry-climate models participating in this Assessment. The relative importance of the different sources of natural variability in stratospheric ozone has been assessed using multiple linear regression. When possible, the connection between the sources of natural variability and ozone has been addressed by analyzing the processes that determine it. Understanding and quantifying the underlying natural ozone variations are necessary to quantify the impact of anthropogenic perturbations of the ozone layer and to make reliable predictions of future ozone abundances.

The annual cycle is a forced variation of the atmosphere that is reflected in ozone concentrations. Figure 2-22 (panels a and b) shows the annual cycle in ozone concentration at 1 hPa for 40°S and 40°N derived from MLS data compared to the annual cycles calculated by CCMs. Figure 2-22 (panels c and d) shows the annual cycle also at 72°S and 72°N calculated in the lower stratosphere at 46 hPa. The vertical and latitudinal distribution of the annual cycle in stratospheric zonal monthly-mean ozone is well represented in stratosphere- and mesosphere-resolving models with a few outstanding issues. In the lower stratosphere, models tend to have a late occurrence of the polar ozone depletion (Antarctic ozone hole, Figure 2-22c). In the upper stratosphere (Figure 2-22a) the zonal mean MLS data at 40°S show an interesting peak in May and June for three of the four years that is not reproduced by models. SBUV data show a similar peak.

Model simulations reproduce many of the key features of the observed interannual variability of column ozone. All models show the expected minimum in polar variability in the summer season. However, in the NH dynamically active period, most of the models underestimate the interannual polar ozone variability. In the SH some models overestimate while others underestimate interannual variability in ozone.

Most models reproduce the connections between the dynamical processes responsible for the interannual polar ozone variations and the ozone response. Models with poor performance in interannual polar variability also tend to perform poorly in the diagnosed dynamics-ozone connections. There are various techniques that use observations to cause a model to produce a QBO. These improve simulated ozone variability. However, there are biases in the amplitude of the QBO ozone signal from these simulations that are comparable to biases for models with internally generated QBO signals.

2.4.3.2 SOLAR CYCLE

Here we update the extensive discussion of the relationship between ozone and solar radiation associated with the 11-year solar cycle and the 27-day solar rotation period given in WMO (2007). Variations of total ozone

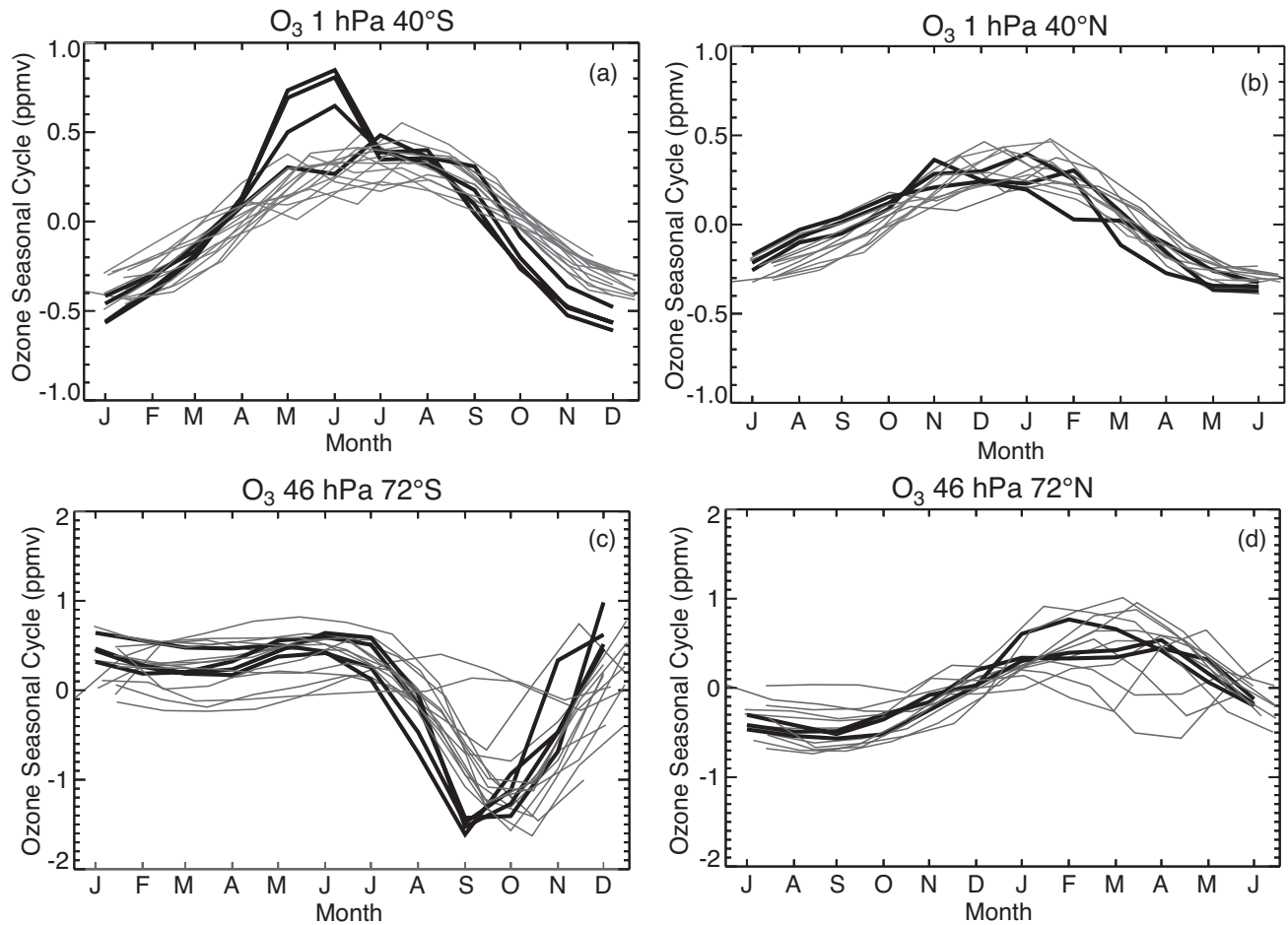


Figure 2-22. (a) and (b): Ozone seasonal cycle (in parts per million by volume) from MLS data at 1 hPa compared to models at 40°S and 40°N. (c) and (d): Same but for 46 hPa and 72°S and 72°N. Heavy lines are MLS data for each of four years (2005–2008); light lines are from models. Adapted from Figure 8.2 in Chapter 8 of SPARC CCMVal (2010).

column in phase with the solar cycle of 2–3% were reported, along with the stratospheric ozone profile response as a function of latitude. The detailed mechanism to explain the ozone response observed in the lower stratosphere remained uncertain. The following updates the discussion of the vertical structure of the tropical solar response given in WMO (2007) using additional observations and model results (see also Gray et al., 2010).

Recent analysis of the CCMVal models shows that although the 11-year solar cycle in column ozone is reproduced by the models, the amplitude of the response varies among models. Differences in radiation, photolysis, and transport all contribute to the spread in response. The latitudinal dependence of the solar response in column ozone derived from observations compares better with that derived from present models than earlier studies (Austin et al., 2008). The large spread at mid to high latitudes is due

to large interannual variability and limits the discussion of extratropical signals.

Recent observational studies using ground-based and satellite data sets agree with previous results, reporting ozone variations in phase with the 11-year and 27-day solar cycle in the upper stratosphere (e.g., Fioletov, 2009; Remsberg, 2008) and the lower stratosphere (e.g., Tourpali, et al., 2007; Sitnov, 2009). Similarly, the vertical structure of the solar signal in SAGE I and II data (Randel and Wu, 2007) shows a maximum response in the tropical upper stratosphere, a smaller (statistically insignificant) response in the middle stratosphere (~30–35 km), and a secondary maximum in the tropical lower stratosphere. This structure of the stratospheric ozone response in the tropics is supported by analysis of ground-based Umkehr measurements at the Mauna Loa station (Tourpali et al., 2007).

The QBO complicates the statistical detection of the solar signal. Smith and Matthes (2008) found that the presence of a QBO in their simulation could contaminate the detection of the solar signal when 2–4 solar cycles were included in the analysis. The near coincidence of the El Chichón and Mt. Pinatubo volcanic eruptions in 1982 and 1991 with two solar maxima also complicates the quantification of solar signals derived from data. Thus, there is still uncertainty in quantifying the solar cycle by statistical analysis from observations, particularly in the lower stratosphere. Chapter 8 of SPARC CCMVal (2010) finds that the direct solar response in temperature and ozone in the upper stratosphere is well represented, but the vertical structure in the tropics below 10 hPa varies considerably among the models and between models and observations. Chapter 8 also notes large uncertainties in the middle to lower stratosphere that are the result of short observational records, possible aliasing of signals from QBO and volcanoes, as well as possible nonlinear interactions of the solar cycle signal with QBO, ENSO, and volcanic signals.

Recent model analyses show an improved representation of the vertical distribution of the solar signal in ozone in the tropics as compared to WMO (2007). However, reasons for the better agreement in the 2-D and 3-D models are still under discussion and conflicting explanations for the tropical solar ozone response in the lower stratosphere are presented. Austin et al. (2008) noted that models participating in the first CCMVal exercise reproduced the observed vertical structure of the stratospheric tropical solar ozone signal, although the magnitude of the response was smaller than derived from observations. Climate forcings, including observed sea surface temperatures (SSTs) as well as time-dependent solar cycle forcings, were considered essential to simulating this response. Neither the QBO nor the upper atmospheric effects of energetic particles were found to be necessary to explain the observed solar cycle response of ozone or temperature. Large discrepancies among the models and a small (insignificant) solar signal found in the tropical lower stratosphere in models that did not include solar forcing suggest possible influences from other processes (SST variations and aliasing between the signals) or from random variability in the records (Austin et al., 2008).

Schmidt and Brasseur (2006) used the Hamburg Model of the Neutral and Ionized Atmosphere (HAMMONIA) to simulate the difference between solar maximum and solar minimum. They produced a solar signal in the tropical lower stratosphere using climatological sea surface temperatures and a repeating solar cycle. This solar signal is independent of the presence of a self-consistently produced QBO (Schmidt et al., 2010). Tsutsui et al. (2009) found a small, not significant (0.6%) solar cycle response of ozone in the tropical lower strato-

sphere in a simulation using the Whole-Atmosphere Community Climate Model (WACCM) forced with climatological SSTs and a time-varying solar cycle. However, McCormack et al. (2007) highlight the importance of the presence of a QBO for the solar signal in tropical ozone in their 2-D model simulations. Their internally generated QBO is itself modified by the solar cycle. Additional complications arise from aliasing between ENSO and the solar cycle in the tropical lower stratosphere (Marsh and Garcia, 2007). Recent statistical analysis applied to observations and model simulations includes a proxy term that accounts for ENSO variations (Randel et al., 2009; Chapter 8 of SPARC CCMVal, 2010).

In summary, the upper stratospheric ozone response (2–3% between solar minimum and solar maximum) is reproduced by the CCMVal models and is a direct radiative effect of heating and photochemistry. The lower stratospheric solar cycle in tropical ozone appears to be caused indirectly through a dynamical response to solar ultraviolet variations. The origin of such a dynamical response to the solar cycle is not fully understood.

2.4.3.3 VOLCANIC AND AEROSOL EFFECTS

Sulfate volcanic aerosols affect stratospheric circulation and temperature, provide surfaces for chemical heterogeneous reactions, and lead to ozone depletion (Hofmann and Solomon, 1989). The aerosols produced by Mt. Pinatubo, which erupted in June 1991, decayed by 1996. No major volcanic eruptions have occurred between 1996 and present, but efforts to quantify fully the effects of volcanic aerosols on stratospheric ozone continue, in part due to the importance of quantifying potential effects of continuous injection of sulfur into the stratosphere that has been discussed as a “geoengineering” approach to counteract global warming from increased greenhouse gases (e.g., Crutzen, 2006; Rasch et al., 2008). Geoengineering is discussed further in Section 3.2.6 of Chapter 3.

1-D, 2-D, and 3-D models have been used to determine the chemical and dynamical effects of volcanic aerosols (e.g., Zhao et al., 1995; Tie et al., 1994; Stolarski et al., 2006). The polar vortex strengthens in NH after a volcanic eruption because of the changes in the equator-to-pole temperature gradient in the lower stratosphere (Stenchikov et al., 2002). A stronger polar vortex increases the probability of formation of polar stratospheric clouds, thereby enhancing the rate of heterogeneous chemical destruction of stratospheric ozone (Tabazadeh et al., 2002). The effects on stratospheric ozone depletion in the wake of a volcanic eruption are largest when chlorine and bromine levels are largest (Tie and Brasseur, 1995). The surface area density (SAD) of sulfate aerosols in models, the crucial input parameter to simulate this aspect of ozone depletion,

is usually prescribed based on observations. Comparisons of simulations with observations suggest that there are no significant missing processes or greatly inaccurate reaction rates (e.g., Fahey et al., 1993; Dessler et al., 1997).

Analysis of CCMVal-2 models (SPARC CCMVal, 2010) shows that the simulated post-eruption changes in total column ozone are well correlated with changes in lower stratospheric chlorine monoxide. Although most models use the same aerosol SAD data set to drive the anomalous post-eruption chemistry, the sensitivity to aerosols and the background SAD values differ among models, leading to different amounts of chlorine activation and associated ozone loss. Mäder et al. (2007) used statistical analysis of total ozone data from 158 ground stations to show that the SAD had the largest impact on the decrease of total ozone in the Northern Hemisphere. This is consistent with the conclusions in WMO (2007) that the Mt. Pinatubo aerosols appeared to have a stronger effect on ozone in the Northern Hemisphere than in the Southern Hemisphere.

Telford et al. (2009), using a nudged CCM (UK Chemistry and Aerosols (UKCA)) simulation, concluded that the depletion of stratospheric ozone was produced mainly as a result of photochemical changes due to heterogeneous reactions, but there was some evidence for dynamically induced ozone reduction, especially in the NH midlatitudes. Fleming et al. (2007) found that the interannual dynamical variability in two-dimensional model simulations acts to reinforce the ozone perturbation in the NH midlatitudes, while in the SH the observationally derived circulation mitigates or even cancels the aerosol-induced chemical ozone reactions. Robock et al. (2007), using National Centers for Environmental Prediction (NCEP) and European Centre for Medium-Range Weather Forecasts (ECMWF) analyses and Goddard Institute for Space Studies (GISS) Model E, and Feng et al. (2007), using a 3-D CTM, did not find a clear signal of chemical ozone loss in the SH midlatitudes after the eruption of Mt. Pinatubo. In contrast Brunner et al. (2006), using Candido Assimilated Three-dimensional Ozone (CATO), demonstrated a significant effect of volcanic aerosols on ozone in SH mid (south of about 45°) and high latitudes. In summary, observations and model simulations found a significant effect of Mt. Pinatubo volcanic aerosols on stratospheric ozone in the NH compared to the SH. The absence of a stronger observation of ozone loss in the SH is not yet understood.

Polar ozone is also sensitive to volcanic enhancement of stratospheric aerosols. There have been no new findings on this subject since WMO (2007), but results are summarized here due to the potential importance of an increase in stratospheric aerosols through geoengineering as discussed above and in Section 3.2.6. Studies of the Arctic winter 1991/1992 consistently find enhanced polar ozone loss due to the presence of Mt. Pinatubo aerosol

(Rex et al., 2004; Tilmes et al., 2008b) although the quantitative estimates of the volcanically induced signal differ. Further, Portmann et al. (1996) showed that Antarctic ozone depletion in the 1980s and early 1990s was influenced by enhanced sulfate aerosol SAD, and speculated that the ozone hole might have been detected later than the mid-1980s if there had been no increase in aerosol loading from El Chichón and several earlier minor eruptions. Portmann et al. (1996) also suggested that future Arctic ozone depletion could be severe in unusually cold winters with large volcanic aerosol SAD present. Several studies attempt to discern the effects of volcanic aerosol perturbations on PSC characteristics (Deshler et al., 1994; David et al., 1998; Fromm et al., 2003). These studies are inconclusive, largely because it is much more difficult to distinguish PSCs – especially STS – when the background (non-PSC) sulfate aerosol level is elevated and varies temporally.

As noted above, there have been no recent major volcanic eruptions, but there is evidence that the background stratospheric aerosol layer is changing. Hofmann et al. (2009b) analyzed ground-based measurements to show that stratospheric aerosol amount exhibits an increasing trend since 2000, attributing the background stratospheric aerosol since 2002 to an increase in the SO₂ emissions caused by an increase in global coal consumption, mainly in China. Hofmann et al. (2009b) estimate the contributions to the increase in the stratospheric aerosol from major volcanic activity and from increased tropical upwelling due to change in the Brewer-Dobson circulation, concluding that these are not significant. However, analysis of observations from the Cloud-Aerosol Lidar with Orthogonal Polarization (CALIOP) suggests that small volcanic eruptions may play a role. CALIOP data show significant changes in aerosol concentration in the tropical stratosphere between 2006 and 2008 (Vernier et al., 2009). CALIOP data showed slow ascent of the Soufriere plume in 2006 from 20 to 25 km, consistent with the Brewer-Dobson circulation and remnants of aerosols from minor volcanic eruptions such as Manam in 2005. Quantitative attribution of the sources of the observed change in background aerosols has not been accomplished.

2.4.3.4 EVALUATION OF SIMULATED TRANSPORT

The evaluation of transport emphasizes the model ability to reproduce observations that are directly related to large-scale physical processes affecting ozone distribution, such as tropical ascent and Antarctic vortex isolation. The reader is referred to Chapter 5 of the SPARC CCMVal (2010) report for detailed evaluation of individual models.

The distributions of long-lived trace gases in the stratosphere are controlled by transport processes, mainly

by the balance between the diabatic circulation and quasi-horizontal mixing (e.g., Holton, 1986). Transport affects the ozone distribution directly and indirectly. In the lower stratosphere ozone is long lived, and large-scale transport from source regions is important to its spatial and temporal distribution. Transport affects ozone indirectly by determining the mixture of chemicals that affect ozone loss at a given location. In Chapter 5 of SPARC CCMVal (2010), diagnostics for circulation and mixing were developed from observations and applied to CCMs. These evaluations identified key processes essential for realistic transport. Chapter 5 concluded that for the credible prediction of future stratospheric composition, the following transport requirements are essential: (1) realistic tropical ascent in the lower stratosphere; (2) realistic mixing between the tropics and extratropics in the lower and middle stratosphere; (3) generation of an isolated lower stratospheric Antarctic vortex in spring; (4) local conservation of chemical family mixing ratios (e.g., Cl_y); and (5) good agreement on all mean-age diagnostics. A summary of the performance of participating CCMs on these criteria is given below.

An adequate tracer advection scheme must conserve chemical families such as total inorganic chlorine (Cl_y) for credible predictions of future ozone levels. Conservation of Cl_y means that models should not produce higher levels of Cl_y in the upper stratosphere than released in the form of organic chlorine at the surface. Three CCMs failed to conserve total chlorine, undermining their credibility for assessment of ozone trends due to chlorine. A fourth model had excess stratospheric chlorine due to insufficient tropospheric removal of hydrogen chloride (HCl).

For more than a decade, model transport has been evaluated using comparisons of simulated and observationally derived mean age at 50 hPa in the midlatitudes and tropics (e.g., Hall et al., 1999; Eyring et al., 2006). These comparisons revealed several issues with model transport. However, at 50 hPa, age distributions computed by many models participating in CCMVal-2 compare well with those derived from observations even though other diagnostics reveal persistent transport issues. The average mean age diagnostic (AMA) was developed in the SPARC CCMVal (2010) report to broaden the comparisons with observationally derived ages in order to assess a model's overall transport fidelity. AMA is based on mean age comparisons at seven locations in the lower and middle stratosphere between 60°S and 60°N. The mean age is a sensitive function of both the circulation and mixing, and the distribution of mean ages throughout the stratosphere reflects the balance between them, which varies as a function of height. While compensating errors in ascent and quasi-horizontal mixing can result in good mean age in some altitudes, it is unlikely that a model will have perfectly balanced compensating errors in both

the lower and middle stratosphere, making the AMA diagnostic a more stringent test of transport than mean age at 50 hPa alone.

Although AMA is a strict diagnostic, fortuitous agreement with mean ages derived from observations is possible because excessive recirculation increases mean age while a fast circulation decreases it. Together they can produce compensating transport errors. It is therefore important to independently assess both the circulation and mixing in models. Significant problems with tropical stratospheric transport have been identified in half of the 18 participating CCMs. Tropical ascent and tropical-midlatitude (T-M) mixing across the subtropics are crucial to distributing ODSs in the stratosphere, and deficiencies in the transport of ODSs affect modeled abundances of the products of ODS destruction (Cl_y) everywhere. Ten of the 18 CCMs were found to have realistic ascent in the tropical lower stratosphere. Of the remaining eight, two models showed a very slow circulation, while six had faster-than-observed ascent rates. T-M mixing, essentially a measure of the degree of isolation of the tropics, was evaluated using as many as four diagnostics in the lower and middle stratosphere. Nine of the ten CCMs with realistic ascent rates also showed reasonable mixing across the subtropics. Of the other nine models, the two models with slow circulations had too little T-M mixing while the other seven showed too much mixing between the tropics and midlatitudes. Strong T-M mixing increases the simulated mean age by allowing older midlatitude air to re-enter the tropics and recirculate through the stratosphere, increasing mean age everywhere. The wide range of independent observations from which the diagnostics are derived strengthens the usefulness and credibility of these evaluations.

Other essential transport processes for simulation of the ozone response to changing chlorine levels are strong descent in the southern winter vortex and the presence of a barrier to mixing between the vortex and midlatitudes in early spring in the Antarctic. Chapter 5 of SPARC CCMVal (2010) showed that vortex isolation is uncorrelated with the AMA, tropical ascent, and T-M mixing and therefore must be evaluated in addition to the other circulation and mixing diagnostics. Of the nine models showing both good tropical ascent and T-M mixing, seven also showed realistic, isolated descent at the end of austral winter. Lower stratospheric vortex isolation in spring, which is crucial to maintaining the high levels of Cl_y necessary for a credible ozone hole, was found to be sufficient in only eight of 18 CCMs. Of the eight CCMs producing an isolated vortex, only four also showed realistic tropical ascent, T-M mixing, average mean age, and polar descent. Those models are CMAM, GEOSCCM, UM-SLIMCAT, and WACCM. (See Table 3-1 of Chapter 3 for descriptions of the CCMs.)

2.4.3.5 EVALUATION OF THE CHEMICAL MECHANISM AND ITS IMPLEMENTATION

Chapter 6 of CCMVal-2 (SPARC CCMVal, 2010) presents the first major attempt at quantifying the behavior of stratospheric chemistry modules within various global 3-D CCMs. Eight of the 18 models participating in CCMVal-2 took part in a photolysis intercomparison (PhotoComp). The chemical mechanism within CCMs was evaluated by comparison of radical species output by each CCM to calculations conducted using a benchmark photochemical steady state (PSS) model, constrained by the abundance of long-lived species and sulfate surface area density (SAD) from each CCM. This comparison was conducted for 14 of the 18 groups. Quantitative metrics were developed for both PhotoComp and PSS, based on equation (4) of Waugh and Eyring (2008). Careful attention was devoted to proper definition of uncertainties. The majority of models showed good agreement with the PhotoComp benchmark.

Models showed a range of agreement with the evaluation of fast chemistry, with some models showing very good to excellent representation of both radicals and their precursors. The radicals in some models show significant discrepancies with the PSS benchmark; in some cases the precursors disagree with a suite of atmospheric observations included in the evaluation (Chapter 6, SPARC CCMVal, 2010). The most realistic representations of fast chemistry were found to be provided by the WACCM, EMAC, GEOSCCM, CMAM, and UM-SLIMCAT models (Figure 6.11 of SPARC CCMVal, 2010). Results for these models are highlighted in subsequent figures.

The PSS evaluation provides an important new tool for quantitative evaluation of the chemical mechanism within CCMs based on analysis of archived model output. A particular CCM model has been observed to exhibit a much larger sensitivity of ozone to anthropogenic halogens than any of the other CCMs; the PSS evaluation shows that this sensitivity is the result of omission of the HCl production from $\text{ClO} + \text{OH}$ in their chemical mechanism (Chapter 6 of SPARC CCMVal, 2010). Previously, chemical mechanisms have been evaluated either by exchange of code or by various groups performing prescribed calculations, both of which are arduous tasks.

The comparisons carried out for CCMVal-2 also showed that models used widely varying distributions of sulfate SAD, even for simulations designed to simulate past behavior (Chapter 6 of SPARC CCMVal, 2010). These differences may be due to the specification of the SAD climatology as a function of geometric altitude, a coordinate not commonly used in CCMs.

One notable difference among the various CCMs was the abundance of Cl_y at the tropopause. Some models have near-zero Cl_y ($\ll 50$ parts per trillion (ppt)) while

other models have much larger values ($\gg 50$ ppt). Models with high levels of Cl_y at the tropopause tend to have excess Cl_y throughout the lowermost stratosphere. These differences in Cl_y are likely due to various representations of HCl uptake and removal in the troposphere (Chapter 6 of SPARC CCMVal, 2010). This is an important detail because models with the higher values of Cl_y in the lowermost stratosphere display greater sensitivity to future changes in stratospheric H_2O and temperature than models with near-zero Cl_y .

2.4.3.6 EVALUATION OF SIMULATIONS OF THE UPPER TROPOSPHERE/LOWER STRATOSPHERE

Chemistry-climate models are important for disentangling and quantifying the effects of halogens on ozone from those of climate change. In the upper troposphere/lower stratosphere (UTLS, approximately defined here as the region between 5 and 22 km), dynamical variability and its expected response to climate change are large. The ability of CCMs to represent the basic characteristics of the dynamical and chemical structure of the UTLS has been tested in Chapter 7 of SPARC CCMVal (2010; also see Gettelman et al., 2009; Gettelman et al., 2010). Various characteristics of the tropical and extratropical chemical and dynamical structures have been evaluated using both quantitative and qualitative diagnostics derived from robust relationships found in aircraft and satellite observations, or reanalyses data sets. The tested characteristics include the representation of the tropical tropopause layer, the tropopause inversion layer, the extratropical tropopause transition layer, and the seasonal cycles in tropical cold point temperatures, lowermost stratospheric mass, and tropical and extratropical water vapor and ozone.

Most CCMs represent the basic dynamical and chemical characteristics of both the tropics and the extratropics well. Models mostly reproduce the annual cycle of tropical cold point temperatures in the tropics, with the right amplitude and timing. However, they show some significant biases in the annual mean cold point temperature. Similar findings are found for the representation of the seasonal cycle in ozone. However, amplitude, timing, and mean value of tropical water vapor does not follow the tropical cold point temperature as expected, which indicates errors in transport and/or microphysics in the models.

In the extratropics, the dynamical structure including zonal mean winds, the seasonal cycle in the lowermost stratospheric mass, and the seasonality and latitudinal behavior of the tropopause inversion layer are well captured. This implies that both the climatological distribution of radiatively active species and the radiative transfer in the models are realistic. The models fail to reproduce the observed sharpness in the tropopause inversion layer, most likely due to limited spatial resolution. The seasonal cycles

in ozone and water vapor are generally well reproduced but indicate a too large (small) amplitude at 100 (200) hPa. The models also resolve the strong tracer gradients across the extratropical tropopause, indicating that simulation of the Brewer-Dobson and the tropospheric baroclinic circulations is at least qualitatively realistic. Models that perform particularly well in the extratropics are CMAM, E39CA, GEOSCCM, and WACCM (Chapter 7 of SPARC CCMVal, 2010). Models that perform less well have issues that include insufficient vertical and horizontal resolution or use of a diffusive numerical transport scheme.

Outstanding deficiencies in the models that affect the ozone distribution and introduce uncertainties in UTLS evaluations are the lack of comprehensive representations of tropospheric chemistry involving nonmethane carbons, of wet and dry deposition, and of lightning NO_x . CCMs include varying lightning NO_x parameterizations, however, the most common one dates back to Price and Rind (1992), which has been shown in recent chemistry transport model studies to be inadequate in generating observed NO_x levels in lightning-affected regions in the upper troposphere (Hudman et al., 2007; Sauvage et al., 2007; Parrington et al., 2008).

2.4.4 Recovery Detection and Attribution

Section 2.1 discussed the data obtained over the past decades including a time-series analysis directed toward determining the current stage of ozone recovery as defined in WMO (2007). Here we discuss the problem of attribution of changes in ozone to changes in chlorine and bromine in the stratosphere.

The past evolution of ozone has been influenced by changes in ODSs and also by changes in greenhouse gas (GHG) concentrations. GHGs influence stratospheric ozone in two ways. In the upper stratosphere, cooling due to increased GHG concentrations leads to an ozone increase by slowing the temperature-dependent catalytic loss cycles. In the lower stratosphere where ozone is long-lived, radiatively driven dynamical changes to the Brewer-Dobson circulation that result from increased GHG concentrations affect the ozone distribution through transport. Attribution of past trends is complicated by the need to untangle the effects of the increases and leveling off of ODSs from the effects of continued increases in GHGs. The implications of these processes on the future development of the ozone layer are discussed in detail in Chapter 3 of this Assessment.

2.4.4.1 DYNAMICAL CONTRIBUTIONS TO APPARENT TREND

In addition to the slow trend in ozone expected due to changing GHGs, dynamical variability in short time series of measurements or model simulations can give rise

to an apparent trend. WMO (2007) summarized a number of studies using chemistry and transport models (CTMs) driven by analyzed winds and studies using empirical relations between planetary wave activity and circulation to address the question of dynamical contribution to Northern Hemisphere midlatitude ozone trend. WMO (2007) concluded that about 30% of the observed negative trend from 1979 to the mid-1990s could be attributed to changes in the lower stratospheric circulation based on both empirical and model studies.

Numerous model and observational studies have demonstrated the importance of dynamical contributions to ozone trends. In an extension of previous studies, Feng et al. (2007) used a CTM to show how spurious trends could result from the use of analyzed winds. They concluded that their simulation with nearly constant ODSs could reproduce the increase in NH midlatitude ozone from the 1990s. Brunner et al. (2006) empirically analyzed ozone data to show that the Brewer-Dobson circulation was a dominant contributor to interannual variability at both high and low latitudes. They further showed that this variability accounted for some of the ozone increase seen in the Northern Hemisphere since the mid-1990s. Fleming et al. (2007) used a 2-D model with winds derived from planetary wave forcing derived from ERA-40 and also from NCEP. They found a good fit to the overall ozone column variability from 1979 through 2005 that appears to have a dynamical contribution to both the downward trend between 1979 and the mid-1990s and the upward trend since then. Harris et al. (2008) examined both chemical and dynamical influences on decadal ozone trends, primarily in the Northern Hemisphere. They found that recent increases in ozone were linked to dynamical processes in the lower stratosphere.

Overall, studies agree that dynamical variability contributed to both the downward trend in the NH through the mid-1990s and to the upward trend in total ozone since the mid-1990s. In addition, Fleming et al. (2007) found little impact of dynamical variability on the fit to the EESC curve for the overall time period from 1979 through 2005.

2.4.4.2 GREENHOUSE GAS EFFECTS ON OZONE TRENDS

In addition to the possible trends due to interannual variability, the change in composition due to the increasing GHGs may cause ozone trends through changes in chemistry and dynamics, as noted previously. CCMs consistently predict a strengthening of the stratospheric Brewer-Dobson circulation (BDC) due to climate change (Butchart and Scaife, 2001; Butchart et al., 2006; McLandress and Shepherd, 2009) that leads to changes in the spatial distribution of ozone (Shepherd, 2008; Li et

al., 2009; Hegglin and Shepherd, 2009). Shepherd (2008) showed that CMAM results indicated an eventual recovery to values above 1980 (or 1960) (i.e., super-recovery) in the mid and high latitudes and under-recovery in the tropics. Both Shepherd (2008) and Li et al. (2009) found nearly latitude-independent increases in upper stratospheric ozone due to temperature decreases in CMAM and GEOSCCM, respectively. Both studies also found lower stratospheric ozone decreases in the tropics and increases elsewhere due to the simulated change in the BDC. In CMAM the effects from the upper and lower stratosphere largely cancel in the 60°S–60°N mean total ozone. According to CMAM, total ozone in the tropics will remain below pre-1980 values, whereas in the midlatitudes, and in particular in the NH between 35°N and 60°N, total ozone will increase to values about 5% above pre-1980 levels in the second half of the 21st century. The GEOSCCM calculates lower stratospheric ozone changes that approximately cancel when averaged globally (Li et al., 2009), so that the resulting change in global mean total ozone is dominated by the upper stratospheric ozone increase.

The studies by Shepherd (2008) and Li et al. (2009) showed the combined effect of GHGs and ODSs on stratospheric ozone, but did not quantify past and future changes to changes in ODSs or GHGs. Shepherd and Jonsson (2008) argued that carbon dioxide (CO₂)-induced cooling had masked about 20% of the ODS-induced ozone depletion. Waugh et al. (2009), using calculations from the GEOSCCM to separate the effect of ODSs and GHGs, found that simulated stratospheric ozone changes during the past decades were clearly dominated by ODSs, except for the tropical lower stratosphere. Here the calculated ozone change during past decades due to the increased strength of the BDC (enhanced tropical upwelling) exceeded the calculated effect of ODSs.

CCMs suggest that GHG-induced changes in temperature and in the BDC may partly be responsible for past ozone changes. Therefore, it is important to assess the realism of the simulated circulation changes. Changes in the strength of the Brewer-Dobson circulation have not been unambiguously detected from observations. Engel et al. (2009) have analyzed balloonborne measurements of CO₂ and sulfur hexafluoride (SF₆) over the past 30 years to derive possible trends in stratospheric age of air. They found a small but insignificant increase of the age of air in the midlatitude middle stratosphere, in contrast to the small decrease in age of air due to the increased BDC calculated with CCMs. The results from this analysis can neither confirm nor deny the model results because of the large error bars and shortness of the record (see also Waugh, 2009). Because the simulated change in the BDC is most apparent in the tropical lower stratosphere where the ozone vertical gradient is steep, CCMs predict a change in ozone there that may be detectable in a long, stable time series of observa-

tions. There are significant issues with ozone trends in the tropical lower stratosphere due to insufficient length of the observational record as discussed below in Section 2.4.5.3.

2.4.4.3 POLAR LOSS AND DILUTION TO MIDLATITUDES

WMO (2007) discussed in detail the importance of export of ozone-depleted air from the polar vortices to mid-latitude trends, attributing about 30% (50%) of the northern (southern) midlatitude trends in total ozone for 1979 to 1995 to this process. Results from multiannual simulations are generally consistent with detailed process studies for a few specific years in both hemispheres. Andersen and Knudsen (2006) conclude that longitudinal differences in the export of ozone-depleted air accounts for the longitudinal dependence of winter and springtime ozone trends at northern midlatitudes. The simulation of polar loss and its comparison to data are discussed in Section 2.4.5.4 below.

2.4.5 Simulation of Ozone Changes for the Last Three Decades

Previous sections discussed specific perturbations of stratospheric ozone in current chemistry-climate models. The CCMVal-2 report evaluates these models with a particular emphasis on their representation of processes by comparison to measurements of the current or recent past atmosphere. In this section we consider the ability of these models to reproduce the observed ozone trends over the last three decades by comparison to the data shown in Section 2.1.

2.4.5.1 TOTAL OZONE TRENDS

Figure 2-23 shows the total ozone trend for 1979–1995 as a function of latitude computed by multiple linear regression (MLR) as described in Section 2.1.2. The sensitivity of total ozone to EESC is calculated by applying the MLR to the entire data period (1978–2009), and the trend is shown for the time period during which EESC increased linearly (1979–1995). The models are also fit with EESC from 1978 through the end of the REF-B1 simulation (usually 2004 to 2007). Note that the EESC fit obtained in this manner is more sensitive to the shape of the EESC function than to the length of record (see Section 2.1.2). The models generally reproduce the latitude dependence of the total ozone trend derived from the merged ozone data, but differ in some significant details. Most models produce a negative trend in the tropics while the data show no trend. Red lines are from three models (CMAM, GEOSCCM, WACCM) that rated highest in CCMVal-2 evaluations of transport, photochemistry, and UTLS discussed in

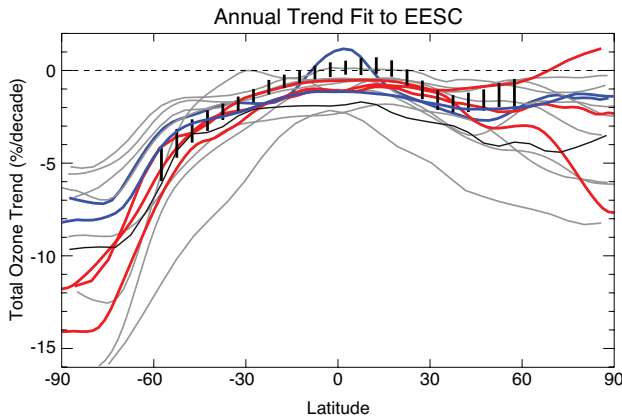


Figure 2-23. Latitude dependence of the annual total ozone trend (%/decade) from 13 of the 18 models used in CCMVal-2 and the merged ozone data set. Trends derived from measurements with 2σ uncertainties are indicated by vertical bars. Red lines are from three models (CMAM, GEOSCCM, WACCM) that rated highest in all three CCMVal-2 tests. Blue lines are from two models (UMSLIMCAT and EMAC) that rated highest in one or two of the three CCMVal-2 tests. Model trends for 1978–1996 are calculated by fitting to EESC using output from 1978 through the end of the REF-B1 simulation. Model descriptions are given in Table 3-1 of Chapter 3.

Sections 2.4.3.4–2.4.3.6 above. Blue lines are from two models (UMSLIMCAT and EMAC) that rated highest in one or two of the three CCMVal-2 tests.

In the southern midlatitudes, with one exception, the model trends vary with latitude in a manner similar to the trend derived from observations, but with significant spread in the magnitude of model trends. A similar spread is found for northern midlatitude trends. The model results show less spread when output beginning in 1960 is used to determine the fit to EESC (not shown), particularly in the north-polar region where interannual variability is large. In the tropics and midlatitudes, the models highlighted as having the best representations of transport, chemistry, or the UTLS generally are more similar to each other than the collection of all model simulations. The same is not true for polar regions. In the tropics most models show a negative trend in total column ozone that does not agree with the trend deduced from either satellite or ground-based data sets. One exception is the EMAC model that has a region of significant positive trend over a portion of the tropics due to an ozone increase in the tropical troposphere; however, the EMAC positive trend disagrees with the trend derived from measurements.

This raises the question of whether the discrepancy in the tropics could be the result of increased tropospheric ozone that is of the same magnitude as the decrease in stratospheric ozone. Most of the models in this comparison do not include tropospheric chemistry or tropospheric physical processes, such as wet and dry deposition and the production of NO_x (and O_3) by lightning. In the tropics, about 10% of the ozone column is in the troposphere. To offset the 1% per decade decrease found in model simulations would require a $\sim 10\%$ per decade increase in tropospheric ozone from the late 1970s through about the mid-1990s. Studies have searched for evidence of a tropospheric trend. Ziemke et al. (2005), using a 25-year record of tropospheric column ozone (TCO) derived from TOMS and SBUV(2) data (1979–2003), showed a zero trend ($\pm \sim 1\text{DU}$ per decade) in the tropics in the Pacific. Beig and Singh (2007) used TOMS data along with the Model for Ozone and Related Chemical Tracers (MOZART) model to derive a trend versus longitude that is negative but insignificant over most of the tropics, but positive and significant over the Indonesian region ($\sim 7\text{--}9\%$ /decade). This trend appears to be the result of large fires in that region leading to ozone increases in the last few years that dominate the change in the record. Clain et al. (2009) derive marginally positive trends from ozonesonde records at Reunion Island (20.8°S , 55.5°E) and Irene, South Africa (25.9°S , 28.2°E). In summary, observational studies to date find no conclusive evidence for a tropospheric O_3 trend large enough to explain the difference between simulated and observed trends in total column ozone, thus the reasons for model disagreement with the observed tropical trend remain a mystery.

Figure 2-24a-d shows the annual average total ozone time series from the merged ozone data set and from each of the CCMs for four regions. The quasi-global average from 60°S to 60°N is shown in Figure 2-24a. In general the models reproduce the overall behavior of the data. The four models showing the best transport representation are highlighted in red and show a smaller difference than the ensemble of all models. Some of the models include forcing due to solar cycle, volcanoes, and QBO while others do not. Although there is a spread in the magnitude of the ozone change from the beginning of the record to the last few years, the models agree with the data that the total ozone has been relatively constant over the last 7–8 years at about 2–4% below 1980 values. The midlatitude time series shown in Figure 2-24b and 2-24d show similar behavior with more variability in the data and among models. Figure 2-24c shows results for the tropics where an apparent solar cycle is prominent in the data and most of the models run below the data, consistent with the trends shown in Figure 2-23.

2.4.5.2 MIDLATITUDE PROFILE TRENDS

In previous Assessments it was noted that 2-D models without temperature feedback showed better agreement with observed ozone trends in the upper stratosphere than models that did include the feedback. The CCMs used here have improved somewhat in this regard. Figure 2-25 and Figure 2-26 show trends deduced from measurements (SAGE, SAGE adjusted SBUV(2), SBUV(2), and ozonesondes) for the northern and southern midlatitudes, respectively. The trends calculated from SAGE for the upper stratosphere have been converted to pressure coordinates and have been adjusted to account for the temperature trend and the accompanying change of altitude at a given pressure level and the conversion of number density

mixing ratio (see Section 2.1.4; Rosenfield et al., 2005). The model results presented in both figures are all from simulations including temperature feedback.

The northern midlatitude simulated trends show a spread in the maximum upper stratospheric depletion that is centered near the trend deduced from data. The red region in Figure 2-25a shows the range of the 3 models with high ratings in each of CCMVal-2 evaluations of the transport, chemistry, and UTLS. The red plus blue regions show the range of those 3 models plus the 3 that were with high ratings in at least one evaluation. The range of deduced ozone trends for these 6 models is narrower than for the entire suite of models (gray shading) and centered near the trend derived from satellite observations. The derived trends from Umkehr measurements are somewhat larger

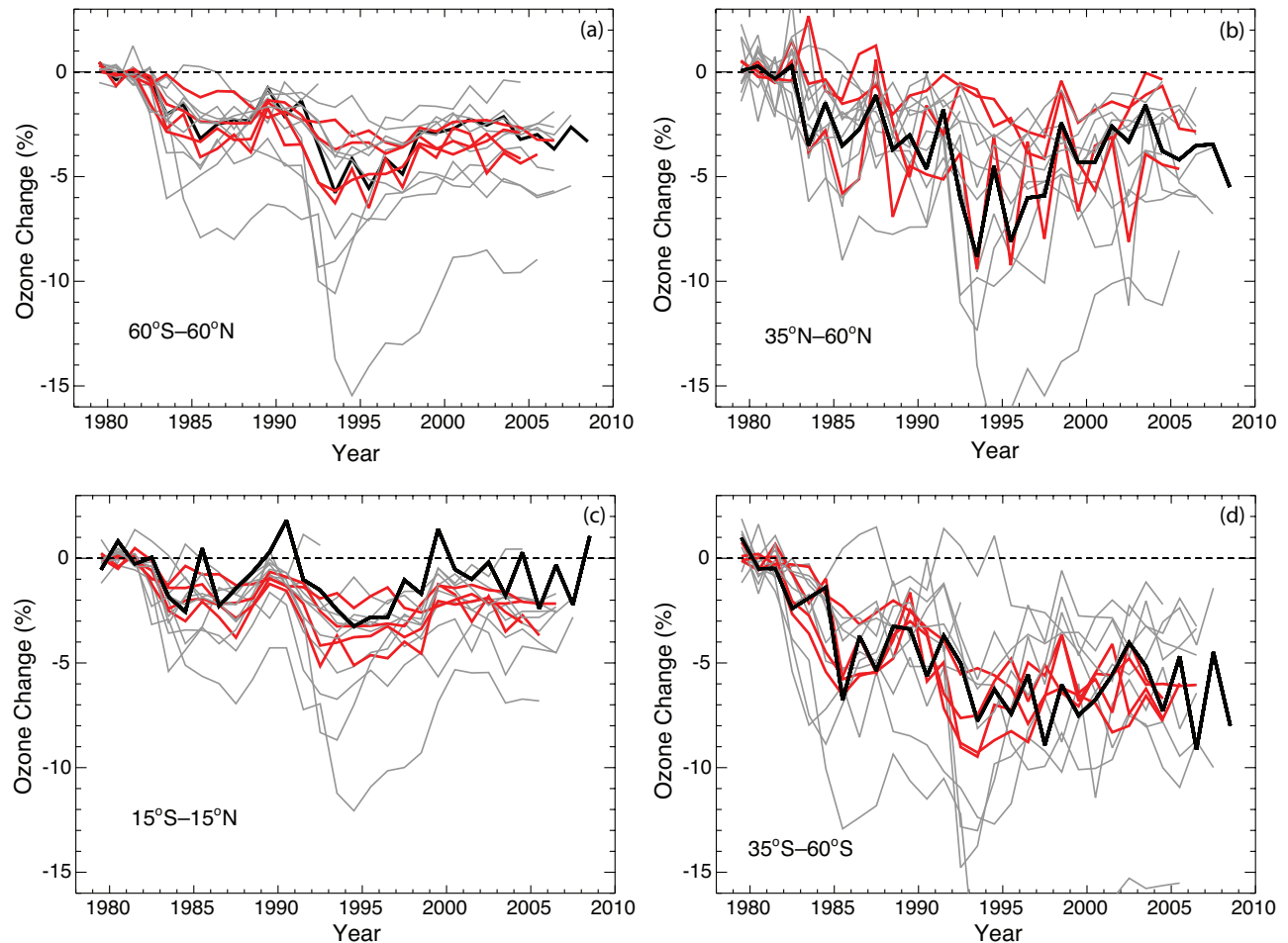


Figure 2-24. (a) Quasi-global time series of annual mean total ozone change (%) from 1980 value calculated from merged ozone data set in heavy black line and from 13 models in lighter lines. Changes in both models and observations are computed relative to the average for 1979–1981. Red lines are results from the four models that rated highest in the CCMVal-2 transport evaluation (CMAM, GEOSCCM, UMSLIMCAT, WACCM). The light gray line with large depletion appears to be an outlier to the rest of the models. (b) Same for northern midlatitudes. (c) Same for tropics. (d) Same for southern midlatitudes.

Figure 2-25. Altitude profile of calculated ozone trend (%/decade) at northern midlatitudes from 17 models. Trends derived from measurements are as defined in Figures 2-4 and 2-7. Panel (a): Trends for the period 1979–1996 are obtained by fitting to EESC. Trends derived from measurements with 2σ uncertainties are indicated by horizontal lines. The solid line is the trend derived from SAGE I + SAGE II data. The dashed line is trend derived from SAGE-corrected SBUV(2) data. The dash-dot line is the trend derived from SBUV(2) data. The dash-dot-dot line is the trend derived from sonde data. The long dashed line is the trend derived from Umkehr data. Red shading is the range of 3 models with high ratings in all 3 evaluations. Blue shading adds the range of 3 models that were highest in at least 1 evaluation. Panel (b): Altitude profile of trends calculated from model simulations for the time period 2000–2009, when the beginning of recovery is expected. Shaded regions are the same as in (a). Although the simulated upward trends and trends from measurements are broadly consistent, the observed increase cannot presently be attributed to ODS decrease because of observational uncertainty, natural ozone variability, and stratospheric cooling. Note that both stratospheric cooling and ODS decrease lead to a projected upper stratospheric ozone increase.

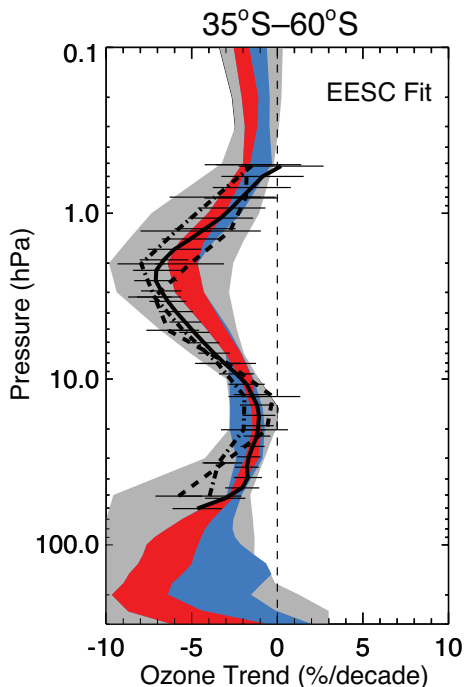
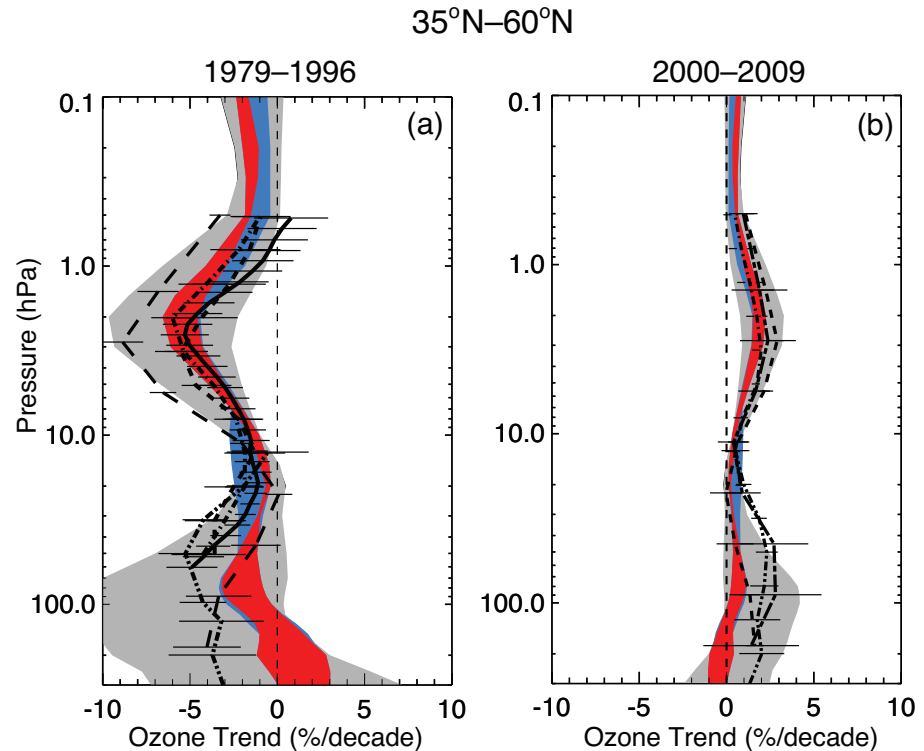


Figure 2-26. Same as 2-25a for the southern midlatitudes.

than the models and the trends derived from satellite measurements. The spread among models is larger in the lower stratosphere but is still significantly reduced by use of the diagnostics to filter results. Here the models that perform best on the diagnostics tended to have smaller trends than those deduced from ozonesonde measurements.

Figure 2-25b shows trends calculated from model simulations for the period after 2000 when the beginning of recovery is expected. Although the simulated upward trends and trends from measurements are broadly consistent, the observed increase cannot presently be attributed to ODS decrease because of observational uncertainty, natural ozone variability, and stratospheric cooling. Note that both stratospheric cooling and ODS decrease lead to a projected upper stratospheric ozone increase.

In the southern midlatitude (Figure 2-26) upper stratosphere, trends from the models that perform best on the diagnostics are somewhat smaller than those deduced from measurements. In the southern midlatitude lower stratosphere, the range of ozone trends deduced from models is somewhat more narrow for simulations that perform best on the CCMVal-2 diagnostics. In both the northern

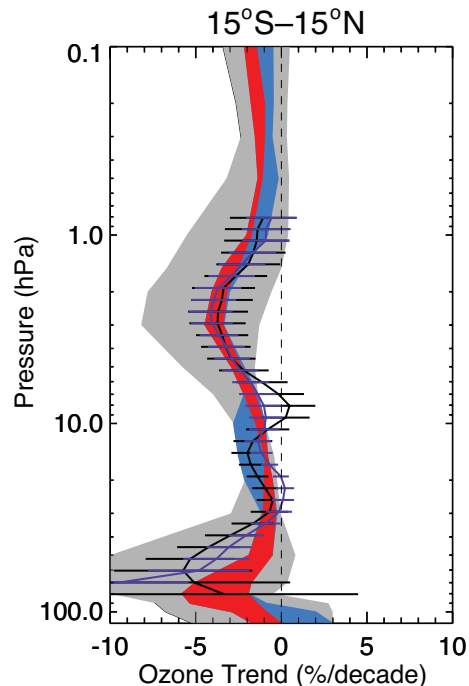


Figure 2-27. Ozone trends (%/decade) computed from CCMVal-2 simulations by 17 models as a function of altitude for the tropics. Black line: trend derived from SAGE II data alone. Purple line: trend derived from SAGE I + SAGE II data. The range of model simulations is as in Figure 2-25a.

and southern midlatitudes, the transport diagnostic selects simulations with smaller ozone depletion. Although we do not have enough sonde data to compare to southern midlatitude trends in the lower stratosphere, it appears that the simulated trends are smaller than trends derived from measurements at the northern midlatitudes.

2.4.5.3 TROPICAL PROFILE TRENDS

In the tropical lower stratosphere the models predict a decrease in column ozone due to increased upwelling (e.g., Butchart et al., 2006), in contrast to trends deduced from total column ozone measurements. The trends in the tropics computed from the simulations by 17 models are shown as a function of pressure in Figure 2-27. Almost all of the simulations show a similar pattern, with a decrease in the upper stratosphere centered at about 2–3 hPa and a smaller, narrower decrease in the lower stratosphere between the tropopause and about 60 hPa. The increase in tropical upwelling bringing up air with lower ozone amounts into the lower stratosphere and mixing of ozone-depleted air into the lower tropical stratosphere may both contribute to this trend.

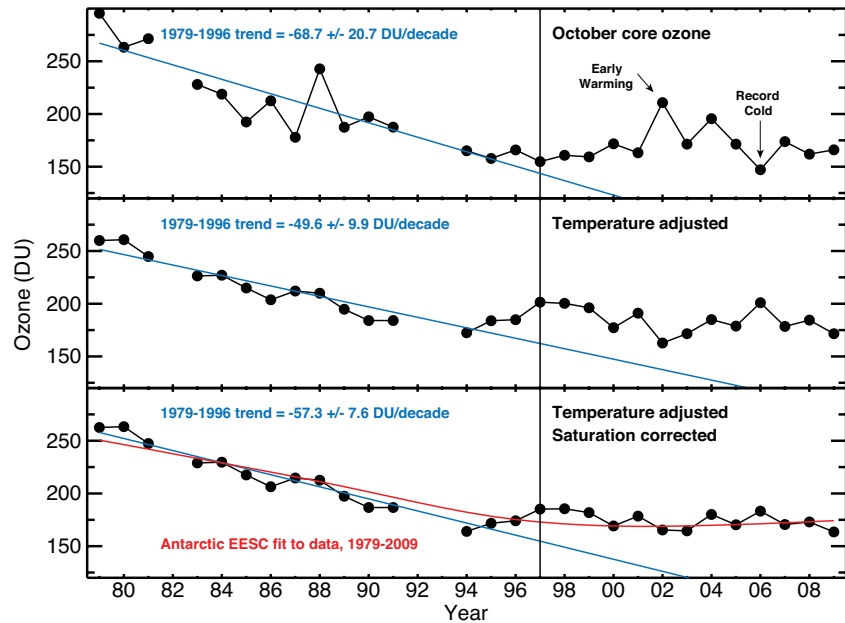
There is evidence for this lower stratospheric negative trend in data as shown by the SAGE I and SAGE I+II results in Figure 2-27. These trends are an update of Randel and Wu (2007). The results for SAGE I+II rely on the relative calibration of SAGE I to SAGE II, and are consistent with the results from SAGE II only and with the simulated trends. Brunner et al. (2006) used the CATO data set that uses measurements of total ozone and the analyses from ECMWF to infer global distributions of ozone. They found a narrow region of negative ozone trends in the tropical lower stratosphere and noted that these were consistent with those found for 1984–2000 in SAGE II data as reported in WMO (2003). As discussed in Section 2.4.5.1, the near-zero trend in tropical total ozone measurements is inconsistent with the negative trend found in the integrated SAGE I + SAGE II stratospheric profiles, and the tropospheric ozone column does not increase enough to resolve this discrepancy. The disagreement between trends obtained from vertically integrated SAGE data and trends obtained from the merged TOMS/SBUV(2) column ozone data set was discussed in WMO (2007).

2.4.5.4 POLAR TRENDS

Yang et al. (2008) report that Antarctic ozone is in the first stage of recovery. Ozone within the springtime Antarctic vortex is affected by both chemical and dynamical processes (Newman et al., 2006). Yang et al. (2008) used correlations between monthly means of total ozone column and temperatures to construct ozone anomaly time series, which reflect variations in ozone due to chemical forcing (Figure 2-28). The ozone anomaly time series reveals a statistically significant leveling off of ozone column since 1997, relative to the previous rate of decline. Yang et al. (2008) estimate ozone loss saturation by comparing the frequency distribution of measured ozone with the distribution expected from a reconstruction of ozone that hypothetically allows ozone abundances to drop below zero. This analysis indicates that the recent leveling off of the total ozone anomaly time series is due to changes in Antarctic halogen loading rather than loss saturation (bottom panel, Figure 2-28). They also identified the minimum of the second derivative of Antarctic EESC as a useful quantitative means to specify the break point for a piecewise linear fit to the data (further discussed in Chapter 1 of this Assessment).

As noted in the previous Assessment (WMO, 2007), trends in Arctic ozone are much more difficult to assess due to strong year-to-year variability of meteorological conditions and the dependence of inferred trends in temperature or ozone on start and end date. Furthermore, the trend in Arctic temperature is not sufficient to assess the impact of long-term changes on ozone (see

Figure 2-28. Time series of Dobson/Brewer measurements of total column ozone (Dobson units) in the core of the Antarctic vortex during October. Top panel: observed ozone column. Middle panel: resulting time series after removing effects of monthly mean temperature variations from the time series. Bottom panel: resulting time series after removing effects of loss saturation and monthly mean temperature variations from the time series. The blue line indicates the downward trend in column ozone for the respective time series, calculated for 1979 to 1996 and forecasted linearly afterward. Linear trends and 95% confidence intervals, DU/decade, are given. The red line in the bottom panel shows a fit of Antarctic EESC to the time series, considering data for the entire record. Years of “record cold” and of a sudden, “early warming” are indicated. Temperatures were warmer than usual in 1988, corresponding to the anomalously high levels of ozone observed that year. The vortex remained intact following the rise in temperature, hence 1988 is not classically considered to have experienced a sudden, “early warming.” From Yang et al. (2008), updated to include data for 2008 and 2009.



Years of “record cold” and of a sudden, “early warming” are indicated. Temperatures were warmer than usual in 1988, corresponding to the anomalously high levels of ozone observed that year. The vortex remained intact following the rise in temperature, hence 1988 is not classically considered to have experienced a sudden, “early warming.” From Yang et al. (2008), updated to include data for 2008 and 2009.

Section 4.1.1.1 of WMO, 2007). Since the previous Assessment, temperature conditions in the Arctic vortex have not been extremely cold for any particular ozone loss season. Chemical loss of Arctic ozone for recent years falls along the compact, near-linear relation with V_{PSC} (volume of air in the vortex exposed to temperature below the threshold for formation of PSCs) identified by Rex et al. (2004).

Much progress has been achieved in the evaluation of the representation of polar ozone loss in CCMs since the previous Assessment. The CCMVal-2 effort has provided important new insight into the chemical, dynamical, and radiative properties of CCMs (Chapter 6 of SPARC CCMVal, 2010). The chemical modules contained in CCMs are similar to the schemes used in off-line 3-D CTMs and other models known to produce good simulations of polar ozone loss under specified meteorological conditions (e.g., Chipperfield et al., 2005; Friele et al., 2006; von Hobe et al., 2007). However, use of a realistic and complete description of the relevant chemical (and microphysical) processes related to polar ozone depletion is only the first step toward obtaining an accurate representation of springtime polar ozone loss in coupled CCMs. The host general circulation model (GCM) must also simulate the correct descent over the pole, the correct timing and isolation of the polar vortex, and realistic temperatures that allow PSCs to form in the model.

Most CCMs include simplified schemes for PSC microphysics. Chapter 6 of SPARC CCMVal (2010) analyzed how well observed distributions of HNO_3 , H_2O , and HCl in the Antarctic were simulated by the CCMs. The models generally reproduced observed H_2O but overestimated HNO_3 . The CCMs generally use simplified equilibrium denitrification schemes and this discrepancy for HNO_3 will be affected by deficiencies in transport. Although conversion of HCl to active chlorine is essentially complete in most CCMs near 500–600 K, as expected from observations, the CCMs overestimate HCl at lower altitudes. This indicates incomplete chlorine activation in some CCMs, which would contribute to an underestimate of the simulated column ozone loss.

Figure 2-29 shows the time dependence of chemical loss of column ozone for the Arctic (top panel) and Antarctic (bottom panel) for 15 CCMs. Ozone loss derived from observations made by the Halogen Occultation Experiment (HALOE) instrument on the Upper Atmosphere Research Satellite (UARS) is also shown. The chemical loss of column ozone is calculated using analysis of the relationship between ozone and N_2O using archived records from each CCM. Chapter 6 of SPARC CCMVal (2010) shows that this method to quantify chemical ozone loss is reasonable because the simulated ozone versus N_2O relationship is well organized along isopleths, as observed. Also, Figure 2-29 shows that prior to ~1980 there

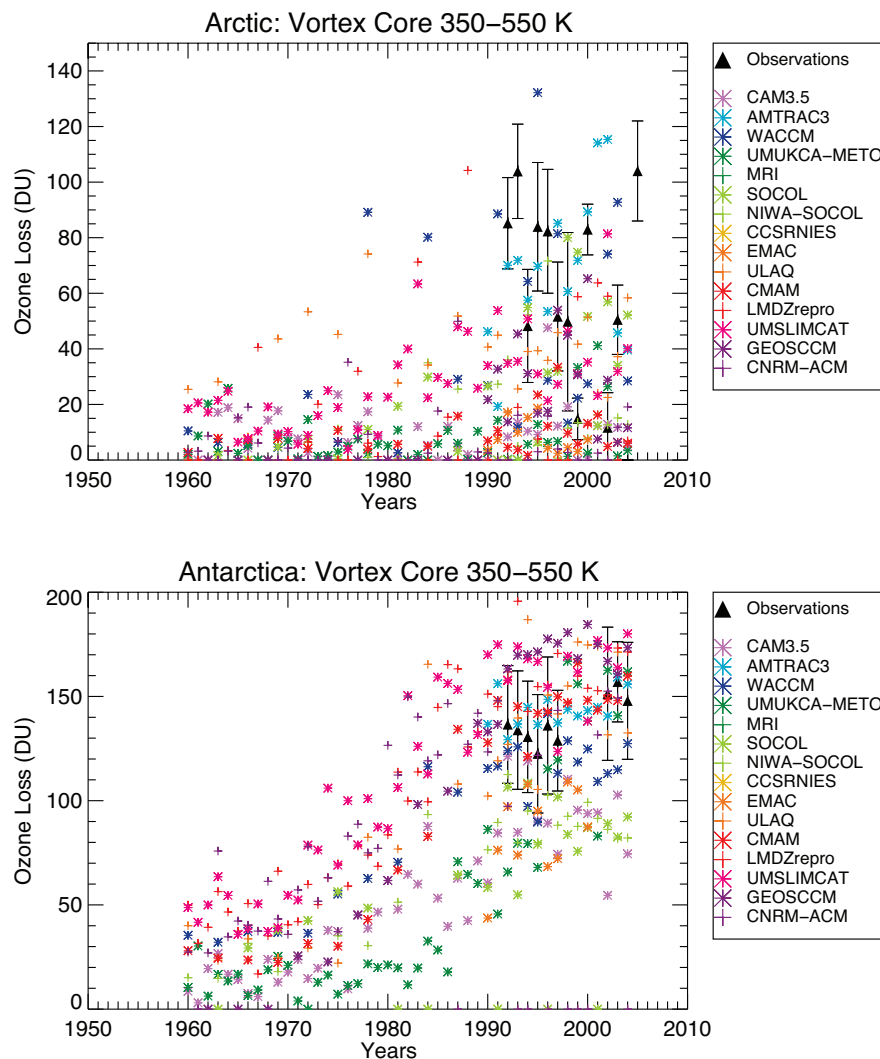


Figure 2-29. Chemical ozone depletion (Dobson units) in the polar vortex from January through April (top panel) and July through October (bottom panel) between 350 and 550 K. Results from observations (black triangles) were derived from HALOE on UARS for the polar vortex core. Model results are shown in different colors and calculated for equivalent latitudes poleward of 80°. Model descriptions are given in Table 3-1 of Chapter 3. (Reproduction of Figure 6.36, Chapter 6 of SPARC CCMVal, 2010).

is chemical loss of column ozone during the ozone loss season. Note that methyl chloride (CH_3Cl) supplies a natural background level of ~ 0.6 ppb Cl_y and anthropogenic ODSs were also increasing during this time period. Cl_y from both of these sources leads to chemical loss of ozone in the early part of the displayed time series, should meteorological conditions result in chlorine activation. Note that the loss due to CH_3Cl is natural and helps determine background levels of polar ozone prior to the buildup of Cl_y due to anthropogenic release of ODSs.

Figure 2-29 shows that modeled chemical loss of column ozone compares better with loss derived from observations in the Antarctic than in the Arctic. There are long-standing discrepancies between model behavior and observations related to the polar lower stratosphere, particularly for the Arctic (e.g., Eyring et al., 2006). CCMs tend to exhibit a cold bias in the Antarctic lower stratosphere and a concomitant westerly circulation that is too strong. The polar vortex then persists later into spring

than observed. Analysis of the CCM tracer transport shows that the different CCMs vary widely in their ability to produce an isolated lower stratospheric Antarctic vortex, with about half of them producing sufficient isolation for the altitude region and time period critical for ozone loss. In the Arctic, where observed temperatures are nearer the threshold for PSC formation, the CCMs are on average warm-biased and there is a large amount of model-to-model variation. The CCMs underestimate the observed frequency of cold Arctic winters. Because the CCMs are generally warm biased in the Arctic they tend to underestimate observed chemical loss of column ozone in the NH. In the SH CCMs are generally cold biased, and simulated column ozone loss generally scatter about the range of column loss derived from observations. In the SH ozone loss tends to saturate in the cold, isolated vortex. Another factor that may contribute to the spread in model results in Figure 2-29 is that although the standard CCMVal-2 runs only included bromine from long-lived

source gases, some models included ~6 pptv extra bromine to be more consistent with the actual stratospheric loading. This increases the loss computed for these models.

2.4.5.5 TRENDS AND RECOVERY IN THE UPPER TROPOSPHERE AND LOWER STRATOSPHERE

The upper troposphere and lower stratosphere (UTLS) are key regions where ozone changes can affect radiative forcing, and hence climate. At middle and high latitudes, up to 30% of total ozone resides in the lower stratosphere, i.e., the region between the tropopause and 100 hPa (Logan, 1999). WMO (2007) noted that apparent trends in this region were mostly the result of interannual variability and could not be ascribed to ODSs. It also concluded that changes in transport were a major contributor to the increase in midlatitude total ozone since the mid-1990s, particularly in the lowermost stratosphere (tropopause to 380K). Yang et al. (2006) showed that abundance of partial column ozone above 18 km altitude has risen slightly since 1997 in response to the decline in the atmospheric abundance of ODSs, whereas partial column ozone between the tropopause and 18 km rose much faster since 1997 than could be attributed to the decline in ODSs. The increases in total column were shown to differ significantly from the recovery in ozone expected solely from declining levels of ODS.

Vyushin et al. (2007), Mäder et al. (2007), and Harris et al. (2008) highlight the importance of accounting for dynamical variability and also volcanic aerosol in statistical models explaining observed changes in total ozone. Brunner et al. (2006) draw similar conclusions from analysis of vertically resolved ozone trends for the period 1979–2004 obtained by multiple linear regression analysis of the CATO ozone data set (see also WMO, 2007). Following the approach of Newchurch et al. (2003), Brunner et al. (2006) fitted their regression model to the reference period 1979–1995 during which EESC was increasing, but analyzed the residuals for the period 1996–2004 using different sets of explanatory variables. Their results show that a combination of EESC, QBO, and solar forcing is not sufficient to explain the recent ozone trend, as significantly positive residuals remained in the extratropical lower stratosphere for the period 1996–2004. However, most of the variations since 1996 could be explained when also accounting for volcanic aerosol and the Eliassen Palm (EP)-flux as a proxy for the wave forcing of the stratospheric circulation. This result demonstrates the importance of interannual variations in dynamics in producing the recent variations in ozone in the lower stratosphere. Brunner et al. (2006) also replaced EESC by a linear trend, assuming a continuation of the negative trend between 1979 and 1995. This resulted in an increase of the residuals that is much stronger than that resulting from

omission of aerosols or EP-flux, demonstrating the importance of the Montreal Protocol in addition to natural variability for explaining the recent observed ozone changes.

The main driver for the natural variations in UTLS ozone is climate variability, as has been extensively discussed in the WMO (2007). This includes variability in the stratospheric mean meridional circulation (e.g., Fusco and Salby, 1999) as well as variability in the tropospheric circulation through synoptic scale wave activity (e.g., Weiss et al., 2001). Recent studies explore the impact of climate variability on vertically resolved ozone in the UTLS. Thouret et al. (2006) used ozone measurements from the MOZAIC program to show that ozone in the upper troposphere is positively correlated with the North Atlantic Oscillation (NAO) index (the dominant mode of variability in surface pressure in the North Atlantic) while ozone in the lower stratosphere is anticorrelated with the extremes of the Northern Annular Mode (NAM) index (extension of the NAO to the full hemisphere) calculated at 150 hPa. Hess and Lamarque (2007), using the MOZART CTM driven by NCEP meteorological analyses, found that ozone is reduced throughout the troposphere at latitudes higher than 50°N during the positive phase of the Arctic Oscillation (AO, the surface manifestation of the NAM). This decrease can be linked to a decrease in ozone transported from the stratosphere. The El Niño-Southern Oscillation (ENSO) may also influence UTLS ozone. Fischer et al. (2008), using three different CCMs, found that ENSO forces a strengthening of the Brewer-Dobson circulation, which leads to lower total ozone in the tropics and higher total ozone at higher latitudes. While their study does not discuss the vertically resolved impact of the ENSO, the change in the Brewer-Dobson circulation is likely to have an impact on ozone in the lower stratosphere.

The question remains concerning how much the underlying long-term climate change may have contributed to the observed ozone changes. Hegglin and Shepherd (2009) use a stratosphere-resolving chemistry-climate model (CMAM) to study the effect of climate change on the stratospheric ozone distribution and derive expected trends of -1%, -3%, and +1% per decade in the SH lower stratosphere, the tropical lower stratosphere, and the NH lower stratosphere, respectively. They assumed a linear ozone response to climate change between 1960 and 2100. These numbers are consistent with those derived by Li et al. (2009) and are also confirmed in a multi-model comparison by Gettelman et al. (2010) except for the SH lower stratosphere, where the results were statistically not significant. These CCM results suggest that climate change may have masked around 30% of the ozone decrease due to EESC in the NH.

The evaluation of time series of ozone measurements at 200–100 hPa between 1960 and 2010 shows that the increase in ozone due to climate change is strongly

modulated by ozone depletion and recovery, with a larger signature in the SH than in the NH (Gettelman et al., 2010). This modulation is characterized by strong decreases in lower stratospheric ozone up to around the year 2000, followed by a strong increase, qualitatively agreeing with observations in this region (compare to Figure 2-7). However, the decline of lower stratospheric ozone in the tropics has not yet been shown unambiguously as stated earlier. WMO (2003, 2007) further pointed out the importance of decadal scale variability in dynamics that modulates the underlying slow dynamical contribution from climate change. The degree to which the decrease and increase are driven by such decadal scale variability is not known.

The changes in lower stratospheric ozone are likely to affect upper tropospheric (UT) ozone. Mid- and upper tropospheric ozone trends exhibit strong regional differences and are not yet well understood (Staehelin et al., 2001). CTMs with realistic ozone precursor emissions but without realistic stratospheric chemistry fail to reproduce either tropospheric background levels (Parrish et al., 2009) or observed trends (Fiore et al., 2009). In addition, Ordoñez et al. (2007) present observational evidence of a significant correlation between ozone at 150 hPa and tropospheric background ozone at two European mountain sites over the period 1992–2004, indicating local coupling of these air masses through stratosphere-to-troposphere exchange. At northern high latitudes, stratospheric ozone is estimated to contribute up to 40% to ozone at 500 hPa and up to 30% at northern midlatitudes (Terao et al., 2008). Hsu and Prather (2009) show the strong modulation of stratosphere-troposphere exchange (STE) ozone fluxes by the QBO, also pointing to stratospheric control of UT ozone.

It is likely that changes in the STE ozone fluxes induced by climate change need to be taken into account to understand observed UT ozone changes. Hegglin and Shepherd (2009) using the CMAM find that the simulated stratospheric ozone flux into the troposphere changes over the time period between 1960 and 2000 due to effects of both ozone depletion/recovery and climate change. Changes in the NH stratospheric ozone flux are around 6%, while changes in the SH are about –8%. A multi-model comparison of STE ozone fluxes performed during CCMVal-2 agrees with the global mean predictions (Chapter 10 of SPARC CCMVal, 2010). While the predicted STE ozone fluxes seem to be biased high by around 20% when compared to observations, the models' range of STE ozone flux is much smaller than found in previous studies used for the IPCC (2007). The impact of STE ozone flux on tropospheric chemistry is discussed further in Section 4.4.4 of Chapter 4.

In summary, evaluations of observed ozone changes show evidence of a statistically significant positive

change in ozone in the lower stratosphere; a part of this change may be attributed to decreasing ODSSs. Dynamical changes are still mainly responsible for these changes, at least in the NH. CCMs simulate increases in lower stratospheric ozone and suggest that up to 30% of the ozone depletion was masked by the dynamical changes due to climate change. While the importance of lower stratospheric ozone changes on upper tropospheric ozone has been recognized, understanding of upper tropospheric ozone trends remains incomplete.

REFERENCES

- Adriani, A., P. Massoli, G. Di Donfrancesco, F. Cairo, M.L. Moriconi, and M. Snels, Climatology of polar stratospheric clouds based on lidar observations from 1993 to 2001 over McMurdo Station, Antarctica, *J. Geophys. Res.*, *109*, D24211, doi: 10.1029/2004JD004800, 2004.
- Andersen, S.B., and B.M. Knudsen, The influence of polar vortex ozone depletion on NH mid-latitude ozone trends in spring, *Atmos. Chem. Phys.*, *6*, 2837–2845, 2006.
- Andreae, M.O., and A. Gelencsér, Black carbon or brown carbon? The nature of light-absorbing carbonaceous aerosols, *Atmos. Chem. Phys.*, *6*, 3131–3148, doi: 10.5194/acp-6-3131-2006, 2006.
- Angell, J.K., and M. Free, Ground-based observations of the slowdown in ozone decline and onset of ozone increase, *J. Geophys. Res.*, *114*, D07303, doi: 10.1029/2008JD010860, 2009.
- Antón, M., D. Loyola, M. López, J.M. Vilaplana, M. Bañón, W. Zimmer, and A. Serrano, Comparison of GOME-2/MetOp total ozone data with Brewer spectroradiometer data over the Iberian Peninsula, *Ann. Geophys.*, *27*, 1377–1386, 2009.
- Arola, A., S. Kazadzis, N. Krotkov, A. Bais, J. Gröbner, and J.R. Herman, Assessment of TOMS UV bias due to absorbing aerosols, *J. Geophys. Res.*, *110*, D23211, doi: 10.1029/2005JD005913, 2005.
- Arola, A., S. Kazadzis, A. Lindfors, N. Krotkov, J. Kujanpää, J. Tamminen, A. Bais, A. di Sarra, J.M. Villaplana, C. Brogniez, A.M. Siani, J. Janouch, P. Weihs, A. Webb, T. Koskela, N. Kouremeti, D. Meloni, V. Buchard, F. Auriol, I. Ialongo, M. Staneck, S. Simic, A. Smedley, and S. Kinne, A new approach to correct for absorbing aerosols in OMI UV, *Geophys. Res. Lett.*, *36*, L22805, doi: 10.1029/2009GL041137, 2009.
- Atkinson, R., D.L. Baulch, R.A. Cox, J.N. Crowley, R.F. Hampson, R.G. Hynes, M.E. Jenkin, M.J. Rossi, and J. Troe, Evaluated kinetic and photochemical data for atmospheric chemistry: Volume III - gas phase reactions of inorganic halogens, *Atmos.*

- Chem. Phys.*, 7 (4), 981-1191, 2007. (Cited as IUPAC, 2007.)
- Austin, J., K. Tourpali, E. Rozanov, H. Akiyoshi, S. Bekki, G. Bodeker, C. Brühl, N. Butchart, M. Chipperfield, M. Deushi, V.I. Formichev, M.A. Giorgetta, L. Gray, K. Kodera, F. Lott, E. Manzini, D. Marsh, K. Matthes, T. Nagashima, K. Shibata, R.S. Stolarski, H. Struthers, and W. Tian, Coupled chemistry climate model simulations of the solar cycle in ozone and temperature, *J. Geophys. Res.*, 113 (D11), doi: 10.1029/2007JD009391, 2008.
- Avallone, L.M., and D.W. Toohey, Tests of halogen photochemistry using in situ measurements of ClO and BrO in the lower polar stratosphere, *J. Geophys. Res.*, 106 (D10), 10411-10422, 2001.
- Badosa, J., R.L. McKenzie, M. Kotkamp, J. Calbó, J.A. González, P.V. Johnston, M. O'Neill, and D.J. Anderson, Towards closure between measured and modelled UV under clear skies at four diverse sites, *Atmos. Chem. Phys.*, 7 (11), 2817-2837, 2007.
- Bais, A.F., and D. Lubin (Lead Authors), A. Arola, G. Bernhard, M. Blumthaler, N. Chubarova, C. Erlick, H.P. Gies, N. Krotkov, K. Lantz, B. Mayer, R.L. McKenzie, R.D. Piacentini, G. Seckmeyer, J.R. Slusser, and C.S. Zerefos, Surface ultraviolet radiation: Past, present, and future, Chapter 7 in *Scientific Assessment of Ozone Depletion: 2006*, Global Ozone Research and Monitoring Project—Report No. 50, 572 pp., World Meteorological Organization, Geneva, Switzerland, 2007.
- Balis, D., J.-C. Lambert, M. Van Roozendaal, R. Spurr, D. Loyola, Y. Livschitz, P. Valks, V. Amiridis, P. Gerard, J. Granville, and C. Zehner, Ten years of GOME/ERS2 total ozone data—the new GOME data processor (GDP) version 4: 2. Ground-based validation and comparisons with TOMS V7/V8, *J. Geophys. Res.*, 112, D07307, doi: 10.1029/2005JD006376, 2007.
- Barnard, J.C., R. Volkamer, and E.I. Kassianov, Estimation of the mass absorption cross section of the organic carbon component of aerosols in the Mexico City Metropolitan Area, *Atmos. Chem. Phys.*, 8 (22), 6665-6679, 2008.
- Barret, B., M. De Mazière, and P. Demoulin, Retrieval and characterization of ozone profiles from solar infrared spectra at the Jungfraujoeh, *J. Geophys. Res.*, 107, 4788, doi: 10.1029/2001JD001298, 2002.
- Beig, G., and V. Singh, Trends in tropical tropospheric column ozone from satellite data and MOZART model, *Geophys. Res. Lett.*, 34, L17801, doi: 10.1029/2007GL030460, 2007.
- Bergstrom, R.W., P. Pilewskie, P.B. Russell, J. Redemann, T.C. Bond, P.K. Quinn, and B. Sierau, Spectral absorption properties of atmospheric aerosols, *Atmos. Chem. Phys.*, 7 (23), 5937-5943, 2007.
- Bergstrom, R.W., K.S. Schmidt, O. Coddington, P. Pilewskie, H. Guan, J.M. Livingston, J. Redemann, and P.B. Russell, Aerosol spectral absorption in the Mexico City area: Results from airborne measurements during MILAGRO/INTEX B, *Atmos. Chem. Phys.*, 10 (13), 6333-6343, doi: 10.5194/acp-10-6333-2010, 2010.
- Bernhard, G., C.R. Booth, and J.C. Eghamjian, Comparison of UV irradiance measurements at Summit, Greenland; Barrow, Alaska; and South Pole, Antarctica, *Atmos. Chem. Phys.*, 8 (16), 4799-4810, doi: 10.5194/acp-8-4799-2008, 2008.
- Bernhard, G., C.R. Booth, and J.C. Eghamjian, Climatology of ultraviolet radiation at high latitudes derived from measurements of the National Science Foundation's ultraviolet spectral irradiance monitoring network, Chapter 3 in *UV Radiation in Global Climate Change: Measurements, Modeling and Effects on Ecosystems*, edited by W. Gao, D.L. Schmoldt, and J.R. Slusser, 550 pp., Springer-Verlag and Tsinghua University Press, ISBN: 978-3-642-03312-4, 48-72, 2010.
- Bhartia, P.K., C.G. Wellemeyer, S.L. Taylor, N. Nath, and A. Gopalan, Solar Backscatter Ultraviolet (SBUV) version 8 profile algorithm, in *Ozone Vol. I, Proceedings of the XX Quadrennial Ozone Symposium*, 1-8 June 2004, Kos, Greece, edited by C.S. Zerefos, 295-296, International Ozone Commission, Athens, Greece, 2004.
- Biele, J., A. Tsias, B.P. Luo, K.S. Carslaw, R. Neuber, G. Beyerle, and T. Peter, Nonequilibrium coexistence of solid and liquid particles in Arctic stratospheric clouds, *J. Geophys. Res.*, 106 (D19), 22991-23007, doi: 10.1029/2001JD900188, 2001.
- Blum, U., K.H. Fricke, K.P. Müller, J. Siebert, and G. Baumgarten, Long-term lidar observations of polar stratospheric clouds at Esrange in northern Sweden, *Tellus*, 57B, 412-422, 2005.
- Bodeker, G.E., H. Shiona, and H. Struthers, The NIWA assimilated total column ozone data base and assimilated trace gas profile data base for validation of CCMs, paper presented at *CCMVal 2005 Workshop*, October 2005, Boulder, Colo., available: http://www.pa.op.dlr.de/workshops/CCMVal2005/CCMVal2005_abstract.html, 2005.
- Booth, C.R., and S. Madronich, Radiation amplification factors: Improved formulation accounts for large increases in ultraviolet radiation associated with Antarctic ozone depletion, in *Ultraviolet Radiation in Antarctica: Measurement and Biological Effects*, edited by C.S. Weiler and P.S. Penhale, *AGU Antarctic Res. Ser.*, 62, 39-52, 1994.
- Borkowski, J.L., Modelling UV radiation variations at

- different time scales, *Ann. Geophys.*, *26*, 441-446, 2008.
- Brunner, D., J. Staehelin, J.A. Maeder, I. Wohltmann, and G.E. Bodeker, Variability and trends in total and vertically resolved stratospheric ozone based on the CATO ozone data set, *Atmos. Chem. Phys.*, *6* (12), 4985-5008, doi: 10.5194/acp-6-4985-2006, 2006.
- Buchard, V., C. Brogniez, F. Auriol, B. Bonnel, J. Lenoble, A. Tanskanen, B. Bojkov, and P. Veefkind, Comparison of OMI ozone and UV irradiance data with ground-based measurements at two French sites, *Atmos. Chem. Phys.*, *8* (16), 4517-4528, doi: 10.5194/acp-8-4517-2008, 2008.
- Burkholder, J.B., J.J. Orlando, and C.J. Howard, Ultraviolet-absorption cross sections of Cl₂O₂ between 210 and 410 nm, *J. Phys. Chem.*, *94*, 687-695, 1990.
- Burrows, J.P., M. Weber, M. Buchwitz, V. Rozanov, A. Ladstädter-Weißmayer, A. Richter, R. de Beek, R. Hoogen, K. Bramstedt, K.-U. Eichmann, M. Eisinger, and D. Perner, The Global Ozone Monitoring Experiment (GOME): Mission concept and first scientific results, *J. Atmos. Sci.*, *56*, 151-175, 1999.
- Butchart, N., and A.A. Scaife, Removal of chlorofluorocarbons by increased mass exchange between the stratosphere and troposphere in a changing climate, *Nature*, *410* (6830), 799-802, 2001.
- Butchart, N., A.A. Scaife, M. Bourqui, J. de Grandpré, S.H.E. Hare, J. Kettleborough, U. Langematz, E. Manzini, F. Sassi, K. Shibata, D. Shindell, and M. Sigmond, Simulations of anthropogenic change in the strength of the Brewer-Dobson circulation, *Clim. Dyn.*, *27* (7-8), 727-741, doi: 10.1007/s00382-006-0162-4, 2006.
- Butkovskaya, N., A. Kukui, and G. Le Bras, HNO₃ forming channel of the HO₂ + NO reaction as a function of pressure and temperature in the ranges of 72–600 Torr and 223–323 K, *J. Phys. Chem. A*, *111*, 9047-9053, doi: 10.1021/jp074117m, 2007.
- Butkovskaya, N., M.-T. Rayez, J.-C. Rayez, A. Kukui, and G. Le Bras, Water vapor effect on the HNO₃ yield in the HO₂ + NO reaction: Experimental and theoretical evidence, *J. Phys. Chem. A*, *113*, 11327-11342, doi: 10.1021/jp811428p, 2009.
- Canty, T., E.D. Rivière, R.J. Salawitch, G. Berthet, J.-B. Renard, K. Pfeilsticker, M. Dorf, A. Butz, H. Bösch, R.M. Stimpfle, D.M. Wilmouth, E.C. Richard, D.W. Fahey, P.J. Popp, M.R. Schoeberl, L.R. Lait, and T.P. Bui, Nighttime OCIO in the winter Arctic vortex, *J. Geophys. Res.*, *110*, D01301, doi: 10.1029/2004JD005035, 2005.
- Cariolle, D., M.J. Evans, M.P. Chipperfield, N. Butkovskaya, A. Kukui, and G. Le Bras, Impact of the new HNO₃-forming channel of the HO₂ + NO reaction on tropospheric HNO₃, NO_x, HO_x and ozone, *Atmos. Chem. Phys.*, *8* (14), 4061-4068, doi: 10.5194/acp-8-4061-2008, 2008.
- Carl, S.A., A highly sensitive method for time-resolved detection of O(¹D) applied to precise determination of absolute O(¹D) reaction rate constants and O(³P) yields, *Phys. Chem. Chem. Phys.*, *7*, 4051-4053, doi: 10.1039/b513576c, 2005.
- Carslaw, K.S., B.P. Luo, S.L. Clegg, Th. Peter, P. Brimblecombe, and P.J. Crutzen, Stratospheric aerosol growth and HNO₃ gas phase depletion from coupled HNO₃ and water uptake by liquid particles, *Geophys. Res. Lett.*, *21* (23), 2479-2482, 1994.
- Cede, A., J. Herman, A. Richter, N. Krotkov, and J. Burrows, Measurements of nitrogen dioxide total column amounts using a Brewer double spectrophotometer in direct sun mode, *J. Geophys. Res.*, *111*, D05304, doi: 10.1029/2005JD006585, 2006.
- Chen, H.-Y., C.-Y. Lien, W.-Y. Lin, Y.T. Lee, and J.J. Lin, UV absorption cross sections of ClOOCl are consistent with ozone degradation models, *Science*, *324*, 781-784, doi: 10.1126/science.1171305, 2009.
- Chipperfield, M.P., and V.E. Fioletov (Lead Authors), B. Bregman, J. Burrows, B.J. Connor, J.D. Haigh, N.R.P. Harris, A. Hauchecorne, L.L. Hood, S.R. Kawa, J.W. Krzyścin, J.A. Logan, N.J. Muthama, L. Polvani, W.J. Randel, T. Sasaki, J. Stähelin, R.S. Stolarski, L.W. Thomason, and J.M. Zawodny, Global ozone: Past and present, Chapter 3 in *Scientific Assessment of Ozone Depletion: 2006*, Global Ozone Research and Monitoring Project—Report No. 50, 572 pp., World Meteorological Organization, Geneva, Switzerland, 2007.
- Chipperfield, M., W. Feng, and M. Rex, Arctic ozone loss and climate sensitivity: Updated three-dimensional model study, *Geophys. Res. Lett.*, *32*, L11813, doi: 10.1029/2005GL022674, 2005.
- Chubarova, N.Y., UV variability in Moscow according to the long-term UV measurements and reconstruction model, *Atmos. Chem. Phys.*, *8* (12), 3025-3031, doi: 10.5194/acp-8-3025-2008, 2008.
- Clain, G., J.L. Baray, R. Delmas, R. Diab, J. Leclair de Bellevue, P. Keckhut, F. Posny, J.M. Metzger, and J.P. Cammas, Tropospheric ozone climatology at two Southern Hemisphere tropical/subtropical sites, (Reunion Island and Irene, South Africa) from ozonesondes, LIDAR, and in situ aircraft measurements, *Atmos. Chem. Phys.*, *9* (5), 1723-1734, doi: 10.5194/acp-9-1723-2009, 2009.
- Coldewey-Egbers, M., M. Weber, L.N. Lamsal, R. de Beek, M. Buchwitz, and J.P. Burrows, Total ozone retrieval from GOME UV spectral data using the weighting function DOAS approach, *Atmos. Chem. Phys.*, *5* (4), 1015-1025, doi: 10.5194/acp-5-1015-2005, 2005.

- Cordero, R.R., G. Seckmeyer, D. Pissulla, L. DaSilva, F. Labbe, Uncertainty evaluation of the spectral UV irradiance evaluated by using the UVSPEC Radiative Transfer Model, *Opt. Commun.*, 276, 44-53, doi: 10.1016/j.optcom.2007.04.008, 2007.
- Cordero, R.R., G. Seckmeyer, D. Pissulla, L. DaSilva, and F. Labbe, Uncertainty evaluation of spectral UV irradiance measurements, *Meas. Sci. Technol.*, 19 (4), 045104, 1-15, doi: 10.1088/0957-0233/19/4/045104, 2008a.
- Cordero, R.R., G. Seckmeyer, D. Pissulla, and F. Labbe, Uncertainty of experimental integrals: Application to the UV index calculation, *Metrologia*, 45 (1), 1-10, doi: 10.1088/0026-1394/45/1/001, 2008b.
- Corr, C.A., N. Krotkov, S. Madronich, J.R. Slusser, B. Holben, W. Gao, J. Flynn, B. Lefer, and S.M. Kreidenweis, Retrieval of aerosol single scattering albedo at ultraviolet wavelengths at the T1 site during MILAGRO, *Atmos. Chem. Phys.*, 9 (15), 5813-5827, doi: 10.5194/acp-9-5813-2009, 2009.
- COST 726 (European Cooperation in Science and Technology), Final report of COST action 726 – *Long Term Changes and Climatology of UV Radiation over Europe*, edited by Z. Lityńska, P. Koepke, H. De Backer, J. Gröbner, A. Schmalwieser, and L. Vuilleumier, COST Earth System Science and Environmental Management, Luxembourg: Office for Official Publications of the European Communities, 137 pp., available: <http://www.cost726.org/>, in press, 2010.
- Cox, R.A., and G.D. Hayman, The stability and photochemistry of dimers of the ClO radical and implications for Antarctic ozone depletion, *Nature*, 332 (6167), 796-800, doi: 10.1038/332796a0, 1988.
- Crutzen, P.J., Albedo enhancement by stratospheric sulfur injections: A contribution to resolve a policy dilemma?, *Clim. Change*, 77 (3-4), 211-220, doi: 10.1007/s10584-006-9101-y, 2006.
- Curylo, A., J. Krzyścin, and B. Bogdańska, UV reconstruction with long time series global radiation measurements, in *Proceedings of the UV Conference "One Century of UV Radiation Research,"* 18-20 September 2007, Davos, Switzerland, edited by J. Gröbner, 211-212, 2007.
- David, C., S. Bekki, S. Godin, G. Mégie, and M.P. Chipperfield, Polar stratospheric clouds climatology over Dumont d'Urville between 1989 and 1993 and the influence of volcanic aerosols on their formation, *J. Geophys. Res.*, 103, 22163-22180, 1998.
- David, C., P. Keckhut, A. Armetta, J. Jumelet, M. Snels, M. Marchand, and S. Bekki, Radiosonde stratospheric temperatures at Dumont d'Urville (Antarctica): Trends and link with polar stratospheric clouds, *Atmos. Chem. Phys.*, 10 (8), 3813-3825, doi: 10.5194/acp-10-3813-2010, 2010.
- DeMore, W.B., and E. Tschuikow-Roux, Ultraviolet spectrum and chemical reactivity of the chlorine monoxide dimer, *J. Phys. Chem.*, 94 (15), 5856-5860, doi: 10.1021/j100378a046, 1990.
- den Outer, P.N., H. Slaper, and R.B. Tax, UV radiation in the Netherlands: Assessing long-term variability and trends in relation to ozone and clouds, *J. Geophys. Res.*, 110, D02203, 1-11, doi: 10.1029/2004JD004824, 2005.
- den Outer, P.N., H. Slaper, J. Kaurola, A. Lindfors, A. Kazantzidis, A.F. Bais, U. Feister, J. Junk, M. Janouch, and W. Josefsson, Reconstructing erythral ultraviolet radiation levels in Europe for the past 4 decades, *J. Geophys. Res.*, 115, D10102, doi: 10.1029/2009JD012827, 2010.
- Deshler, T., B.J. Johnson, and W.R. Rozier, Changes in the character of polar stratospheric clouds over Antarctica in 1992 due to the Pinatubo volcanic aerosol, *Geophys. Res. Lett.*, 21 (4), 273-276, 1994.
- Deshler, T., J.L. Mercer, H.G.J. Smit, R. Stubi, G. Levrat, B.J. Johnson, S.J. Oltmans, R. Kivi, A.M. Thompson, J. Witte, J. Davies, F.J. Schmidlin, G. Brothers, and T. Sasaki, Atmospheric comparison of electrochemical cell ozonesondes from different manufacturers, and with different cathode solution strengths: The Balloon Experiment on Standards for Ozonesondes, *J. Geophys. Res.*, 113, D04307, doi: 10.1029/2007JD008975, 2008.
- Dessler, A.E., D.B. Considine, J.E. Rosenfield, S.R. Kawa, A.R. Douglass, and J.M. Russell III, Lower stratospheric chlorine partitioning during the decay of the Mt. Pinatubo aerosol cloud, *Geophys. Res. Lett.*, 24 (13), 1623-1626, 1997.
- Dhomse, S., M. Weber, I. Wohltmann, M. Rex, and J.P. Burrows, On the possible causes of recent increases in NH total ozone from a statistical analysis of satellite data from 1979 to 2003, *Atmos. Chem. Phys.*, 6 (5), 1165-1180, doi: 10.5194/acp-6-1165-2006, 2006.
- Diaz, S., C. Camilión, G. Deferrari, H. Fuenzalida, R. Armstrong, C. Booth, A. Paladini, S. Cabrera, C. Casiccia, C. Lovengreen, J. Pedroni, A. Rosales, H. Zagarese, and M. Vernet, Ozone and UV radiation over southern South America: Climatology and anomalies, *Photochem. Photobiol.*, 82 (4), 834-843, doi: 10.1562/2005-09-26-RA-697, 2006.
- Dillon, T.J., A. Horowitz, and J.N. Crowley, The atmospheric chemistry of sulphuryl fluoride, SO₂F₂, *Atmos. Chem. Phys.*, 8 (6), 1547-1557, doi: 10.5194/acp-8-1547-2008, 2008.
- Drdla, K., B.W. Gandrud, D. Baumgardner, J.C. Wilson, T.P. Bui, D. Hurst, S.M. Schauffler, H. Jost, J.B. Greenblatt, and C.R. Webster, Evidence for the

- widespread presence of liquid-phase particles during the 1999-2000 Arctic winter, *J. Geophys. Res.*, *108* (D5), 8318, doi: 10.1029/2001JD001127, 2003.
- Dunlea, E.J., and A.R. Ravishankara, Measurement of the rate coefficient for the reaction of O(¹D) with H₂O and re-evaluation of the atmospheric OH production rate, *Phys. Chem. Chem. Phys.*, *6*, 3333-3340, doi: 10.1039/b402483d, 2004.
- Eckermann, S.D., L. Hoffmann, M. Höpfner, D.L. Wu, and M.J. Alexander, Antarctic NAT PSC belt of June 2003: Observational validation of the mountain wave seeding hypothesis, *Geophys. Res. Lett.*, *36*, L02807, doi: 10.1029/2008GL036629, 2009.
- Engel, A., T. Möbius, H. Bönisch, U. Schmidt, R. Heinz, I. Levin, E. Atlas, S. Aoki, T. Nakazawa, S. Sugawara, F. Moore, D. Hurst, J. Elkins, S. Schauffler, A. Andrews, and K. Berine, Age of stratospheric air unchanged within uncertainties over the past 30 years, *Nature Geosci.*, *2*, 28-31, doi: 10.1038/GEO388, 2009.
- Eskes, H.J., R.J. van der A, E.J. Brinksma, J.P. Veefkind, J.F. de Haan, and P.J.M. Valks, Retrieval and validation of ozone columns derived from measurements of SCIAMACHY on Envisat, *Atmos. Chem. Phys. Discuss.*, *5*, 4429-4475, doi: 10.5194/acpd-5-4429-2005, 2005.
- Eyring, V., N. Butchart, D.W. Waugh, H. Akiyoshi, J. Austin, S. Bekki, G.E. Bodeker, B.A. Boville, C. Brühl, M.P. Chipperfield, E. Cordero, M. Dameris, M. Deushi, V.E. Fioletov, S.M. Frith, R.R. Garcia, A. Gettelman, M.A. Giorgetta, V. Grewe, L. Jourdain, D.E. Kinnison, E. Mancini, E. Manzini, M. Marchand, D.R. Marsh, T. Nagashima, P.A. Newman, J.E. Nielsen, S. Pawson, G. Pitari, D.A. Plummer, E. Rozanov, M. Schraner, T.G. Shepherd, K. Shibata, R.S. Stolarski, H. Struthers, W. Tian, and M. Yoshiki, Assessment of temperature, trace species, and ozone in chemistry-climate model simulations of the recent past, *J. Geophys. Res.*, *111*, D22308, doi: 10.1029/2006JD007327, 2006.
- Fahey, D.W., S.R. Kawa, E.L. Woodbridge, P. Tin, J.C. Wilson, H.H. Jonsson, J.E. Dye, D. Baumgardner, S. Borrmann, D.W. Toohey, L.M. Avallone, M.H. Proffitt, J. Margitan, M. Loewenstein, J.R. Podolske, R.J. Salawitch, S.C. Wofsy, M.K.W. Ko, D.E. Anderson, M.R. Schoeberl, and K.R. Chan, In situ measurements constraining the role of sulfate aerosols in midlatitude ozone depletion, *Nature*, *363* (6429), 509-514, doi: 10.1038/363509a0, 1993.
- Fahey, D.W., R.S. Gao, K.S. Carslaw, J. Kettleborough, P.J. Popp, M.J. Northway, J.C. Holecek, S.C. Ciciora, R.J. McLaughlin, T.L. Thompson, R.H. Winkler, D.G. Baumgardner, B. Gandrud, P.O. Wennberg, S. Dhaniyala, K. McKinney, Th. Peter, R.J. Salawitch, T.P. Bui, J.W. Elkins, C.R. Webster, E.L. Atlas, H. Jost, J.C. Wilson, R.L. Herman, A. Kleinböhl, and M. von König, The detection of large HNO₃-containing particles in the winter Arctic stratosphere, *Science*, *291*, 1026-1031, 2001.
- Farman, J.C., B.G. Gardiner, and J.D. Shanklin, Large losses of total ozone in Antarctica reveal seasonal ClO_x/NO_x interaction, *Nature*, *315*, 207-210, 1985.
- Feister, U., J. Junk, M. Woldt, A. Bais, A. Helbig, M. Janouch, W. Josefsson, A. Kazantzidis, A. Lindfors, P.N. den Outer, and H. Slaper, Long-term solar UV radiation reconstructed by ANN modelling with emphasis on spatial characteristics of input data, *Atmos. Chem. Phys.*, *8* (12), 3107-3118, doi: 10.5194/acp-8-3107-2008, 2008.
- Felton, M.A. Jr., T.A. Kovacs, A.H. Omar, and C.A. Hostetler, *Classification of Polar Stratospheric Clouds using LIDAR Measurements from the SAGE III Ozone Loss and Validation Experiment*, Tech. Rep. ARL-TR-4154, 36 pp., U.S. Army Research Laboratory, Adelphi, Md., 2007.
- Feng, W., M.P. Chipperfield, M. Dorf, K. Pfeilsticker, and P. Ricaud, Mid-latitude ozone changes: Studies with a 3-D CTM forced by ERA-40 analyses, *Atmos. Chem. Phys.*, *7* (9), 2357-2369, doi: 10.5194/acp-7-2357-2007, 2007.
- Fioletov, V.E., Estimating the 27-day and 11-year solar cycle variations in tropical upper stratospheric ozone, *J. Geophys. Res.*, *114*, D02302, doi: 10.1029/2008JD010499, 2009.
- Fioletov, V.E., L.J.B. McArthur, J.B. Kerr, and D.I. Wardle, Long-term variations of UV-B irradiance over Canada estimated from Brewer observations and derived from ozone and pyranometer measurements, *J. Geophys. Res.*, *106* (D19), 23009-23027, 2001.
- Fioletov, V.E., G.E. Bodeker, A.J. Miller, R.D. McPeters, and R. Stolarski, Global and zonal total ozone variations estimated from ground-based and satellite measurements: 1964-2000, *J. Geophys. Res.*, *107* (D22), 4647, doi: 10.1029/2001JD001350, 2002.
- Fioletov, V.E., G. Labow, R. Evans, E.W. Hare, U. Köhler, C.T. McElroy, K. Miyagawa, A. Redondas, V. Savastiouk, A.M. Shalamyansky, J. Staehelin, K. Vanicek, and M. Weber, Performance of ground-based total ozone network assessed using satellite data, *J. Geophys. Res.*, *113*, D14313, doi: 10.1029/2008JD009809, 2008.
- Fiore, A.M., F.J. Dentener, O. Wild, C. Cuvelier, M.G. Schultz, P. Hess, C. Textor, M. Schulz, R.M. Doherty, L.W. Horowitz, I.A. MacKenzie, M.G. Sanderson, D.T. Shindell, D.S. Stevenson, S. Szopa, R. Van Dingenen, G. Zeng, C. Atherton, D. Bergmann, I. Bey, G. Carmichael, W.J. Collins, B.N. Duncan, G. Faluvegi, G. Folberth, M. Gauss, S. Gong, D. Hau-

- glustaine, T. Holloway, I.S.A. Isaksen, D.J. Jacob, J.E. Jonson, J.W. Kaminski, T.J. Keating, A. Lupu, E. Marmer, V. Montanaro, R.J. Park, G. Pitari, K.J. Pringle, J.A. Pyle, S. Schroeder, M.G. Vivanco, P. Wind, G. Wojcik, S. Wu, and A. Zuber, Multimodel estimates of intercontinental source-receptor relationships for ozone pollution, *J. Geophys. Res.*, *114*, D04301, doi: 10.1029/2008JD010816, 2009.
- Fischer, A.M., D.T. Shindell, B. Winter, M.S. Bourqui, G. Faluvegi, E. Rozanov, M. Schraner, and S. Brönnimann, Stratospheric winter climate response to ENSO in three chemistry-climate models, *Geophys. Res. Lett.*, *35*, L13819, doi: 10.1029/2008GL034289, 2008.
- Fleming, E.L., C.H. Jackman, D.K. Weisenstein, and M.K.W. Ko, The impact of interannual variability on multidecadal total ozone simulations, *J. Geophys. Res.*, *112*, D10310, doi: 10.1029/2006JD007953, 2007.
- Flynn, L.E., (editor), *Solar Backscatter Ultraviolet Instrument (SBUV/2) Version 8 Ozone Retrieval Algorithm Theoretical Basis Document (V8 ATBD)*, NOAA National Environmental, Satellite, Data, and Information Service, Center for Satellite Applications and Research, available: http://www.star.nesdis.noaa.gov/smcd/spb/calibration/icvs/sbuv/doc/SBUV2_V8_ATBD_020207.pdf, 2007.
- Frieler, K., M. Rex, R.J. Salawitch, T. Canty, M. Streibel, R.M. Stimpfle, K. Pfeilsticker, M. Dorf, D.K. Weisenstein, and S. Godin-Beekmann, Toward a better quantitative understanding of polar stratospheric ozone loss, *Geophys. Res. Lett.*, *33*, L10812, doi: 10.1029/2005GL025466, 2006.
- Frith, S., R. Stolarski, and P.K. Bhartia, Implications of Version 8 TOMS and SBUV data for long-term trend analysis, in *Ozone Vol. I, Proceedings of the XX Quadrennial Ozone Symposium*, 1-8 June 2004, Kos, Greece, edited by C.S. Zerefos, 65-66, International Ozone Commission, Athens, Greece, 2004.
- Fromm, M., J. Alfred, and M. Pitts, A unified, long-term, high-latitude stratospheric aerosol and cloud database using SAM II, SAGE II, and POAM II/III data: Algorithm description, database definition, and climatology, *J. Geophys. Res.*, *108* (D12), 4366, doi: 10.1029/2002JD002772, 2003.
- Fusco, A.C., and M.L. Salby, Interannual variations of total ozone and their relationship to variations of planetary wave activity, *J. Clim.*, *12* (6), 1619-1629, 1999.
- Gadhavi, H., R.T. Pinker, and I. Laszlo, Estimates of surface ultraviolet radiation over north America using Geostationary Operational Environmental Satellites observations, *J. Geophys. Res.*, *113*, D21205, doi: 10.1029/2007JD009308, 2008.
- Gardiner, T., A. Forbes, M. de Mazière, C. Vigouroux, E. Mahieu, P. Demoulin, V. Velazco, J. Notholt, T. Blumenstock, F. Hase, I. Kramer, R. Sussmann, W. Stremme, J. Mellqvist, A. Strandberg, K. Ellingsen, and M. Gauss, Trend analysis of greenhouse gases over Europe measured by a network of ground-based remote FTIR instruments, *Atmos. Chem. Phys.*, *8* (22), 6719-6727, doi: 10.5194/acp-8-6719-2008, 2008.
- Gottelman, A., T. Birner, V. Eyering, H. Akiyoshi, S. Bekki, C. Brühl, M. Dameris, D.E. Kinnison, F. Lefevre, F. Lott, E. Mancini, G. Pitari, D.A. Plummer, E. Rozanov, K. Shibata, A. Stenke, H. Struthers, and W. Tian, The tropical tropopause layer 1960–2100, *Atmos. Chem. Phys.*, *9* (5), 1621-1637, doi: 10.5194/acp-9-1621-2009, 2009.
- Gottelman, A., M.I. Hegglin, S.-W. Son, J. Kim, M. Fujiwara, T. Birner, S. Kremser, M. Rex, J.A. Añel, H. Akiyoshi, J. Austin, S. Bekki, P. Braesike, C. Brühl, N. Butchart, M. Chipperfield, M. Dameris, S. Dhomse, H. Garny, S.C. Hardiman, P. Jöckel, D.E. Kinnison, J.F. Lamarque, E. Mancini, M. Marchand, M. Michou, O. Morgenstern, S. Pawson, G. Pitari, D. Plummer, J.A. Pyle, E. Rozanov, J. Scinocca, T.G. Shepherd, K. Shibata, D. Smale, H. Teyssèdre, and W. Tian, Multimodel assessment of the upper troposphere and lower stratosphere: Tropics and trends, *J. Geophys. Res.*, *115*, D00M08, doi: 10.1029/2009JD013638, 2010.
- Gray, L.J., J. Beer, M. Geller, J.D. Haigh, M. Lockwood, K. Matthes, U. Cubasch, D. Fleitmann, G. Harrison, L. Hood, J. Luterbacher, G.A. Meehl, D. Shindell, B. van Geel, and W. White, Solar influence on climate, *Rev. Geophys.*, *48*, RG4001, doi: 10.1029/2009RG000282, 2010.
- Gröbner, J., M. Blumthaler, S. Kazadzis, A. Bais, A. Webb, J. Schreder, G. Seckmeyer, and D. Rembges, Quality assurance of spectral solar UV measurements: Results from 25 UV monitoring sites in Europe, 2002 to 2004, *Metrologia*, *43*, S66-S71, doi: 10.1088/0026-1394/43/2/S14, 2006.
- Gröbner, J., G. Hülsen, L. Vuilleumier, M. Blumthaler, J.M. Vilaplana, D. Walker, and J.E. Gil, *Report of the PMOD/WRC-COST Calibration and Intercomparison of Erythral Radiometers*, Davos, Switzerland, 28 July–23 August 2006, 108 pp., European Cooperation in Science and Technology (COST), available: ftp.pmodwrc.ch/pub/publications/PMOD_COST726_BBreport.pdf, 2007.
- Hall, T.M., D.W. Waugh, K.A. Boering, and R.A. Plumb, Evaluation of transport in stratospheric models, *J. Geophys. Res.*, *104* (D15), 18815-18839, 1999.
- Harris, N.R.P., E. Kyrö, J. Staehelin, D. Brunner, S.-B. Andersen, S. Godin-Beekmann, S. Dhomse, P.

- Hadjinicolaou, G. Hansen, I. Isaksen, A. Jrrar, A. Karpetchko, R. Kivi, B. Knudsen, P. Krizan, J. Lastovicka, J. Maeder, Y. Orsolini, J.A. Pyle, M. Rex, K. Vanicek, M. Weber, I. Wohltmann, P. Zanis, and C. Zerefos, Ozone trends at northern mid- and high latitudes – a European perspective, *Ann. Geophys.*, *26*, 1207-1220, 2008.
- Hase, F., Inversion von Spurengasprofilen aus Hochaufgelösten Bodengebundenen FTIR-Messungen in Absorption, Wissenschaftliche Berichte Forschungszentrum Karlsruhe, FZKA 6512; Ph.D. thesis, 156 pp., ISSN 0947-8620, available: <http://www-imk.fzk.de/asf/ftir/diss/hase.pdf>, 2000.
- Hassler, B., G.E. Bodeker, and M. Dameris, Technical Note: A new global database of trace gases and aerosols from multiple sources of high vertical resolution measurements, *Atmos. Chem. Phys.*, *8* (17), 5403-5421, doi: 10.5194/acp-8-5403-2008, 2008.
- Hegglin, M.I., and T.G. Shepherd, Large climate-induced changes in stratosphere-to-troposphere ozone flux and ultraviolet index, *Nature Geosci.*, *2*, 687-691, doi: 10.1038/NCEO604, 2009.
- Herman, J.R., Global increase in UV irradiance during the past 30 years (1979–2008) estimated from satellite data, *J. Geophys. Res.*, *115*, D04203, doi: 10.1029/2009JD012219, 2010.
- Herman, J.R., G. Labow, N.C. Hsu, and D. Larko, Changes in cloud cover derived from reflectivity time series using SeaWiFS, N7-TOMS, EP-TOMS, SBUV-2, and OMI radiance data, *J. Geophys. Res.*, *114*, D01201, doi: 10.1029/2007JD009508, 2009.
- Hess, P.G., and J.-F. Lamarque, Ozone source attribution and its modulation by the Arctic oscillation during the spring months, *J. Geophys. Res.*, *112*, D11303, doi: 10.1029/2006JD007557, 2007.
- Hicke, J.A., J. Slusser, K. Lantz, and F.G. Pascual, Trends and interannual variability in surface UVB radiation over 8 to 11 years observed across the United States, *J. Geophys. Res.*, *113*, D21302, doi: 10.1029/2008JD009826, 2008.
- Hickson, K.M., L.F. Keyser, and S.P. Sander, Temperature dependence of the HO₂ + ClO reaction. 2. Reaction kinetics using the discharge flow-resonance fluorescence technique, *J. Phys. Chem. A*, *111*, 8126-8138, doi: 10.1021/jp0689464, 2007.
- Hitchcock, P., T.G. Shepherd, and C. McLandress, Past and future conditions for polar stratospheric cloud formation simulated by the Canadian middle atmosphere model, *Atmos. Chem. Phys.*, *9* (2), 483-495, doi: 10.5194/acp-9-483-2009, 2009.
- Hofmann, D.J., and S. Solomon, Ozone destruction through heterogeneous chemistry following the eruption of El Chichón, *J. Geophys. Res.*, *94* (D4), 5029-5041, 1989.
- Hofmann, D.J., and S.J. Oltmans, Anomalous Antarctic ozone during 1992: Evidence for Pinatubo volcanic aerosol effects, *J. Geophys. Res.*, *98* (D10), 18555-18562, 1993.
- Hofmann, D.J., B.J. Johnson, and S.J. Oltmans, Twenty-two years of ozonesonde measurements at the South Pole, *Int. J. Remote Sens.*, *30* (15-16), 3995-4008, doi: 10.1080/01431160902821932, 2009a.
- Hofmann, D., J. Barnes, M. O'Neill, M. Trudeau, and R. Neely, Increase in background stratospheric aerosol observed with lidar at Mauna Loa Observatory and Boulder, Colorado, *Geophys. Res. Lett.*, *36*, L15808, doi: 10.1029/2009GL039008, 2009b.
- Holton, J.R., Meridional distribution of stratospheric trace constituents, *J. Atmos. Sci.*, *43* (12), 1238-1242, 1986.
- Höpfner, M., B.P. Luo, P. Massoli, F. Cairo, R. Spang, M. Snels, G. Di Donfrancesco, G. Stiller, T. von Clarmann, H. Fischer, and U. Biermann, Spectroscopic evidence for NAT, STS, and ice in MIPAS infrared limb emission measurements of polar stratospheric clouds, *Atmos. Chem. Phys.*, *6* (5), 1201-1219, doi: 10.5194/acp-6-1201-2006, 2006a.
- Höpfner, M., N. Larsen, R. Spang, B. Luo, J. Ma, S.H. Svendsen, S.D. Eckermann, B. Knudsen, P. Massoli, F. Cairo, G. Stiller, T. v. Clarmann, and H. Fischer, MIPAS detects Antarctic stratospheric belt of NAT PSCs caused by mountain waves, *Atmos. Chem. Phys.*, *6* (5), 1221-1230, doi: 10.5194/acp-6-1221-2006, 2006b.
- Höpfner, M., M.C. Pitts, and L.R. Poole, Comparison between CALIPSO and MIPAS observations of polar stratospheric clouds, *J. Geophys. Res.*, *114*, D00H05, doi: 10.1029/2009JD012114, 2009.
- Hsu, J., and M.J. Prather, Stratospheric variability and tropospheric ozone, *J. Geophys. Res.*, *114*, D06102, doi: 10.1029/2008JD010942, 2009.
- Huder, K.J., and W.B. DeMore, Absorption cross-sections of the ClO dimer, *J. Phys. Chem.*, *99*, 3905-3908, 1995.
- Hudman, R.C., D.J. Jacob, S. Turquety, E.M. Leibensperger, L.T. Murray, S. Wu, A.B. Gilliland, M. Avery, T.H. Bertram, W. Brune, R.C. Cohen, J.E. Dibb, F.M. Flocke, A. Fried, J. Holloway, J.A. Neuman, R. Orville, A. Perring, X. Ren, G.W. Sachse, H.B. Singh, A. Swanson, and P.J. Wooldrige, Surface and lightning sources of nitrogen oxides over the United States: Magnitudes, chemical evolution, and outflow, *J. Geophys. Res.*, *112*, D12S05, doi: 10.1029/2006JD007912, 2007.
- Hülsem, G., J. Gröbner, A. Bais, M. Blumthaler, P. Disterhoft, B. Johnsen, K.O. Lantz, C. Meleti, J. Schreder, J.M. Vilaplana Guerrero, and L. Ylianttila, Intercomparison of erythemal broadband radiometers

- calibrated by seven UV calibration facilities in Europe and the USA, *Atmos. Chem. Phys.*, *8* (16), 4865-4875, doi: 10.5194/acp-8-4865-2008, 2008.
- Ialongo, I., G.R. Casale, and A.M. Siani, Comparison of total ozone and erythral UV data from OMI with ground-based measurements at Rome station, *Atmos. Chem. Phys.*, *8* (12), 3283-3289, doi: 10.5194/acp-8-3283-2008, 2008.
- Ialongo, I., V. Buchard, C. Brogniez, G.R. Casale, and A.M. Siani, Aerosol Single Scattering Albedo retrieval in the UV range: An application to OMI satellite validation, *Atmos. Chem. Phys.*, *10* (2), 331-340, doi: 10.5194/acp-10-331-2010, 2010.
- Innis, J.L., and A.R. Klekociuk, Planetary wave and gravity wave influence on the occurrence of polar stratospheric clouds over Davis Station, Antarctica, seen in lidar and radiosonde observations, *J. Geophys. Res.*, *111*, D22102, doi: 10.1029/2006JD007629, 2006.
- IPCC (Intergovernmental Panel on Climate Change), *Climate Change 2007: Synthesis Report, Contribution of Working Groups I, II and III to the Fourth Assessment Report of the Intergovernmental Panel on Climate Change*, edited by Core Writing Team, R.K. Pachauri, and A. Reisinger, IPCC, Geneva, Switzerland, 104 pp., 2007.
- IUPAC (International Union of Pure and Applied Chemistry), 2007: see Atkinson et al., 2007.
- Janjai, S., S. Buntung, R. Wattan, and I. Masiri, Mapping solar ultraviolet radiation from satellite data in a tropical environment, *Remote Sens. Environ.*, *114* (3), 682-691, doi: 10.1016/j.rse.2009.11.008, 2010.
- Janouch, M., and L. Metelka, Modeling UV spectra with help of neural networks, in *Proceedings of the UV Conference "One Century of UV Radiation Research,"* 18-20 September 2007, Davos, Switzerland, edited by J. Gröbner, 207-208, 2007.
- Jin, B., I.-C. Chen, W.-T. Huang, C.-Y. Lien, N. Guchhait, and J.J. Lin, Photodissociation cross section of ClOOCl at 330 nm, *J. Phys. Chem. A.*, *114*, 4791-4797, doi: 10.1021/jp909374k, 2010.
- JMA (Japan Meteorological Agency), *Climate Change Monitoring Report 2008*, 87 pp., Japan Meteorological Agency, Tokyo, available: <http://ds.data.jma.go.jp/tcc/tcc/products/gwp/CCMR2008.pdf>, 2009.
- Johnsen, B., B. Kjeldstad, T.N. Aalerud, L.T. Nilsen, J. Schreder, M. Blumthaler, G. Bernhard, C. Topaloglou, O. Meinander, A. Bagheri, J.R. Slusser, and J. Davis, Intercomparison and harmonization of UV Index measurements from multiband filter radiometers, *J. Geophys. Res.*, *113*, D15206, doi: 10.1029/2007JD009731, 2008.
- Jones, A., J. Urban, D.P. Murtagh, P. Eriksson, S. Brohede, C. Haley, D. Degenstein, A. Bourassa, C. von Savigny, T. Sonkaew, A. Rozanov, H. Bovensmann, and J. Burrows, Evolution of stratospheric ozone and water vapour time series studied with satellite measurements, *Atmos. Chem. Phys.*, *9* (16), 6055-6075, doi: 10.5194/acp-9-6055-2009, 2009.
- JPL (Jet Propulsion Laboratory) 02-25: see Sander et al, 2003.
- JPL (Jet Propulsion Laboratory) 06-2: see Sander et al, 2006.
- JPL (Jet Propulsion Laboratory) 09-31: see Sander et al, 2009.
- Junk, J., U. Feister, and A. Helbig, Reconstruction of daily solar UV radiation from 1893 to 2002 in Potsdam, Germany, *Int. J. Biometeorol.*, *51* (6), 505-512, doi: 10.1007/s00484-007-0089-4, 2007.
- Kawa, S.R., R.S. Stolarski, P.A. Newman, A.R. Douglass, M. Rex, D.J. Hofmann, M.L. Santee, and K. Frieler, Sensitivity of polar stratospheric ozone loss to uncertainties in chemical reaction kinetics, *Atmos. Chem. Phys.*, *9* (22), 8651-8660, doi: 10.5194/acp-9-8651-2009, 2009.
- Kazadzis, S., A. Bais, V. Amiridis, D. Balis, C. Meleti, N. Kouremeti, C.S. Zerefos, S. Rapsomanikis, M. Petrakakis, A. Kelesis, P. Tzoumaka, and K. Keletkoglou, Nine years of UV aerosol optical depth measurements at Thessaloniki, Greece, *Atmos. Chem. Phys.*, *7* (8), 2091-2101, doi: 10.5194/acp-7-2091-2007, 2007.
- Kazadzis, S., A. Bais, A. Arola, N. Krotkov, N. Kouremeti, and C. Meleti, Ozone Monitoring Instrument spectral UV irradiance products: comparison with ground based measurements at an urban environment, *Atmos. Chem. Phys.*, *9* (2), 585-594, doi: 10.5194/acp-9-585-2009, 2009a.
- Kazadzis, S., A. Bais, D. Balis, N. Kouremeti, M. Zempila, A. Arola, E. Giannakaki, V. Amiridis, and A. Kazantzidis, Spatial and temporal UV irradiance and aerosol variability within the area of an OMI satellite pixel, *Atmos. Chem. Phys.*, *9* (14), 4593-4601, doi: 10.5194/acp-9-4593-2009, 2009b.
- Kazantzidis, A., A. Bais, K. Garane, S. Kazadzis, and C. Meleti, Estimation of UV irradiance from ancillary data and comparison with measurements at Thessaloniki, Greece (40.5°N, 23°E), in *Remote Sensing of Clouds and the Atmosphere XI*, edited by J.R. Slusser, K. Schäfer, and A. Comerón, Proc. SPIE, 6362, 636228, doi: 10.1117/12.689813, 2006.
- Kivi, R., E. Kyrö, T. Turunen, N.R.P. Harris, P. von der Gathen, M. Rex, S.B. Andersen, and I. Wohltmann, Ozonesonde observations in the Arctic during 1989–2003: Ozone variability and trends in the lower stratosphere and free troposphere, *J. Geophys. Res.*, *112*, D08306, doi: 10.1029/2006JD007271, 2007.

- Kovalenko, L.J., K.W. Jucks, R.J. Salawitch, G.C. Toon, J.-F. Blavier, D.G. Johnson, A. Kleinböhl, N.J. Livesey, J.J. Margitan, H.M. Pickett, M.L. Santee, B. Sen, R.A. Stachnik, and J.W. Waters, Observed and modeled HOCl profiles in the midlatitude stratosphere: Implication for ozone loss, *Geophys. Res. Lett.*, *34*, L19801, doi: 10.1029/2007GL031100, 2007.
- Krzyżcin, J.W., and J.L. Borkowski, Variability of the total ozone trend over Europe for the period 1950–2004 derived from reconstructed data, *Atmos. Chem. Phys.*, *8* (11), 2847–2857, doi: 10.5194/acp-8-2847-2008, 2008.
- Krzyżcin, J.W., and B. Rajewska-Więch, Trends in the ozone vertical distribution from the Umkehr observations at Belsk 1963–2007, *Int. J. Remote Sens.*, *30* (15), 3917–3926, doi: 10.1080/014311609002821866, 2009.
- Krzyżcin, J.W., P.S. Sobolewski, J. Jarosławski, J. Podgórski, and B. Rajewska-Więch, Erythral UV observations at Belsk, Poland, in the period 1976–2008: Data homogenization, climatology, and trends, *Acta Geophysica*, *59* (1) 155–182, 2011.
- Kuttippurath, J., S. Godin-Beekmann, F. Lefèvre, and A. Pazmiño, Ozone depletion in the Arctic winter 2007–2008, *Int. J. Remote Sens.*, *30* (15–16), 4071–4082, doi: 10.1080/01431160902821965, 2009.
- Kvalevåg, M.M., G. Myhre, and C.E. Lund Myhre, Extensive reduction of surface UV radiation since 1750 in world's populated regions, *Atmos. Chem. Phys.*, *9* (20), 7737–7751, doi: 10.5194/acp-9-7737-2009, 2009.
- Lee-Taylor, J., S. Madronich, C. Fischer, and B. Mayer, A climatology of UV radiation, 1979–2000, 65S–65N, Chapter 1 in *UV Radiation in Global Climate Change: Measurements, Modeling and Effects on Ecosystems*, edited by W. Gao, D.L. Schmoldt, and J. Slusser, 550 pp., Springer-Verlag and Tsinghua University Press, ISBN: 978-3-642-03312-4, 1–20, 2009.
- Lerot, C., M. Van Roozendael, J. van Geffen, J. van Gent, C. Fayt, R. Spurr, G. Lichtenberg, and A. von Barmen, Six years of total ozone column measurements from SCIAMACHY nadir observations, *Atmos. Meas. Tech.*, *2*, 87–98, doi: 10.5194/amt-2-87-2009, 2009.
- Li, F., R.S. Stolarski, and P.A. Newman, Stratospheric ozone in the post-CFC era, *Atmos. Chem. Phys.*, *9* (6), 2207–2213, doi: 10.5194/acp-9-2207-2009, 2009.
- Lien, C.Y., W.Y. Lin, H.Y. Chen, W.T. Huang, B. Jin, I.C. Chen, and J.J. Lin, Photodissociation cross sections of ClOOCl at 248.4 and 266 nm, *J. Chem. Phys.*, *131* (17), 174301, 2009.
- Lindfors, A., J. Kaurola, A. Arola, T. Koskela, K. Lakkala, W. Josefsson, J.A. Olseth, and B. Johnsen, A method for reconstruction of past UV radiation based on radiative transfer modeling: Applied to four stations in northern Europe, *J. Geophys. Res.*, *112*, D23201, doi: 10.1029/2007JD008454, 2007.
- Logan, J., An analysis of ozonesonde data for the lower stratosphere: Recommendations for testing models, *J. Geophys. Res.*, *104* (D13), 16151–16170, 1999.
- Lowe, D., and A.R. MacKenzie, Polar stratospheric cloud microphysics and chemistry, *J. Atmos. Solar-Terr. Phys.*, *70*, 13–40, doi: 10.1016/j.jastp.2007.09.011, 2008.
- Loyola, D.G., R.M. Coldewey-Egbers, M. Dameris, H. Garny, A. Stenke, M. Van Roozendael, C. Lerot, D. Balis, and M. Koukouli, Global long-term monitoring of the ozone layer — a prerequisite for predictions, *Int. J. Remote Sens.*, *30*, 4295–4318, doi: 10.1080/01431160902825016, 2009a.
- Loyola, D.G., R.M. Coldewey-Egbers, W. Zimmer, M. Koukouli, D. Balis, C. Lerot, M. Van Roozendael, and M. Dameris, Total ozone trends derived from the 14-years merged GOME/SCIAMACHY/GOME-2 data record, *Proc. ESA Atmospheric Science Conference*, 7–11 September 2009, Barcelona, Spain, European Space Agency, ESA SP-676, available: http://uv-vis.aeronomie.be/publications/proceedings/2009a_loyola.pdf, 2009b.
- Mäder, J.A., J. Staehelin, D. Brunner, W.A. Stahel, I. Wohltmann, and T. Peter, Statistical modeling of total ozone: Selection of appropriate explanatory variables, *J. Geophys. Res.*, *112*, D11108, doi: 10.1029/2006JD007694, 2007.
- Marley, N.A., J.S. Gaffney, M. Tackett, N.C. Sturchio, L. Heraty, N. Martinez, K.D. Hardy, A. Marchany-Rivera, T. Guilderson, A. MacMillan, and K. Steelman, The impact of biogenic carbon sources on aerosol absorption in Mexico City, *Atmos. Chem. Phys.*, *9* (5), 1537–1549, doi: 10.5194/acp-9-1537-2009, 2009.
- Marsh, D.R., and R.R. Garcia, Attribution of decadal variability in lower-stratospheric tropical ozone, *Geophys. Res. Lett.*, *34*, L21807, doi: 10.1029/2007GL030935, 2007.
- Martins, J.V., P. Artaxo, Y.J. Kaufman, A.D. Castanho, and L.A. Remer, Spectral absorption properties of aerosol particles from 350–2500 nm, *Geophys. Res. Lett.*, *36*, L13810, doi: 10.1029/2009GL037435, 2009.
- Massoli, P., M. Maturilli, and R. Neuber, Climatology of Arctic polar stratospheric clouds as measured by lidar in Ny-Ålesund, Spitsbergen (79°N, 12°E), *J. Geophys. Res.*, *111*, D09206, doi: 10.1029/2005JD005840, 2006.

- Maturilli, M., R. Nueber, P. Massoli, F. Cairo, A. Adriani, M.L. Moriconi, and G. Di Donfrancesco, Differences in Arctic and Antarctic PSC occurrence as observed by lidar in Ny-Ålesund (79°N, 12°E) and McMurdo (78°S, 167°E), *Atmos. Chem. Phys.*, 5 (8), 2081-2090, doi: 10.5194/acp-5-2081-2005, 2005.
- Matus, M.H., M.T. Nguyen, D.A. Dixon, K.A. Peterson, and J.S. Francisco, ClClO₂ is the most stable isomer of Cl₂O₂. Accurate coupled cluster energetics and electronic spectra of Cl₂O₂ isomers, *J. Phys. Chem. A*, 112, 9623-9627, doi: 10.1021/jp806220r, 2008.
- McCormack, J.P., D.E. Siskind, and L.L. Hood, Solar-QBO interaction and its impact on stratospheric ozone in a zonally averaged photochemical transport model of the middle atmosphere, *J. Geophys. Res.*, 112, D16109, doi: 10.1029/2006JD008369, 2007.
- McDonald, A.J., S.E. George, and R.M. Woollands, Can gravity waves significantly impact PSC occurrence in the Antarctic?, *Atmos. Chem. Phys.*, 9 (22), 8825-8840, doi: 10.5194/acp-9-8825-2009, 2009.
- McElroy, M.B., R.J. Salawitch, S.C. Wofsy, and J.A. Logan, Reductions of Antarctic ozone due to synergistic interactions of chlorine and bromine, *Nature*, 321, 759-762, doi: 10.1038/321759a0, 1986.
- McKenzie, R., G. Bodeker, G. Scott, J. Slusser, and K. Lantz, Geographical differences in erythemally-weighted UV measured at mid-latitude USDA sites, *Photochem. Photobiol. Sci.*, 5 (3), 343-352, doi: 10.1039/B510943D, 2006.
- McKenzie, R.L., C. Weinreis, P.V. Johnston, B. Liley, H. Shiona, M. Kotkamp, D. Smale, N. Takegawa, and Y. Kondo, Effects of urban pollution on UV spectral irradiances, *Atmos. Chem. Phys.*, 8 (18), 5683-5697, doi: 10.5194/acp-8-5683-2008, 2008.
- McKenzie, R.L., J.B. Liley, and L.O. Björn, UV radiation: Balancing risks and benefits, *Photochem. Photobiol.*, 85, 88-98, doi: 10.1111/j.1751-1097.2008.00400.x, 2009.
- McLandress, C., and T.G. Shepherd, Simulated anthropogenic changes in the Brewer-Dobson circulation, including its extension to high latitudes, *J. Clim.*, 22, 1516-1540, doi: 10.1175/2008JCLI2679.1, 2009.
- McLinden, C.A., S. Tegtmeier, and V. Fioletov, Technical note: A SAGE-corrected SBUV zonal-mean ozone data set, *Atmos. Chem. Phys.*, 9 (20), 7963-7972, doi: 10.5194/acp-9-7963-2009, 2009.
- Meinander, O., A. Kontu, K. Lakkala, A. Heikkilä, L. Ylianttila, and M. Toikka, Diurnal variations in the UV albedo of arctic snow, *Atmos. Chem. Phys.*, 8 (21), 6551-6563, doi: 10.5194/acp-8-6551-2008, 2008.
- Miller, A.J., A. Cai, G. Taio, D.J. Wuebbles, L.E. Flynn, S.-K. Yang, E.C. Weatherhead, V. Fioletov, I. Petropavlovskikh, X.-L. Meng, S. Guillas, R.M. Nagatani, and G.C. Reinsel, Examination of ozonsonde data for trends and trend changes incorporating solar and Arctic oscillation signals, *J. Geophys. Res.*, 111, D13305, doi: 10.1029/2005JD006684, 2006.
- Molina, L.T., and M.J. Molina, Production of Cl₂O₂ from the self-reaction of the ClO radical, *J. Phys. Chem.*, 91, 433-436, 1987.
- Moore, T.A., M. Okumura, J.W. Seale, and T.K. Minton, UV photolysis of ClOOCl, *J. Phys. Chem. A*, 103 (12), 1691-1695, 1999.
- Müller, R., J.-U. Groöß, C. Lemmen, D. Heinze, M. Dameris, and G. Bodeker, Simple measures of ozone depletion in the polar stratosphere, *Atmos. Chem. Phys.*, 8 (2), 251-264, doi: 10.5194/acp-8-251-2008, 2008.
- Murata, I., K. Sato, S. Okano, and Y. Tomikawa, Measurements of stratospheric ozone with a balloon-borne optical ozone sensor, *Int. J. Remote Sens.*, 30, 3961-3966, doi: 10.1080/01431160902822823, 2009.
- Newchurch, M.J., E.-S. Yang, D.M. Cunnold, G.C. Reinsel, J.M. Zawodny, and J.M. Russell III, Evidence for slowdown in stratospheric ozone loss: First stage of ozone recovery, *J. Geophys. Res.*, 108 (D16), 4507, doi: 10.1029/2003JD003471, 2003.
- Newman, P.A., and M. Rex (Lead Authors), P.O. Canziani, K.S. Carslaw, K. Drdla, S. Godin-Beekmann, D.M. Golden, C.H. Jackman, K. Kreher, U. Langematz, R. Müller, H. Nakane, Y.J. Orsolini, R.J. Salawitch, M.L. Santee, M. von Hobe, and S. Yoden, Polar ozone: Past and present, Chapter 4 in *Scientific Assessment of Ozone Depletion: 2006*, Global Ozone Research and Monitoring Project-Report No. 50, 572 pp., World Meteorological Organization, Geneva, Switzerland, 2007.
- Newman, P.A., E.R. Nash, S.R. Kawa, S.A. Montzka, and S.M. Schauffler, When will the Antarctic ozone hole recover?, *Geophys. Res. Lett.*, 33, L12814, doi: 10.1029/2005GL025232, 2006.
- Noel, V., A. Hertzog, H. Chepfer, and D.M. Winker, Polar stratospheric clouds over Antarctica from the CALIPSO spaceborne lidar, *J. Geophys. Res.*, 113, D02205, doi: 10.1029/2007JD008616, 2008.
- Noel, V., A. Hertzog, and H. Chepfer, CALIPSO observations of wave-induced PSCs with near-unity optical depth over Antarctica in 2006-2007, *J. Geophys. Res.*, 114, D05202, doi: 10.1029/2008JD010604, 2009.
- Ordóñez, C., D. Brunner, J. Staehelin, P. Hadjinicolaou, J.A. Pyle, M. Jonas, H. Wernli, and A.S.H. Prévôt, Strong influence of lowermost stratospheric ozone on lower tropospheric background ozone changes over Europe, *Geophys. Res. Lett.*, 34, L07805, doi:

- 10.1029/2006GL029113, 2007.
- Panicker, A.S., G. Pandithurai, T. Takamura, and R.T. Pinker, Aerosol effects in the UV-B spectral region over Pune, an urban site in India, *Geophys. Res. Lett.*, *36*, L10802, doi: 10.1029/2009GL037632, 2009.
- Papanastasiou, D.K., V.C. Papadimitriou, D.W. Fahey, and J.B. Burkholder, UV absorption spectrum of the ClO dimer (Cl_2O_2) between 200 and 420 nm, *J. Phys. Chem. A*, *113*, 13711-13726, doi: 10.1021/jp9065345, 2009.
- Parrington, M., D.B.A. Jones, K.W. Bowman, L.W. Horowitz, A.M. Thompson, D.W. Tarasick, and J.C. Witte, Estimating the summertime tropospheric ozone distribution over North America through assimilation of observations from the Tropospheric Emission Spectrometer, *J. Geophys. Res.*, *113*, D18307, doi: 10.1029/2007JD009341, 2008.
- Parrish, D.D., D.B. Millet, and A.H. Goldstein, Increasing ozone in marine boundary layer inflow at the west coasts of North America and Europe, *Atmos. Chem. Phys.*, *9* (4), 1303-1323, doi: 10.5194/acp-9-1303-2009, 2009.
- Permien, T., R. Vogt, and R.N. Schindler, Absorption spectra of HOCl and Cl_2O_2 , in *Mechanisms of Gas Phase-Liquid Phase Chemical Transformations*, edited by R.A. Cox, *Air Pollution Report #17*, 149-153, Environmental Research Program of the CEC, EUR 12035 EN, Brussels, Belgium, 1988.
- Petkov, B., V. Vitale, C. Tomasi, U. Bonafè, S. Scaglione, D. Flori, R. Santaguida, M. Gausa, G. Hansen, and T. Colombo, Narrowband filter radiometer for ground-based measurements of global ultraviolet solar irradiance and total ozone, *Appl. Opt.*, *45* (18), 4383-4395, doi: 10.1364/AO.45.004383, 2006.
- Petropavlovskikh, I., C. Ahn, P.K. Bhartia, and L.E. Flynn, Comparison and covalidation of ozone anomalies and variability observed in SBUV(2) and Umkehr northern midlatitude ozone profile estimates, *Geophys. Res. Lett.*, *32*, L06805, doi: 10.1029/2004GL022002, 2005a.
- Petropavlovskikh, I., P.K. Bhartia, and J.J. DeLuisi, New Umkehr ozone profile retrieval algorithm optimized for climatological studies, *Geophys. Res. Lett.*, *32*, L16808, doi: 10.1029/2005GL023323, 2005b.
- Pitts, M.C., L.W. Thomason, L.R. Poole, and D.M. Winker, Characterization of Polar Stratospheric Clouds with spaceborne lidar: CALIPSO and the 2006 Antarctic season, *Atmos. Chem. Phys.*, *7* (19), 5207-5228, doi: 10.5194/acp-7-5207-2007, 2007.
- Pitts, M.C., L.R. Poole, and L.W. Thomason, CALIPSO polar stratospheric cloud observations: Second-generation detection algorithm and composition discrimination, *Atmos. Chem. Phys.*, *9* (19), 7577-7589, doi: 10.5194/acp-9-7577-2009, 2009.
- Plenge, J., R. Flesch, S. Köhl, B. Vogel, R. Müller, F. Stroh, and E. Rühl, Ultraviolet photolysis of the ClO dimer, *J. Phys. Chem. A*, *108*, 4859-4863, 2004.
- Pommereau, J.P., and F. Goutail, O_3 and NO_2 ground-based measurements by visible spectrometry during Arctic winter and spring 1988, *Geophys. Res. Lett.*, *15*, (8) 891-894, 1988.
- Poole, L.R., and M.C. Pitts, Polar stratospheric cloud climatology based on Stratospheric Aerosol Measurement II observations from 1978 to 1989, *J. Geophys. Res.*, *99* (D6), 13083-13089, 1994.
- Pope, F.D., J.C. Hansen, K.D. Bayes, R.R. Friedl, and S.P. Sander, Ultraviolet absorption spectrum of chlorine peroxide, ClOCl, *J. Phys. Chem.*, *111*, 4322-4332, 2007.
- Portmann, R.W., S. Solomon, R.R. Garcia, L.W. Thomason, L.R. Poole, and M.P. McCormick, Role of aerosol variations in anthropogenic ozone depletion in the polar regions, *J. Geophys. Res.*, *101* (D17), 22991-23006, 1996.
- Pougatchev, N.S., B.J. Connor, and C.P. Rinsland, Infrared measurements of the ozone vertical distribution above Kitt Peak, *J. Geophys. Res.*, *100* (D8), 16689-16697, 1995.
- Pribullová, A., and M. Chmelík, Typical distribution of the solar erythemal UV radiation over Slovakia, *Atmos. Chem. Phys.*, *8* (17), 5393-5401, doi: 10.5194/acp-8-5393-2008, 2008.
- Price, C., and D. Rind, A simple lightning parameterization for calculating global lightning distributions, *J. Geophys. Res.*, *97* (D9), 9919-9933, 1992.
- Randel, W.J., and F. Wu, A stratospheric ozone profile data set for 1979-2005: Variability, trends, and comparisons with column ozone data, *J. Geophys. Res.*, *112*, D06313, doi: 10.1029/2006JD007339, 2007.
- Randel, W.J., K.P. Shine, J. Austin, J. Barnett, C. Claud, N.P. Gillett, P. Keckhut, U. Langematz, R. Lin, C. Long, C. Mears, A. Miller, J. Nash, D.J. Seidel, D.W.J. Thompson, F. Wu, and S. Yoden, An update of observed stratospheric temperature trends, *J. Geophys. Res.*, *114*, D02107, doi: 10.1029/2008JD010421, 2009.
- Rasch, P.J., P.J. Crutzen, and D.B. Coleman, Exploring the goengineering of climate using stratospheric sulfate aerosols: The role of particle size, *Geophys. Res. Lett.*, *35*, L02809, doi: 10.1029/2007GL032179, 2008.
- Reinsel, G.C., E.C. Weatherhead, G.C. Tiao, A.J. Miller, R.M. Nagatani, D.J. Wuebbles, and L.E. Flynn, On detection of turnaround and recovery in trend for ozone, *J. Geophys. Res.*, *107* (D10), 4078, doi: 10.1029/2001JD000500, 2002.
- Reinsel, G.C., A.J. Miller, E.C. Weatherhead, L.E. Flynn,

- R. Nagatani, G.C. Tiao, and D.J. Wuebbles, Trend analysis of total ozone data for turnaround and dynamical contributions, *J. Geophys. Res.*, *110*, D16306, doi: 10.1029/2004JD004662, 2005.
- Remsberg, E.E., On the response of Halogen Occultation Experiment (HALOE) stratospheric ozone and temperature to the 11-year solar cycle forcing, *J. Geophys. Res.*, *113*, D22304, doi: 10.1029/2008JD010189, 2008.
- Rex, M., R.J. Salawitch, P. von der Gathen, N.R.P. Harris, M.P. Chipperfield, and B. Naujokat, Arctic ozone loss and climate change, *Geophys. Res. Lett.*, *31*, L04116, doi: 10.1029/2003GL018844, 2004.
- Rex, M., R.J. Salawitch, H. Deckelmann, P. von der Gathen, N.R.P. Harris, M.P. Chipperfield, B. Naujokat, E. Reimer, M. Allaart, S.B. Andersen, R. Bevilacqua, G.O. Braathen, H. Claude, J. Davies, H. De Backer, H. Dier, V. Dorokhov, H. Fast, M. Gerdling, S. Godin-Beekmann, K. Hoppel, B. Johnson, E. Kyrö, Z. Litynska, D. Moore, H. Nakane, M.C. Parrondo, A.D. Risley Jr., P. Skrivankova, R. Stübi, P. Viatte, V. Yushkov, and C. Zerefos, Arctic winter 2005: Implications for stratospheric ozone loss and climate change, *Geophys. Res. Lett.*, *33*, L23808, doi: 10.1029/2006GL026731, 2006.
- Rieder, H.E., F. Holawe, S. Simic, M. Blumthaler, J.W. Krzyściński, J.E. Wagner, A.W. Schmalwieser, and P. Weihs, Reconstruction of erythema UV-doses for two stations in Austria: A comparison between alpine and urban regions, *Atmos. Chem. Phys.*, *8* (20), 6309-6323, doi: 10.5194/acp-8-6309-2008, 2008.
- Robock, A., T. Adams, M. Moore, L. Oman, G. Stenchikov, Southern Hemisphere atmospheric circulation effects of the 1991 Mount Pinatubo eruption, *Geophys. Res. Lett.*, *34*, L23710, doi: 10.1029/2007GL031403, 2007.
- Rodgers, C.D., *Inverse Methods for Atmospheric Sounding: Theory and Practice*, 240 pp., ISBN 981-02-2740X, World Scientific Publishing Co. Ltd., London, UK, 2000.
- Rosenfield, J.E., S.M. Frith, and R.S. Stolarski, Version 8 SBUV ozone profile trends compared with trends from a zonally averaged chemical model, *J. Geophys. Res.*, *110*, D12302, doi: 10.1029/2004JD005466, 2005.
- Rösevall, J.D., D.P. Murthugh, and J. Urban, Ozone depletion in the 2006/2007 Arctic winter, *Geophys. Res. Lett.*, *34*, L21809, doi: 10.1029/2007GL030620, 2007.
- Ruckstuhl, C., R. Philipona, K. Behrens, M. Collaud Coen, B. Dürr, A. Heimo, C. Mätzler, S. Nyeki, A. Ohmura, L. Vuilleumier, M. Weller, C. Wehrli, and A. Zelenka, Aerosol and cloud effects on solar brightening and the recent rapid warming, *Geophys. Res. Lett.*, *35*, L12708, doi: 10.1029/2008GL034228, 2008.
- Salawitch, R.J., D.K. Weisenstein, L.J. Kovalenko, C.E. Sioris, P.O. Wennberg, K. Chance, M.K.W. Ko, and C.A. McLinden, Sensitivity of ozone to bromine in the lower stratosphere, *Geophys. Res. Lett.*, *32* (5), L05811, doi: 10.1029/2004GL021504, 2005.
- Sander, S.P., R.R. Friedl, D.M. Golden, M.J. Kurylo, R.E. Huie, V.L. Orkin, G.K. Moortgat, A.R. Ravishankara, C.E. Kolb, M.J. Molina, and B.J. Finlayson-Pitts, *Chemical Kinetics and Photochemical Data for Use in Atmospheric Studies: Evaluation No. 14, JPL Publication 02-25*, Jet Propulsion Laboratory, Pasadena, Calif., 2003. (Cited as JPL 02-25.)
- Sander, S.P., R.R. Friedl, D.M. Golden, M.J. Kurylo, G.K. Moortgat, H. Keller-Rudek, P.H. Wine, A.R. Ravishankara, C.E. Kolb, M.J. Molina, B.J. Finlayson-Pitts, R.E. Huie, and V.L. Orkin, *Chemical Kinetics and Photochemical Data for Use in Atmospheric Studies: Evaluation No. 15, JPL Publication 06-2*, Jet Propulsion Laboratory, Pasadena, Calif., 2006. (Cited as JPL 06-2.)
- Sander, S.P., J. Abbatt, J.R. Barker, J.B. Burkholder, R.R. Friedl, D.M. Golden, R.E. Huie, C.E. Kolb, M.J. Kurylo, G.K. Moortgat, V.L. Orkin, and P.H. Wine, *Chemical Kinetics and Photochemical Data for Use in Atmospheric Studies: Evaluation Number 16, JPL Publication 09-31*, Jet Propulsion Laboratory, Pasadena, Calif., available at <http://jpldataeval.jpl.nasa.gov>, 2009. (Cited as JPL 09-31.)
- Santee, M.L., I.A. MacKenzie, G.L. Manney, M.P. Chipperfield, P.F. Bernath, K.A. Walker, C.D. Boone, L. Froidevaux, N.J. Livesey, and J.W. Waters, A study of stratospheric chlorine partitioning based on new satellite measurements and modeling, *J. Geophys. Res.*, *113*, D12307, doi: 10.1029/2007JD009057, 2008.
- Santee, M.L., S.P. Sander, N.J. Livesey, and L. Froidevaux, Constraining the chlorine monoxide (ClO)/chlorine peroxide (ClOOCl) equilibrium constant from Aura Microwave Limb Sounder measurements of nighttime ClO, *Proc. Nat. Acad. Sci.*, *107* (15), 6588-6593, doi: 10.1073/pnas.0912659107, 2010.
- Sauvage, B., R.V. Martin, A. van Donkelaar, X. Liu, K. Chance, L. Jaeglé, P.I. Palmer, S. Wu, and T.-M. Fu, Remote sensed and in situ constraints on processes affecting tropical tropospheric ozone, *Atmos. Chem. Phys.*, *7* (3), 815-838, doi: 10.5194/acp-7-815-2007, 2007.
- Scarnato, B., J. Staehelin, T. Peter, J. Gröbner, and R. Stübi, Temperature and slant path effects in Dobson and Brewer total ozone measurements, *J. Geophys. Res.*, *114*, D24303, doi: 10.1029/2009JD012349, 2009.

- Scarnato, B., J. Staehelin, R. Stübi, and H. Schill, Long term total ozone observations at Arosa (Switzerland) with Dobson and Brewer instruments (1988–2007), *J. Geophys. Res.*, *115*, D13306, doi: 10.1029/2009JD011908, 2010.
- Schallhart, B., M. Blumthaler, J. Schreder, and J. Verdebout, A method to generate near real time UV-Index maps of Austria, *Atmos. Chem. Phys.*, *8* (24), 7483–7491, doi: 10.5194/acp-8-7483-2008, 2008.
- Schiermeier, Q., Chemists poke holes in ozone theory, *Nature*, *449*, 382–383, 2007.
- Schmidt, H., and G.P. Brasseur, The response of the middle atmosphere to solar cycle forcing in the Hamburg Model of the neutral and ionized atmosphere, *Space Sci. Rev.*, *125*, 345–356, doi: 10.1007/s11214-006-9068-z, 2006.
- Schmidt, H., G.P. Brasseur, and M.A. Giorgetta, Solar cycle signal in a general circulation and chemistry model with internally generated quasi-biennial oscillation, *J. Geophys. Res.*, *115*, D00114, doi: 10.1029/2009JD012542, 2010.
- Schneider, M., A. Redondas, F. Hase, C. Guirado, T. Blumenstock, and E. Cuevas, Comparison of ground-based Brewer and FTIR total O₃ monitoring techniques, *Atmos. Chem. Phys.*, *8* (18), 5535–5550, doi: 10.5194/acp-8-5535-2008, 2008.
- Schofield, R., K. Frieler, I. Wohltmann, M. Rex, M. von Hobe, F. Stroh, G. Koch, T. Peter, T. Canty, R. Salawitch, and C.M. Volk, Polar stratospheric chlorine kinetics from a self-match flight during SOLVE-II/EUPLEX, *Geophys. Res. Lett.*, *35*, L01807, doi: 10.1029/2007GL031740, 2008.
- Seckmeyer G., M. Glandorf, C. Wichers, R. McKenzie, D. Henriques, F. Carvalho, A. Webb, A.M. Siani, A. Bais, B. Kjeldstad, C. Brogniez, P. Werle, T. Koskela, K. Lakkala, J. Gröbner, H. Slaper, P. den Outer, and U. Feister, Europe's darker atmosphere in the UV-B, *Photochem. Photobiol. Sci.*, *7* (8), 925–930, 2008a.
- Seckmeyer, G., D. Pissulla, M. Glandorf, D. Henriques, B. Johnsen, A. Webb, A.-M. Siani, A. Bais, B. Kjeldstad, C. Brogniez, J. Lenoble, B. Gardiner, P. Kirsch, T. Koskela, J. Kaurola, B. Uhlmann, H. Slaper, P. den Outer, M. Janouch, P. Werle, J. Gröbner, B. Mayer, A. de la Casiniere, S. Simic, and F. Carvalho, Variability of UV irradiance in Europe, *Photochem. Photobiol.*, *84*, 172–179, doi: 10.1111/j.1751-1097.20007.00216.x, 2008b.
- Shepherd, T.G., Dynamics, stratospheric ozone, and climate change, *Atmos.-Ocean*, *46* (1), 117–138, doi: 10.3137/ao.460106, 2008.
- Shepherd, T.G., and A.I. Jonsson, On the attribution of stratospheric ozone and temperature changes to changes in ozone-depleting substances and well-mixed greenhouse gases, *Atmos. Chem. Phys.*, *8* (5), 1435–1444, doi: 10.5194/acp-8-1435-2008, 2008.
- Shindell, D.T., and R.L. de Zafra, Chlorine monoxide in the Antarctic spring vortex 2. A comparison of measured and modeled diurnal cycling over McMurdo Station, 1993, *J. Geophys. Res.*, *101* (D1), 1475–1487, 1996.
- Sinnhuber, B.-M., D.W. Arlander, H. Bovensmann, J.P. Burrows, M.P. Chipperfield, C.-F. Enell, U. Frieß, F. Hendrick, P.V. Johnston, R.L. Jones, K. Kreher, N. Mohamed-Tahrin, R. Müller, K. Pfeilsticker, U. Platt, J.-P. Pommereau, I. Pundt, A. Richter, A.M. South, K.K. Tørnkvist, M. Van Roozendaal, T. Wagner, and F. Wittrock, Comparison of measurements and model calculations of stratospheric bromine monoxide, *J. Geophys. Res.*, *107* (D19), 4398, doi: 10.1029/2001JD000940, 2002.
- Sitnov, S., Influence of the 11-year solar cycle on the effects of the equatorial quasi-biennial oscillation, manifesting in the extratropical northern atmosphere, *Clim. Dyn.*, *32*, 1–17, doi: 10.1007/s00382-007-0362-6, 2009.
- Slusser, J., J. Gibson, D. Bigelow, D. Kolinski, P. Disterhoft, K. Lantz, and A. Beaubien, Langley method of calibrating UV filter radiometers, *J. Geophys. Res.*, *105* (D4), 4841–4849, 2000.
- Smit, H.G.J., W. Straeter, B.J. Johnson, S.J. Oltmans, J. Davies, D.W. Tarasick, B. Goegger, R. Stubi, F.J. Schmidlin, T. Northam, A.M. Thompson, J.C. Witte, I. Boyd, and F. Posny, Assessment of the performance of ECC ozonesondes under quasi-flight conditions in the environmental simulation chamber: Insights from the Juelich Ozone Sonde Intercomparison Experiment (JOSIE), *J. Geophys. Res.*, *112*, D19306, doi: 10.1029/2006JD007308, 2007.
- Smith, A.K., and K. Matthes, Decadal-scale periodicities in the stratosphere associated with the solar cycle and the QBO, *J. Geophys. Res.*, *113*, D05311, doi: 10.1029/2007JD009051, 2008.
- Soller, R., J.M. Nicovich, and P.H. Wine, Temperature-dependent rate coefficients for the reactions of Br(²P_{3/2}), Cl(²P_{3/2}), and O(³P₁) with BrONO₂, *J. Phys. Chem. A*, *105* (9), 1416–1422, 2001.
- Solomon, P., B. Connor, J. Barrett, T. Mooney, A. Lee, and A. Parrish, Measurements of stratospheric ClO over Antarctica in 1996–2000 and implications for ClO dimer chemistry, *Geophys. Res. Lett.*, *29* (15), 1708, doi: 10.1029/2002GL015232, 2002.
- Solomon, S., R.R. Garcia, F.S. Rowland, and D.J. Wuebbles, On the depletion of Antarctic ozone, *Nature*, *321*, 755–758, doi: 10.1038/321755a0, 1986.
- Solomon, S., R.W. Portmann, T. Sasaki, D.J. Hofmann, and D.W.J. Thompson, Four decades of ozonesonde measurements over Antarctica, *J. Geophys. Res.*,

- 110, D21311, doi: 10.1029/2005JD005917, 2005.
- Solomon, S., R.W. Portmann, and D.W.J. Thompson, Contrasts between Antarctic and Arctic ozone depletion, *Proc. Nat. Acad. Sci.*, *104* (2), 445-449, doi: 10.1073/pnas.0604895104, 2007.
- SPARC (Stratospheric Processes And their Role in Climate), *SPARC/IOC/GAW Assessment of Trends in the Vertical Distribution of Ozone*, edited by N. Harris, R. Hudson, and C. Phillips, SPARC Report No. 1, WMO Global Ozone Research and Monitoring Project Report No. 43, 289 pp., Verrières le Buisson, France, 1998.
- SPARC (Stratospheric Processes And their Role in Climate), *The Role of Halogen Chemistry in Polar Stratospheric Ozone Depletion*, Report from the June 2008 Cambridge UK Workshop for an Initiative under the Stratospheric Processes and Their Role in Climate (SPARC) Project of the World Climate Research Programme, authored by M.J. Kurylo, B.-M. Sinnhuber, N.R.P. Harris, M. von Hobe, P.A. Newman, D.W. Fahey, R.S. Gao, R.J. Salawitch, M.P. Chipperfield, J.G. Anderson, M.L. Santee, T.P. Canty, R. Müller, R. Schofield, R.M. Stimpfle, F. Strohm, D.W. Toohey, J. Urban, S.R. Kawa, D.J. Hofmann, K.W. Hoppel, M. Rex, K.D. Bayes, D.A. Dixon, K.W. Jucks, S.P. Sander, J.-U. Groöb, and D.E. Kinnison, 48 pp., available: http://www.atmosp.physics.utoronto.ca/SPARC/HalogenChem_Final_20090213.pdf, 2009.
- SPARC CCMVal (Stratospheric Processes And their Role in Climate), *SPARC Report on the Evaluation of Chemistry-Climate Models*, edited by V. Eyring, T.G. Shepherd, and D.W. Waugh, SPARC Report No. 5, WCRP-132, WMO/TD-No. 1526, 478 pp., available: <http://www.atmosp.physics.utoronto.ca/SPARC>, 2010.
- Staehelin, J., N.R.P. Harris, C. Appenzeller, and J. Eberhard, Ozone trends: A review, *Rev. Geophys.*, *39*, 231-290, 2001.
- Staiger, H., P.N. den Outer, A.F. Bais, H. Feister, B. Johnsen, and L. Vuilleumier, Hourly resolved cloud modification factors in the ultraviolet, *Atmos. Chem. Phys.*, *8* (9), 2493-2508, doi: 10.5194/acp-8-2493-2008, 2008.
- Steinbrecht, W., H. Claude, F. Schöenborn, I.S. McDermid, T. Leblanc, S. Godin-Beekmann, P. Keckhut, A. Hauchecorne, J.A.E. Van Gijssel, D.P.J. Swart, G.E. Bodeker, A. Parrish, I.S. Boyd, N. Kämpfer, K. Hocke, R.S. Stolarski, S.M. Frith, L.W. Thomason, E.E. Remsberg, C. Von Savigny, A. Rozanov, and J.P. Burrows, Ozone and temperature trends in the upper stratosphere at five stations of the Network for the Detection of Atmospheric Composition Change, *Int. J. Remote Sens.*, *30*, 3875-3886, doi: 10.1080/01431160902821841, 2009.
- Stenchikov, G., A. Robock, V. Ramaswamy, M.D. Schwarzkopf, K. Hamilton, and S. Ramachandran, Arctic Oscillation response to the 1991 Mount Pinatubo eruption: Effects of volcanic aerosols and ozone depletion, *J. Geophys. Res.*, *107* (D24), 4803, doi: 10.1029/2002JD002090, 2002.
- Stimpfle, R.M., R.A. Perry, and C.J. Howard, Temperature-dependence of the reaction of ClO and HO₂ radicals, *J. Chem. Phys.*, *71* (12), 5183-5190, doi: 10.1063/1.438293, 1979.
- Stimpfle, R., D.M. Wilmouth, R.J. Salawitch, and J.G. Anderson, First measurements of ClOOC1 in the stratosphere: The coupling of ClOOC1 and ClO in the Arctic polar vortex, *J. Geophys. Res.*, *109*, D03301, doi: 10.1029/2003JD003811, 2004.
- Stolarski, R.S., and S.M. Frith, Search for evidence of trend slow-down in the long-term TOMS/SBUV total ozone data record: The importance of instrument drift uncertainty, *Atmos. Chem. Phys.*, *6*, 4057-4065, 2006.
- Stolarski, R.S., A.R. Douglass, S. Steenrod, and S. Pawson, Trends in stratospheric ozone: Lessons learned from a 3D Chemical Transport Model, *J. Atmos. Sci.*, *63* (3), 1028-1041, 2006.
- Stübi, R., G. Levrat, B. Hoegger, P. Viatte, J. Staehelin, and F. J. Schmidlin, In-flight comparison of Brewer-Mast and electrochemical concentration cell ozonesondes, *J. Geophys. Res.*, *113*, D13302, doi: 10.1029/2007JD009091, 2008.
- Tabazadeh, A., R.P. Turco, K. Drdla, M.Z. Jacobson, and O.B. Toon, A study of Type I polar stratospheric cloud formation, *Geophys. Res. Lett.*, *21* (15), 1619-1622, 1994.
- Tabazadeh, A., Y.S. Djikaev, P. Hamill, and H. Reiss, Laboratory evidence for surface nucleation of solid polar stratospheric cloud particles, *J. Phys. Chem. A*, *106*, 10238-10246, 2002.
- Takahashi, K., Y. Takeuchi, and Y. Matsumi, Rate constants of the O(¹D) reactions with N₂, O₂, N₂O, and H₂O at 295 K, *Chem. Phys. Lett.*, *410*, 196-200, 2005.
- Tanskanen, A., N.A. Krotkov, J.R. Herman, and A. Arola, Surface ultraviolet irradiance from OMI, *Geosci. Remote Sens.*, *44* (5), 1267-1271, doi: 10.1109/TGRS.2005.862203, 2006.
- Tanskanen, A., A. Lindfors, A. Määttä, N. Krotkov, J. Herman, J. Kaurola, T. Koskela, K. Lakkala, V. Fioletov, G. Bernhard, R. McKenzie, Y. Kondo, M. O'Neill, H. Slaper, P. den Outer, A.F. Bais, and J. Tamminen, Validation of daily erythemal doses from Ozone Monitoring Instrument with ground-based UV measurement data, *J. Geophys. Res.*, *112*, D24S44, doi: 10.1029/2007JD008830, 2007.

- Tatarov, B., H. Nakane, Ch. B. Park, N. Sugimoto, and I. Matsui, Lidar observation of long-term trends and variations of stratospheric ozone and temperature over Tsukuba, Japan, *Int. J. Remote Sens.*, *30* (15-16), 3951-3960, doi: 10.1080/01431160902821882, 2009.
- Tegtmeier, S., M. Rex, I. Wohltmann, and K. Krüger, Relative importance of dynamical and chemical contributions to Arctic wintertime ozone, *Geophys. Res. Lett.*, *35*, L17801, doi: 10.1029/2008GL034250, 2008.
- Telford, P., P. Braesicke, O. Morgenstern, and J. Pyle, Re-assessment of causes of ozone column variability following the eruption of Mount Pinatubo using a nudged CCM, *Atmos. Chem. Phys.*, *9* (13), 4251-4260, doi: 10.5194/acp-9-4251-2009, 2009.
- Terao, Y., and J.A. Logan, Consistency of time series and trends of stratospheric ozone as seen by ozonesonde, SAGE II, HALOE, and SBUV(2), *J. Geophys. Res.*, *112*, D06310, doi: 10.1029/2006JD007667, 2007.
- Terao, Y., J.A. Logan, A.R. Douglass, and R.S. Stolarski, Contribution of stratospheric ozone to the interannual variability of tropospheric ozone in the northern extratropics, *J. Geophys. Res.*, *113*, D18309, doi: 10.1029/2008JD009854, 2008.
- Thiel, S., L. Ammannato, A. Bais, B. Bandy, M. Blumthaler, B. Bohn, O. Engelsen, G.P. Gobbi, J. Gröbner, E. Jäkel, W. Junkermann, S. Kazadzis, R. Kift, B. Kjeldstad, N. Kouremeti, A. Kylling, B. Mayer, P.S. Monks, C.E. Reeves, B. Schallhart, R. Scheirer, S. Schmidt, R. Schmitt, J. Schreder, R. Silbernagl, C. Topaloglou, T.M. Thorseth, A.R. Webb, M. Wendisch, and P. Werle, Influence of clouds on the spectral actinic flux density in the lower troposphere (INSPECTRO): Overview of the field campaigns, *Atmos. Chem. Phys.*, *8* (6), 1789-1812, doi: 10.5194/acp-8-1789-2008, 2008.
- Thompson, A.M., J.B. Stone, J.C. Witte, S.K. Miller, R.B. Pierce, R.B. Chatfield, S.J. Oltmans, O.R. Cooper, A.L. Loucks, B.F. Taubman, B.J. Johnson, E. Joseph, T.L. Kucsera, J.T. Merrill, G.A. Morris, S. Hersey, G. Forbes, M.J. Newchurch, F.J. Schmidlin, D.W. Tarasick, V. Thouret, and J.-P. Cammas, Intercontinental Chemical Transport Experiment Ozonesonde Network Study (IONS) 2004: 1. Summertime upper troposphere/lower stratosphere ozone over northeastern North America, *J. Geophys. Res.*, *112*, D12S12, doi: 10.1029/2006JD007441, 2007.
- Thouret, V., J.-P. Cammas, B. Sauvage, G. Athier, R. Zbinden, P. Nédélec, P. Simon, and F. Karcher, Tropopause referenced ozone climatology and inter-annual variability (1994–2003) from the MOZAIC programme, *Atmos. Chem. Phys.*, *6* (4), 1033-1051, doi: 10.5194/acp-6-1033-2006, 2006.
- Tie, X.X., and G.P. Brasseur, The response of stratospheric ozone to volcanic eruptions: Sensitivity to atmospheric chlorine loading, *Geophys. Res. Lett.*, *22* (22), 3035-3038, 1995.
- Tie, X.X., G.P. Brasseur, B. Briegleb, and C. Granier, Two-dimensional simulation of Pinatubo aerosol and its effect on stratospheric ozone, *J. Geophys. Res.*, *99* (D10), 20545-20562, 1994.
- Tilmes, S., R. Müller, J.-U. Groöf, and J.M. Russell III, Ozone loss and chlorine activation in the Arctic winters 1991–2003 derived with the tracer-tracer correlations, *Atmos. Chem. Phys.*, *4* (8), 2181-2213, doi: 10.5194/acp-4-2181-2004, 2004.
- Tilmes, S., R. Müller, A. Engel, M. Rex, and J. M. Russell, Chemical ozone loss in the Arctic and Antarctic stratosphere between 1992 and 2005, *Geophys. Res. Lett.*, *33*, L20812, doi: 10.1029/2006GL026925, 2006.
- Tilmes, S., R. Müller, and R. Salawitch, The sensitivity of polar ozone depletion to proposed geoengineering schemes, *Science*, *320*, 1201-1204, 2008a.
- Tilmes, S., R. Müller, R.J. Salawitch, U. Schmidt, C.R. Webster, H. Oelhaf, C.C. Camy-Peyret, and J.M. Russell III, Chemical ozone loss in the Arctic winter 1991–1992, *Atmos. Chem. Phys.*, *8* (7), 1897-1910, doi: 10.5194/acp-8-1897-2008, 2008b.
- Toohey, D.W., L.M. Avallone, L.R. Lait, P.A. Newman, M.R. Schoeberl, D.W. Fahey, E.L. Woodbridge, and J.G. Anderson, The seasonal evolution of reactive chlorine in the northern hemisphere stratosphere, *Science*, *261* (5125), 1134-1136, doi: 10.1126/science.261-5125.1134, 1993.
- Toon, O., A. Tabazadeh, E. Browell, and J. Jordan, Analysis of lidar observations of Arctic polar stratospheric clouds during January 1989, *J. Geophys. Res.*, *105* (D16), 20589-20615, 2000.
- Tourpali, K., C.S. Zerefos, D.S. Balis, and A.F. Bais, The 11-year solar cycle in stratospheric ozone: Comparison between Umkehr and SBUVv8 and effects on surface erythemal irradiance, *J. Geophys. Res.*, *112*, D12306, doi: 10.1029/2006JD007760, 2007.
- Tsutsui, J., K. Nishizawa, and F. Sassi, Response of the middle atmosphere to the 11-year solar cycle simulated with the Whole Atmosphere Community Climate Model, *J. Geophys. Res.*, *114*, D02111, doi: 10.1029/2008JD010316, 2009.
- Van Roozendaal, M., D. Loyola, R. Spurr, D. Balis, J.-C. Lambert, Y. Livschitz, P. Valks, T. Ruppert, P. Kenter, C. Fayt, and C. Zehner, Ten years of GOME/ERS-2 total ozone data – The new GOME data processor (GDP) version 4: 1. Algorithm description, *J. Geophys. Res.*, *111*, D14311, doi: 10.1029/2005JD006375, 2006.
- Verdebout, J., A method to generate surface UV radiation

- maps over Europe using GOME, Meteosat, and ancillary geophysical data, *J. Geophys. Res.*, *105* (D4), 5049-5058, 2000.
- Verdebout, J., A European satellite-derived UV climatology available for impact studies, *Radiat. Prot. Dosim.*, *111* (4), 407-411, 2004a.
- Verdebout, J., A satellite-derived UV radiation climatology over Europe to support impact studies, *Arct. Antarct. Alp. Res.*, *36* (3), 357-363, 2004b.
- Vernet, M., S.B. Diaz, H.A. Fuenzalida, C. Camilion, C.R. Booth, S. Cabrera, C. Casiccia, G. Deferrari, C. Lovengreen, A. Paladini, J. Pedroni, A. Rosales, and H.E. Zagarese, Quality of UVR exposure for different biological systems along a latitudinal gradient, *Photochem. Photobiol.*, *8*, 1329-1345, doi: 10.1039/b904540f, 2009.
- Vernier, J.P., J.P. Pommereau, A. Garnier, J. Pelon, N. Larsen, J. Nielsen, T. Christensen, F. Cairo, L.W. Thomason, T. Leblanc, and I.S. McDermid, Tropical stratospheric aerosol layer from CALIPSO lidar observations, *J. Geophys. Res.*, *114*, D00H10, doi: 10.1029/2009JD011946, 2009.
- Vigouroux C., M. De Mazière, P. Demoulin, C. Servais, F. Hase, T. Blumenstock, I. Kramer, M. Schneider, J. Mellqvist, A. Strandberg, V. Velazco, J. Notholt, R. Sussmann, W. Stremme, A. Rockmann, T. Gardiner, M. Coleman, and P. Woods, Evaluation of tropospheric and stratospheric ozone trends over Western Europe from ground-based FTIR network observations, *Atmos. Chem. Phys.*, *8* (23), 6865-6886, doi: 10.5194/acp-8-6865-2008, 2008.
- Vogel, B., R. Müller, T. Deshler, J.-U. Grooß, J. Karhu, D.S. McKenna, M. Müller, D. Toohey, G.C. Toon, and F. Stroh, Vertical profiles of activated ClO and ozone loss in the Arctic vortex in January and March 2000: In situ observations and model simulations, *J. Geophys. Res.*, *108* (D22), 8334, doi: 10.1029/2002JD002564, 2003.
- Voigt, C., J. Schreiner, A. Kohlman, P. Zink, K. Mauersberger, N. Larsen, T. Deshler, C. Kröger, J. Rosen, A. Adriani, F. Cairo, G. Di Donfrancesco, M. Viterbini, J. Ovarlez, H. Ovarlez, C. David, and A. Dörnbrack, Nitric acid trihydrate (NAT) in polar stratospheric clouds, *Science*, *290*, 1756-1758, 2000.
- von Hobe, M., Revisiting ozone depletion, *Science*, *318*, 1878-1879, 2007.
- von Hobe, M., R.J. Salawitch, T. Canty, H. Keller-Rudek, G.K. Moortgat, J.-U. Grooß, R. Müller, and F. Stroh, Understanding the kinetics of the ClO dimer cycle, *Atmos. Chem. Phys.*, *7* (12), 3055-3069, doi: 10.5194/acp-7-3055-2007, 2007.
- von Hobe, M., F. Stroh, H. Beckers, T. Benter, and H. Willner, The UV/Vis absorption spectrum of matrix-isolated dichlorine peroxide, ClOOC1, *Phys. Chem. Chem. Phys.*, *11*, 1571-1580, doi: 10.1039/b814373k, 2009.
- Vranckx, S., J. Peeters, and S.A. Carl, Absolute rate constant and O(³P) yield for the O(¹D) + N₂O reaction in the temperature range 227 K to 719 K, *Atmos. Chem. Phys.*, *8* (20), 6261-6272, doi: 10.5194/acp-8-6261-2008, 2008.
- Vyushin, D., V.E. Fioletov, and T.G. Shepherd, Impact of long-range correlations on trend detection in total ozone, *J. Geophys. Res.*, *112*, D14307, doi: 10.1029/2006JD008168, 2007.
- Vyushin, D., T.G. Shepherd, and V.E. Fioletov, On the statistical modeling of persistence in total ozone anomalies, *J. Geophys. Res.*, *115*, D16306, doi: 10.1029/2009JD013105, 2010.
- Waibel, A.E., T. Peter, K.S. Carslaw, H. Oelhaf, G. Wetzel, P.J. Crutzen, U. Pöschl, A. Tsias, E. Reimer, and H. Fischer, Arctic ozone loss due to denitrification, *Science*, *283*, 2064-2069, 1999.
- Wang, K., R.E. Dickinson, and S. Liang, Clear sky visibility has decreased over land globally from 1973 to 2007, *Science*, *323* (5921), 1468-1470, doi: 10.1126/science.1167549, 2009.
- Wang, Z., G. Stephens, T. Deshler, C. Trepte, T. Parish, D. Vane, D. Winker, D. Liu, and L. Adhikari, Association of Antarctic polar stratospheric cloud formation on tropospheric cloud systems, *Geophys. Res. Lett.*, *35*, L13806, doi: 10.1029/2008GL034209, 2008.
- Waugh, D., Atmospheric dynamics: The age of stratospheric air, *Nature Geosci.*, *2*, 14-16, doi: 10.1038/nge0397, 2009.
- Waugh, D.W., and T.M. Hall, Age of stratospheric air: Theory, observations, and models, *Rev. Geophys.*, *40*, doi: 10.1029/2000RG000101, 2000.
- Waugh, D.W., and V. Eyring, Quantitative performance metrics for stratospheric-resolving chemistry-climate models, *Atmos. Chem. Phys.*, *8* (18), 5699-5713, doi: 10.5194/acp-8-5699-2008, 2008.
- Waugh, D.W., L. Oman, S.R. Kawa, R.S. Stolarski, S. Pawson, A.R. Douglass, P.A. Newman, and J.E. Nielsen, Impacts of climate change on stratospheric ozone recovery, *Geophys. Res. Lett.*, *36*, L03805, doi: 10.1029/2008GL036223, 2009.
- Weatherhead, E.C., G.C. Reinsel, G.C. Tiao, C.H. Jackman, L. Bishop, S.M.H. Frith, J. DeLuisi, T. Keller, S.J. Oltmans, E.L. Fleming, D.J. Wuebbles, J.B. Kerr, A.J. Miller, J. Herman, R. McPeters, R.M. Nagatani, and J.E. Frederick, Detecting the recovery of total column ozone, *J. Geophys. Res.*, *105* (D17), 22201-22210, 2000.
- Webb, A.R., B.G. Gardine, T.J. Martin, K. Leszczynsk, J. Metzendorf, and V.A. Mohnen, *Guidelines for Site Quality Control of UV Monitoring*, WMO/GAW

- No. 126, WMO TD 884, World Meteorological Organization, Geneva, 39 pp., 1998.
- Webb, A.R., J. Gröbner, and M. Blumthaler, *A Practical Guide to Operating Broadband Instruments Measuring Erythemally Weighted Irradiance*, publication of COST 726 and World Meteorological Organization, 21 pp., European Cooperation in Science and Technology (COST) Office, Luxembourg, available: <http://www.cost726.org/>, 2006.
- Weber, M., L.N. Lamsal, M. Coldewey-Egbers, K. Bramstedt, and J.P. Burrows, Pole-to-pole validation of GOME WFOAS total ozone with ground-based data, *Atmos. Chem. Phys.*, 5 (5), 1341-1355, doi: 10.5194/acp-5-1341-2005, 2005.
- Weber, M., L.N. Lamsal, and J.P. Burrows, Improved SCIAMACHY WFOAS total ozone retrieval: Steps towards homogenising long-term total ozone datasets from GOME, SCIAMACHY, and GOME2, in *Proceedings of the Envisat Symposium 2007*, Montreux, Switzerland, 23-27 April 2007, ESA SP-636, available: <http://envisat.esa.int/envisatsymposium/proceedings/posters/3P4/463281we.pdf>, 2007.
- Weih, P., M. Blumthaler, H.E. Rieder, A. Kreuter, S. Simic, W. Laube, A.W. Schmalwieser, J.E. Wagner, and A. Tanskanen, Measurements of UV irradiance within the area of one satellite pixel, *Atmos. Chem. Phys.*, 8 (18), 5615-5626, doi: 10.5194/acp-8-5615-2008, 2008.
- Weiss, A.K., J. Staehelin, C. Appenzeller, and N.R.P. Harris, Chemical and dynamical contributions to ozone profile trends of the Payerne (Switzerland) balloon soundings, *J. Geophys. Res.*, 106 (D19), 22685-22694, 2001.
- Wetzel, G., H. Oelhaf, O. Kirner, R. Ruhnke, F. Friedl-Vallon, A. Kleinert, G. Maucher, H. Fischer, M. Birk, G. Wagner, and A. Engel, First remote sensing measurements of ClOOCl along with ClO and ClONO₂ in activated and deactivated Arctic vortex conditions using new ClOOCl IR absorption cross sections, *Atmos. Chem. Phys.*, 10 (3), 931-945, doi: 10.5194/acp-10-931-2010, 2010.
- Wilmouth, D.M., R.M. Stimpfle, J.G. Anderson, J.W. Elkins, D.F. Hurst, R.J. Salawitch, and L.R. Lait, Evolution of inorganic chlorine partitioning in the Arctic polar vortex, *J. Geophys. Res.*, 111, D16308, doi: 10.1029/2005JD006951, 2006.
- Wilmouth, D.M., T.F. Hanisco, R.M. Stimpfle, and J.G. Anderson, Chlorine-catalyzed ozone destruction: Cl atom production from ClOOCl photolysis, *J. Phys. Chem. A*, 113, 14099-14108, doi: 10.1021/jp9053204, 2009.
- WMO (World Meteorological Organization), *Scientific Assessment of Ozone Depletion: 1994*, Global Ozone Research and Monitoring Project-Report No. 37, Geneva, Switzerland, 1995.
- WMO (World Meteorological Organization), *Scientific Assessment of Ozone Depletion: 1998*, Global Ozone Research and Monitoring Project-Report No. 44, Geneva, Switzerland, 1999.
- WMO (World Meteorological Organization), *Scientific Assessment of Ozone Depletion: 2002*, Global Ozone Research and Monitoring Project-Report No. 47, Geneva, Switzerland, 2003.
- WMO (World Meteorological Organization), *Scientific Assessment of Ozone Depletion: 2006*, Global Ozone Research and Monitoring Project-Report No. 50, 572 pp., Geneva, Switzerland, 2007.
- WMO (World Meteorological Organization), *Instruments to Measure Solar Ultraviolet Radiation – Part 2: Broadband Instruments Measuring Erythemally Weighted Solar Irradiance*, WMO TD No. 1289, G. Seckmeyer, A. Bais, G. Bernhard, M. Blumthaler, C.R. Booth, K. Lantz, and R.L. McKenzie, 55 pp., Geneva, Switzerland, available: <http://www.wmo.int/pages/prog/arep/gaw/gaw-reports.html>, 2008.
- Wohltmann, I., R. Lehmann, M. Rex, D. Brunner, and J. Mäder, A process-oriented regression model for column ozone, *J. Geophys. Res.*, 112, D12304, doi: 10.1029/2006JD007573, 2007.
- Wuttke, S., J. Verdebout, and G. Seckmeyer, An improved algorithm for satellite-derived UV radiation, *Photochem. Photobiol.*, 77 (1), 52-57, 2003.
- Wuttke, S., G. Seckmeyer, and G. König-Langlo, Measurements of spectral snow albedo at Neumayer, Antarctica, *Ann. Geophys.*, 24, 7-21, 2006a.
- Wuttke, S., G. Seckmeyer, G. Bernhard, J. Ehrhamjian, R. McKenzie, P. Johnston, and M. O'Neill, New spectroradiometers complying with the NDSC standards, *J. Atmos. Oceanic Tech.*, 23, 241-251, 2006b.
- Yang, E.-S., D.M. Cunnold, R.J. Salawitch, M.P. McCormick, J. Russell III, J.M. Zawodny, S. Oltmans, and M.J. Newchurch, Attribution of recovery in lower-stratospheric ozone, *J. Geophys. Res.*, 111, D17309, doi: 10.1029/2005JD006371, 2006.
- Yang, E.-S., D.M. Cunnold, M.J. Newchurch, R.J. Salawitch, M.P. McCormick, J.M. Russell III, J.M. Zawodny, and S.J. Oltmans, First stage of Antarctic ozone recovery, *J. Geophys. Res.*, 113, D20308, doi: 10.1029/2007JD009675, 2008.
- Yang, M., S.G. Howell, J. Zhuang, and B.J. Huebert, Attribution of aerosol light absorption to black carbon, brown carbon, and dust in China – interpretations of atmospheric measurements during EAST-AIRE, *Atmos. Chem. Phys.*, 9 (6), 2035-2050, doi: 10.5194/acp-9-2035-2009, 2009.
- Yang, S.-K., C.S. Long, A.J. Miller, X. He, Y. Yang,

- D.J. Wuebbles, and G. Tiao, Modulation of natural variability on a trend analysis of updated cohesive SBUV(2) total ozone, *Int. J. Remote Sens.*, *30*, 3975-3986, doi: 10.1080/01431160902821924, 2009.
- Zanis, P., E. Maillard, J. Staehelin, C. Zerefos, E. Kosmidis, K. Tourpali, and I. Wohltmann, On the turnaround of stratospheric ozone trends deduced from the reevaluated Umkehr record of Arosa, Switzerland, *J. Geophys. Res.*, *111*, D22307, doi: 10.1029/2005JD006886, 2006.
- Zhao, J., R.P. Turco, and O.B. Toon, A model simulation of Pinatubo volcanic aerosols in the stratosphere, *J. Geophys. Res.*, *100* (D4), 7315-7328, 1995.
- Ziemke, J.R., S. Chandra, and P.K. Bhartia, A 25-year data record of atmospheric ozone in the Pacific from Total Ozone Mapping Spectrometer (TOMS) cloud slicing: Implications for ozone trends in the stratosphere and troposphere, *J. Geophys. Res.*, *110*, D15105, doi: 10.1029/2004JD005687, 2005.